Università degli Studi di Padova

Dipartimento di Ingegneria Industriale
Corso di Laurea in Ingegneria Elettrica

Analysis and Design of Multipole Fractional-Slot PM Assisted REL Motors: Techniques to Increase the Torque Density with Respect to the Standard Solutions

Laureando:

Paolo Marzarotto

Relatore:

Ch.mo Prof. Nicola Bianchi

Analysis and Design of Multipole Fractional-Slot PM Assisted REL Motors: Techniques to Increase the Torque Density with Respect to the Standard Solutions
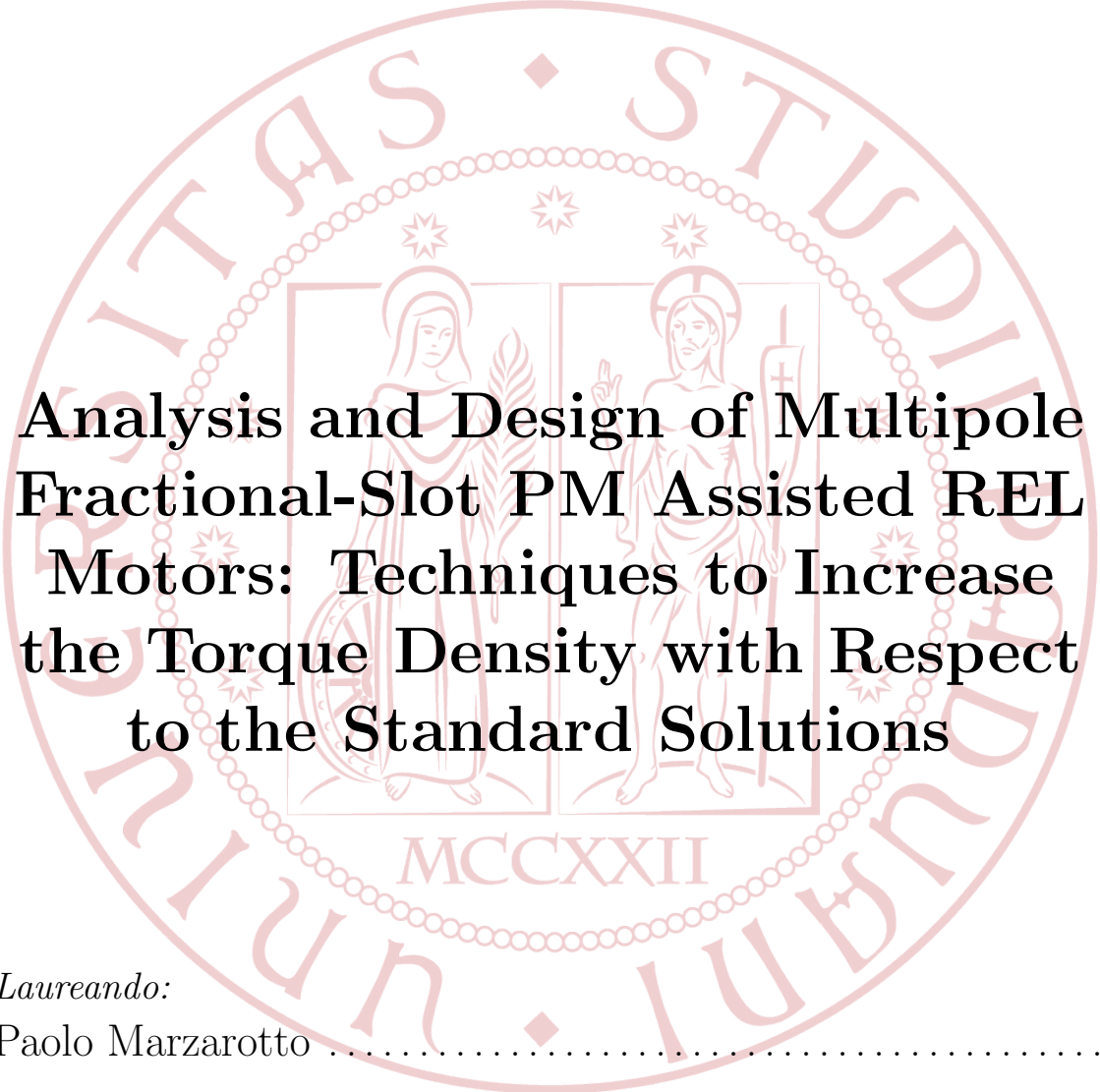
Laureando:
Paolo Marzarotto . . . .

Relatore::
Ch.mo Prof. Nicola Bianchi . . . .

Alla mia famiglia.

Abstract

Fractional-slot concentrated winding (FCSW) synchronous PMARel machines have been gaining interest in the last few years. This is because they have several advantages due to the union of the FCSW and PMs. In particular they are characterized by high-power density, high efficiency, short end turns, low cogging torque and flux-weakening capability. If compared with SPM motors, there is the possibility to use low cost Ferrite PMs instead of NdFeB ones, much more expensive because of the high market demand. Being based on IPM rotor configuration, this kind of motors have as benefits an easier magnet retention but some negative aspects must be considered. The rotor structure is more difficult to size than the SPM one and in terms of torque performance they usually exhibit an higher torque ripple and a lower average torque.

The main aim of this thesis is to analyze different FCSW synchronous PMARel configurations focusing the attention on torque behaviour. This to do a comparison with a SPM motor and a distributed winding (DW) synchronous PMARel motor.

Different techniques will be shown trying to increase the average torque and to decrease the torque ripple, getting as closer as possible to SPM motor torque performance. They are:

- the *Tooth Cut* which is described in Chap.4;

- the *Stator Shifting increasing the slot number* which is reported in Chap.5;

- the *Rotor skewing combined with Stator Shifting* which is described in Chap.6.

The entire study is carried out for a low-speed elevator application. All the motors have been analyzed always at nominal conditions and they have multipole structures since they must work at low-speed.

Contents

Chapter 1

SPM motor

The first analysis deals with the SPM motor and the computation of its parameters. Finite Elements Analysis (FEM) has been used. Two different kinds of permanent magnets are considered, Neodimium - Iron - Boron (NdFeB) and Ferrite, to determine the effects of different materials on motor performance to compare the SPM to PMARel configurations.

1.1 Motor design

The SPM design must be based on some geometrical constraints and other specifications reported in Table 1.1:

<div align="center">

Table 1.1: SPM geometrical specifications

Symbol	Value	Unit	Geometrical constraints
D_e	290	$[mm]$	External diameter
L_{stk}	145	$[mm]$	Stack length
			Other specifications
$2p$	8	-	Poles number
g	1	$[mm]$	Air–gap thickness
n	159	$[rpm]$	Motor speed at nominal conditions
T_N	165	$[Nm]$	Nominal torque

</div>

The PMs material chosen is NdFeB. From the BH curve of the material at $120C$ it's fixed that:

$$\frac{B_{g0}}{B_r} \simeq 0.85 \tag{1.1}$$

It's known that $B_r = 1.1\ T$ and from (3.1) could be obtained:

$$B_{g0} \simeq 0.85 \cdot B_r = 0.85 \cdot 1.1 = 0.935\ [T] \tag{1.2}$$

Always from the NdFeB BH curve, considering that the magnetic field is proportional to the induction, it's fixed $H_{g0} = -140\ kA/m$. Also the working point limit of the magnetic field is fixed, and in particular it corresponds to $H_{knee} = -571.875\ kA/m$. The difference

between these two values represents the available range of magnetic field on which the PMs work:

$$H_{g0} - H_{knee} = -140 + 571.875 \simeq 432 \ [kA/m] \tag{1.3}$$

Deciding to work at nominal conditions with $H_{gN} = 170 \ kA/m$, the peak induction into the air-gap at nominal conditions could be calculated as:

$$\Delta H_s = H_{g0} - H_{gN} = -140 + 170 = 30 \ [kA/m] \tag{1.4}$$

$$\Delta B_s \simeq 0.038 \ [T] \tag{1.5}$$

and so:

$$B_g = B_{g0} - \Delta B_s = 0.936 - 0.038 = 0.898 \ [T] \tag{1.6}$$

From the NdFeB curve at 60 °C the relative magnetic permeability results in:

$$B_r = \mu_r \cdot \mu_0 \cdot H_c \Rightarrow \mu_r = \frac{B_r}{\mu_0 \cdot H_c} = \frac{1.20}{4 \cdot \pi \cdot 10^{-7} \cdot 900000} = 1.061 \tag{1.7}$$

Then the saturation coefficient and the Carter coefficient are estimated as:

$$K_{sat} \simeq 1.5 \qquad\qquad K_{Carter} \simeq 1.1 \tag{1.8}$$

The first one represents the ratio between the total magnetic voltage drop and the magnetic voltage drop related to the air-gap, while the second one considers the effect of the stator slot openings on the flux lines. So the actual thickness of the air-gap will be equal to:

$$g" = g \cdot K_{sat} \cdot K_{Carter} = 1 \cdot 1.65 \cdot 1.1 = 1.65 \ [mm] \tag{1.9}$$

The PMs thickness is calculated as:

$$t_m = \mu_r \cdot g" \cdot \left(\frac{B_{g0}}{B_r - B_{g0}} \right) = 1.061 \cdot 1.65 \cdot \left(\frac{0.935}{1.1 - 0.935} \right) \simeq 10 \ [mm] \tag{1.10}$$

The external and internal rotor diameters could be defined as:

$$D_{re} = D_e - 2 \cdot \left(g + t_m \right) = 190 - 2 \cdot \left(1 + 10 \right) = 168 \ [mm] \tag{1.11}$$

$$D_{ri} = 110 \ [mm] \tag{1.12}$$

As far as the magnets width is concerned, considering that there are 8 poles, each one corresponds to 45 deg mechanical degrees. If it is supposed that the PM occupies about 85 % of the pole, in mechanical degrees it is equal to 37.5 deg. In terms of millimeters all this could be expressed as:

$$h_m = \frac{\pi \cdot D_{re}}{2} \cdot \frac{37.5}{180} \simeq 55 \ [mm] \tag{1.13}$$

At this point the rotor geometry is defined and the sizing could pass to the stator. In particular the slot pitch is exstimated through the De Jong expression reported by $Bianchi$ in [1]:

$$p_s \simeq 1.6 \cdot \sqrt{\frac{D_{re}}{p}} = 1.6 \cdot \sqrt{\frac{190}{4}} = 11.03 \ [mm] \tag{1.14}$$

Then the stator slots number is defined as:

$$Q_s = \frac{\pi \cdot D_{re}}{p_s} = \frac{\pi \cdot 190}{11.03} = 54.12 \tag{1.15}$$

and the number of slots per pole per phase is:

$$q = \frac{Q_s}{2p \cdot m} = \frac{54.12}{8 \cdot 3} = 2.26 \Rightarrow q = 2 \div 2.5 \tag{1.16}$$

The final choice is q = 2 and as a consequence:

$$Q_s = q \cdot 2p \cdot m = 2 \cdot 8 \cdot 3 = 48 \tag{1.17}$$

Also the stator pitch could be calculated definitively, considering higher diameter to take into consideration the slot opening height and the slot link near the air-gap:

$$p_s = \frac{\pi \cdot D}{Q_s} = \frac{\pi \cdot 197.6}{48} = 12.93 \ [mm] \tag{1.18}$$

Estimating that $B_t = 1.77 \ T$ the tooth width could be now expressed as:

$$w_t = \frac{B_{g0} + \Delta B_s}{B_t} \cdot p_s \cdot k_{pack} = \frac{0.935 + 0.038}{1.77} \cdot 12.93 \cdot 0.96 = 6.87 \ [mm] \tag{1.19}$$

So, the slot width will be equal to:

$$w_s = p_s - w_t = 12.93 - 6.87 = 6.06 \ [mm] \tag{1.20}$$

Assuming a $J_s = 6 \ A/mm^2$, it could be possible to define the geometry of the conductors. The mechanical speed and the nominal power are expressed like:

$$\omega_m = n \cdot \frac{2 \cdot \pi}{60} = 159 \cdot \frac{2 \cdot \pi}{60} = 16.65 \ [rad/s] \tag{1.21}$$

$$P_N = T_N \cdot \omega_m = 165 \cdot 16.65 = 2747 \ [W] \tag{1.22}$$

Fixing $cos\varphi = 0.9$, $\eta = 0.73 \ \%$ and $E = 210 \ V$ the current root mean square [rms] value is:

$$I = \frac{P_N}{3 \cdot E \cdot cos\varphi \cdot \eta} = \frac{2747}{3 \cdot 210 \cdot 0.9 \cdot 0.73} = 5.38 \ [A] \tag{1.23}$$

So the cross-section area of the single conductor is calculated as:

$$S_c = \frac{I}{J_s} = \frac{5.38}{6} = 0.9 \ [mm^2] \tag{1.24}$$

and as a consequence the conductor diameter could be analytically defined and then rounded off to a commercial value. So :

$$d_c = \sqrt{\frac{4 \cdot S_c}{\pi}} = \sqrt{\frac{4 \cdot 0.9}{\pi}} = 1.07 \Rightarrow 1.06 \ [mm^2] \tag{1.25}$$

Considering this diameter, the opening slot is defined in terms both of width and height. They are fixed equal to:

$$\omega_{so} = 3.15 \ [mm] \qquad\qquad\qquad h_{so} = 0.75 \ [mm] \qquad\qquad (1.26)$$

As far as the flux is concerned it is defined as:

$$\phi = B_g \cdot \frac{D_{re} \cdot Lstk}{p} \ = 0.898 \cdot \frac{0.19 \cdot 0.145}{4} = 6.18 \ [mWb] \qquad\qquad (1.27)$$

The total conductors is the next parameter which must be defined. Fixing the winding factor equal to $K_w = 1$, the frequency is expressed as:

$$f = \frac{n \cdot p}{60} = \frac{159 \cdot 4}{60} = 10.6 \ [Hz] \qquad\qquad (1.28)$$

and so:

$$N_s = \frac{E}{\frac{\pi}{\sqrt{2}} \cdot f \cdot K_w \cdot \phi} = \frac{210}{\frac{\pi}{\sqrt{2}} \cdot 10.6 \cdot 1 \cdot 6.18 \cdot 10^{-3}} = 1443 \qquad\qquad (1.29)$$

Having defined both stator slots number and the number of total conductors it is possible to calculate the total conductors into a slot. The choice is that to have a two parallel paths winding ($n_{pp} = 2$) and so:

$$n_{cs} = \frac{3 \cdot N_s}{Q_s} = \frac{3 \cdot 1443}{48} \simeq 90 \qquad\qquad (1.30)$$

$$n_c = n_{cs} \cdot n_{pp} = 90 \cdot 2 = 180 \qquad\qquad (1.31)$$

Finally the total cross-section area related to the conductors into a slot is:

$$S_{Cuslot} = n_{cs} \cdot S_c = 90 \cdot 0.9 = 81 \ [mm^2] \qquad\qquad (1.32)$$

Supposing a $K_{fill} = 0.4$ the total slot cross-section area is:

$$S_{slot} = \frac{S_{Cuslot}}{K_{fill}} = \frac{81}{0.4} \simeq 205 \ [mm^2] \qquad\qquad (1.33)$$

To complete the slot sizing remains only to define the slot height. It could be evaluated as:

$$h_s = \frac{Q_s}{2 \cdot \pi} \cdot \left\{ \sqrt{\left[\omega_s^2 + \frac{4 \cdot \pi}{Q_s} \cdot S_{slot}\right]} - \omega_s \right\} = \frac{48}{2 \cdot \pi} \cdot \left\{ \sqrt{\left[6.06^2 + \frac{4 \cdot \pi}{48} \cdot 205\right]} - 6.06 \right\} \simeq 30 \ [mm]$$
$$(1.34)$$

As far as the back iron height is concerned, fixing $B_{bi} = 1.7 \ T$, it is calculated as:

$$h_{bi} = \frac{B_{g0}}{B_{bi}} \cdot \frac{\tau_p}{2} = \frac{B_{g0}}{B_{bi}} \cdot \frac{\pi \cdot D_{re}}{2p \cdot 2} = \frac{0.936}{1.7} \cdot \frac{\pi \cdot 190}{8 \cdot 2} \simeq 20 \ [mm] \qquad\qquad (1.35)$$

Finally it must be verified that the geometrical constraints related to the external diameter are satisfied. It is:

$$D_e = D_{re} + 2 \cdot h_s + 2 \cdot h_{bi} = 190 + 2 \cdot 30 + 2 \cdot 20 = 290 \ [mm] \tag{1.36}$$

and satisfies exactly the request which was done at the beginning of the sizing.
To complete the motor design the winding factor K_w must be correctly defined. It has been decided to design a distributed, chorded and double - layer winding. The chording pitch is equal to 1. The pitch factor and the distribution factor could be calculated. To do this it is foundamental to evaluate the angle between two consecutive slots as:

$$\alpha_s = \frac{360}{Q_s} = \frac{360}{48} = 7.5 \ [deg] \Rightarrow \alpha_s^e = p \cdot \alpha_s = 4 \cdot 7.5 = 30 \ [deg] \tag{1.37}$$

and the chording angle as:

$$\beta_r^e = \alpha_s^e = 30 \ [deg] \tag{1.38}$$

In conclusion:

- Distribution factor:

$$K_d = \frac{sin\left(q \cdot \frac{\alpha_s^e}{2}\right)}{q \cdot sin\left(\frac{\alpha_s^e}{2}\right)} = \frac{sin\left(4 \cdot \frac{30}{2}\right)}{4 \cdot sin\left(\frac{30}{2}\right)} = 0.966 \tag{1.39}$$

- Chording factor:

$$K_p = cos\left(\frac{\beta_r^e}{2}\right) = cos\left(\frac{30}{2}\right) = 0.966 \tag{1.40}$$

- Winding factor:

$$K_w = K_d \cdot K_p = 0.966 \cdot 0.966 = 0.933 \tag{1.41}$$

Through the star of slots method it is possible to define the winding slot matrix which will be used in the simulations. It is reported hereafter:

ka = [-1, -0.5, 0, 0, 0, +0.5, +1, +0.5, 0, 0, 0, -0.5, -1, -0.5, 0, 0, 0, +0.5, +1, +0.5, 0, 0, 0, -0.5, -1, -0.5, 0, 0, 0, +0.5, +1, +0.5, 0, 0, 0, -0.5, -1, -0.5, 0, 0, 0, +0.5, +1, +0.5, 0, 0, 0, -0.5];

kb = [0, 0, 0, -0.5, -1, -0.5, 0, 0, 0, +0.5, +1, +0.5, 0, 0, 0, -0.5, -1, -0.5, 0, 0, 0, +0.5, +1, +0.5, 0, 0, 0, -0.5, -1, -0.5, 0, 0, 0, +0.5, +1, +0.5, 0, 0, 0, -0.5, -1, -0.5, 0, 0, 0, +0.5, +1, +0.5];

kc = [0, +0.5, +1, +0.5, 0, 0, 0, -0.5, -1, -0.5, 0, 0, 0, +0.5, +1, +0.5, 0, 0, 0, -0.5, -1, -0.5, 0, 0, 0, +0.5, +1, +0.5, 0, 0, 0, -0.5, -1, -0.5, 0, 0, 0, +0.5, +1, +0.5, 0, 0, 0, -0.5, -1, -0.5, 0, 0];

To achieve, the motor geometry is reported in Fig. 1.1, and Table 1.2 shows the geometrical parameters:
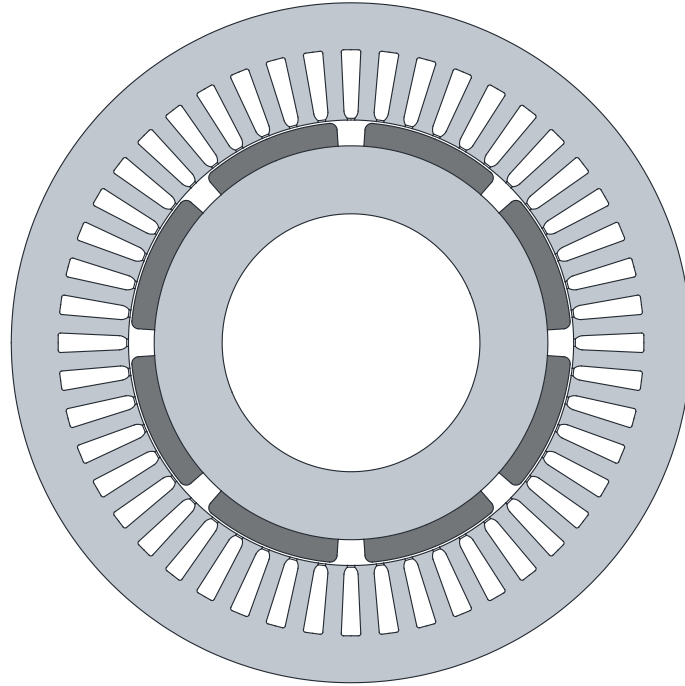
Figure 1.1: SPM cross-section area

Table 1.2: SPM geometrical data

Symbol	Value	Unit	Stator
D_e	290	$[mm]$	External diameter
D_i	190	$[mm]$	Stator inner diameter
Q_s	48	-	Slot number
w_t	7.9	$[mm]$	Tooth width
w_{so}	3.15	$[mm]$	Slot opening width
h_s	30	$[mm]$	Slot height
S_{slot}	205	$[mm^2]$	Slot cross-section area
			Rotor
D_r	168	$[mm]$	Rotor diameter
D_f	110	$[mm]$	Rotor inner diameter
t_m	10	$[mm]$	Magnet thickness
h_m	55	$[mm]$	Magnet width
			Common data
$2p$	8	-	Poles number
L_{stk}	145	$[mm]$	Stack length
g	1	$[mm]$	Air–gap thickness

1.2   Simulations

As said before, the main aim of the simulations is the analysis of the average torque and the torque ripple, while the efficiency and the power factor assume a secondary importance during the development of the study.

Two operating points have been taken into consideration, the first refers to the nominal conditions and the second one corresponds to the overload conditions. Each motor is initially aligned: the reference position $\theta_m = 0 \ deg$ corresponds to the position where the rotor PM axis is out of phase of $-90 \ deg$ with respect to the A-phase axis. After that, it is simulated to determine the optimal electrical angle of the current vector corresponding to the maximum torque. Then, it is simulated to compute the variation of the torque for different rotor positions, fixing both amplitude and angle of the current vector previously found.

The range of mechanical angle, d-q torque and Maxwell torque are defined as done by *Bianchi* in [2]. It results:

$$\theta_m = \frac{360}{m \cdot p} \tag{1.42}$$

where m represents the phase number, and p the number of pole pairs. Since there are geometrical symmetries, half of the range calculated can be considered: all simulations were carried out considering a rotation of 15 deg instead of 30 deg.

As far as the torque computation is concerned, two different approaches are used:

- **d-q torque** based on the following expression

$$T_{dq} = \frac{3}{2} \cdot p \cdot [\Lambda_d \cdot I_q - \Lambda_q \cdot I_d] \tag{1.43}$$

   using the d-q axis currents and flux-linkages obtained by the $T_{abc/dq}$ transformation.

- **Maxwell torque** which is based on the Maxwell stress tensor. The expression is:

$$T_{Mxw} = \frac{L_{Fe}}{g \cdot \mu_0} \cdot \int_S r \cdot B_r \cdot B_\theta \, dS \tag{1.44}$$

   where g is the air gap thickness, r is a generic radius while B_r and B_θ are respectively the radial and azimuthal components of the flux density at the air gap. S_g is the air-gap cross-section area in the 2D simulation.

These two values are always compared. Even if the average torque in both cases is the same it is not the same for the istantaneous values. The torque computed via the Maxwell stress tensor exhibits a larger variation respect the dq torque. For this reason, the ripple computation is based on Maxwell torque and its expression is given by:

$$T_{Ripple} = \frac{|T_{MxwMAX}| - |T_{MxwMIN}|}{T_{MxwAVG}} \cdot 100 \ [\%] \tag{1.45}$$

1.2.1   Materials

In the model analyzed different types of materials were used. In particular, the copper has been defined as linear and with an electrical conductivity equal to $\sigma = 37.5\ MS/m$. As far as the iron is concerned, it has been defined with an electrical conductivity equal to $\sigma = 3\ MS/m$ and a non linear BH curve. This BH curve is reported in Fig. 1.2:
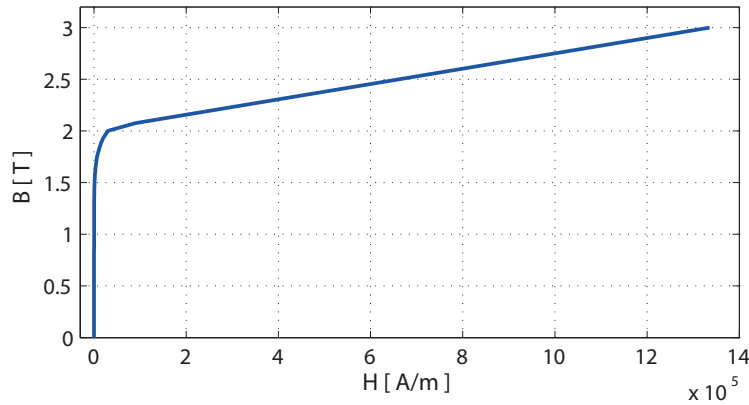
Figure 1.2: Terni BH curve

This lamination is characterized by a low specific losses, that is $P_{specFe} = 1.92\ W/K_g$ at a reference frequency of 50 Hz and at a reference flux density of 1 T.

The comparison in terms of residual induction and coercive magnetic field between the two types of PMs is shown in Fig. 1.3. It's clear how the Ferrite BH curve is smoother than the NdFeB one as aspected.

Figure 1.3: Comparison between N38H and Ferrite BH curves at 120 C

The first PM material is NdFeB, (it is used only in the SPM motor), classified as $N38H$. The main parameters are reported in Table 1.3:

Table 1.3: N38H parameters (120 C)

μ_r	H_c [A/m]	σ [MS/m]	B_{rem} [T]
1.061	-578125	0.555	1.1

Later on a Ferrite PM will be adopted in the model. Its BH curve is cosidered to be linear with the characteristics in Table 1.4:
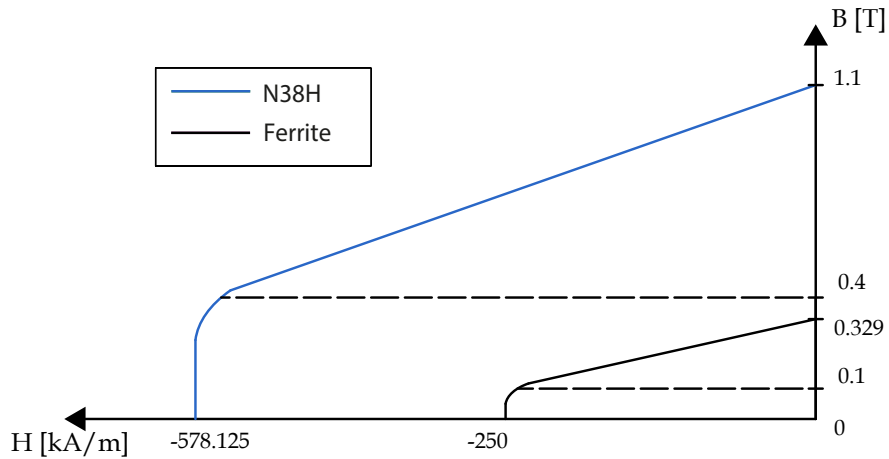
Table 1.4: Ferrite parameters (120 C)

μ_r	H_c [A/m]	σ [MS/m]	B_{rem} [T]
1.048	-250000	0.667	0.329

1.3 Comparison between two different types of SPM

After the design of the motor a comparison is carried out between SPM motor configuration with two different types of PMs. In particolar it is based on the same operating conditions (the same current density into the stator slots) and the same geometrical data. Only the PMs material is changed. For each of them the performance is analyzed at nominal and overload conditions. A distributed winding (DW) is used.

1.3.1 SPM with PM in NdFeB

Nominal conditions

According to $\alpha_{ie} = 90 \ deg$ and $I_{slot} = 695 \ A$ ($J_s = 6 \ A/mm^2$).
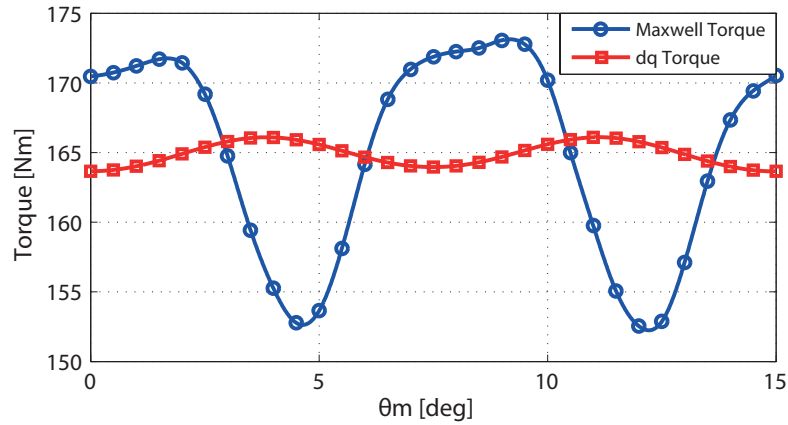Fig. 1.4 shows the torque of the motor versus the rotor angle position:

Figure 1.4: Torque value for different mechanical angles calculated through Maxwell stress tensor and d-q reference at nominal conditions. SPM motor using NdFeB PMs. In the $2p = 8$ pole machine 15 *deg* mechanical degrees correspond to 60 *deg* electrical degrees

The results obtained in terms of average torque and of torque ripple in the two cases are:

Average Maxwell Torque = 165 Nm
Average d-q torque = 164.9 Nm
Torque ripple = 12.44 %

Any considerations could be done about the harmonic content of Maxwell torque. In particular it's clear the presence of a 12th harmonic as main contribute to torque ripple. In fact, in Fig. 1.4 there are two periods in 60 electrical degrees. The effect of the harmonic of 6th, 24th and 36th order is quite irrilevant as shown in Fig. 1.5. It could be noticed in the different peak values of Maxwell torque and also in the difference of pitch in Maxwell torque behaviour from a semi-period to the next one.
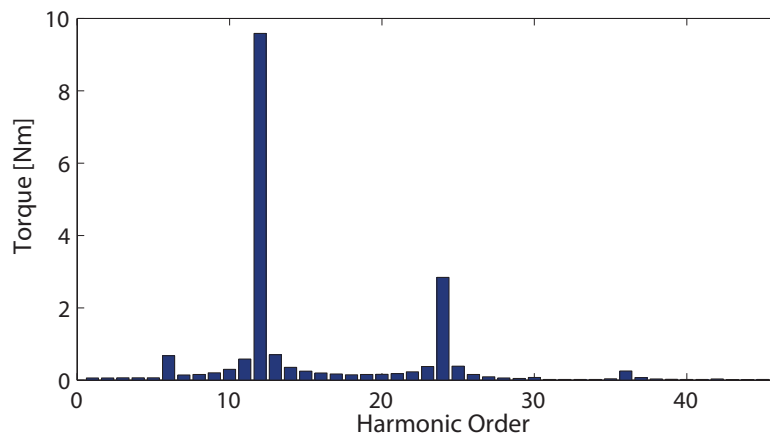

Figure 1.5: Torque ripple harmonic analysis of 8 poles SPM motor using NdFeB PMs at nominal conditions. The fundamental is not considered in this harmonic order

Overload conditions

The maximum torque is calculated according to a peak current into the slot equal to $I_{slot} = 1140\ A$ ($J_s = 9.8\ A/mm^2$)always with an angle $\alpha_{ie} = 90\ deg$.
The results obtained in terms of average torque and ripple in the two cases are:

Average Maxwell Torque = 270.6 Nm
Average d-q torque = 270.2 Nm
Torque ripple = 10.65 %

and they are shown in Fig. 1.6:
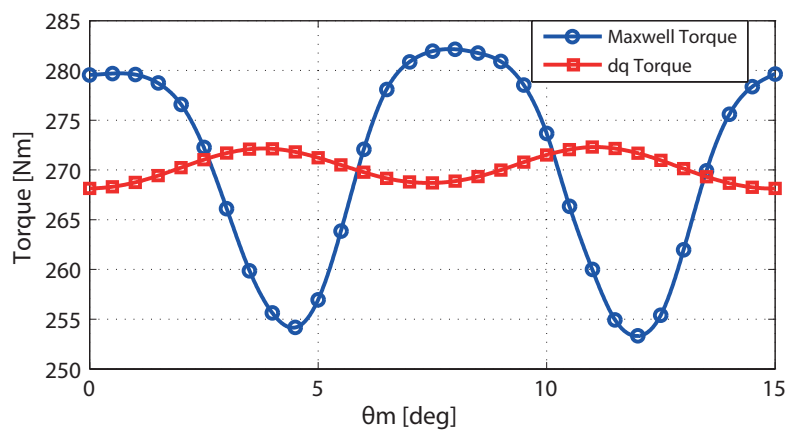
Figure 1.6: Torque value for different mechanical angles calculated through Maxwell stress tensor and d-q reference at overload conditions. SPM motor using NdFeB PMs. In the $2p = 8$ pole machine 15 deg mechanical degrees correspond to 60 deg electrical degrees

In Fig. 1.7 is reported the harmonic analysis related to Maxwell torque at overload conditions:
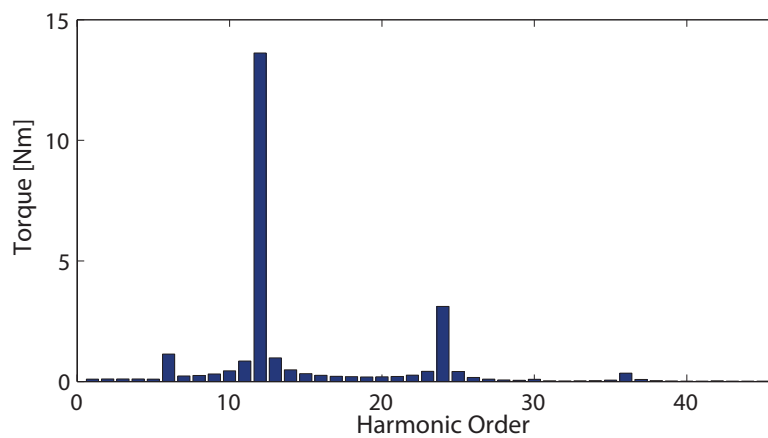
Figure 1.7: Torque ripple harmonic analysis of 8 poles SPM motor using NdFeB PMs at overload conditions. The fundamental is not considered in this harmonic order

Also in this case the reason of torque ripple is due to the presence of the harmonic of 6th, 12th, 24th, 36th order. The main one is again the 12th which has an higher amplitude than before. The other harmonics don't change their amplitudes. However, also if the 12th harmonic is increased, the torque ripple hasn't the same behaviour. In fact it decreases about the 2 % because the average torque increases much more than the 12th one.

1.3.2   SPM with PM in Ferrite

This configuration is the same that has been analyzed previously at the same load conditions. The only thing that has changed is the PMs material. In this case Ferrite is used. Fig. 1.8 and Fig. 1.10 show the torque behaviour versus θ_m at nominal and overload conditions respectively.

Nominal conditions


Figure 1.8: Torque behaviour versus mechanical angles calculated through Maxwell stress tensor and d-q reference. SPM motor using Ferrite PMs. In the $2p = 8$ pole machine 15 *deg* mechanical degrees correspond to 60 *deg* electrical degrees

The results obtained in terms of average torque and ripple are:

Average Maxwell Torque = 70.7 Nm
Average d-q torque = 70.6 Nm
Torque ripple = 9.48 %

The harmonic analysis has been done for Maxwell torque and it is reported in Fig. 1.9. Also in this case the main contribute to torque ripple is given by the 12th harmonic. At the same nominal conditions its amplitude is three times lower than the case with NdFeB PMs. Instead the average Maxwell torque is about 2.35 times lower than the previous case. This consideration explains why the torque ripple is better. The cause of torque ripple decreases in fact more than the average torque. The other harmonics remain the same and so don't have particular influence than before.

Figure 1.9: Torque ripple harmonic analysis of 8 poles SPM motor using Ferrite PMs at nominal conditions. The fundamental is not considered in this harmonic order
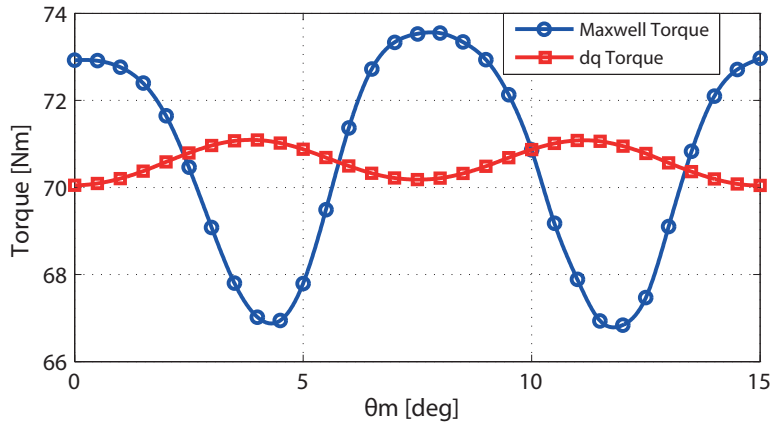
Overload conditions
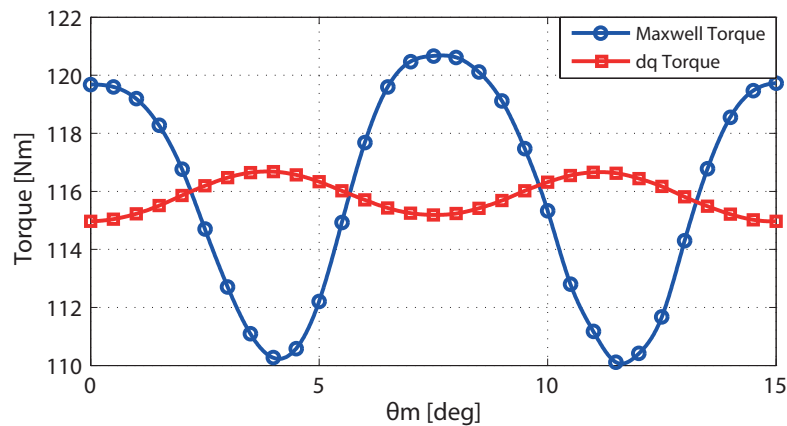
Figure 1.10: Torque behaviour versus mechanical angles calculated through Maxwell stress tensor and d-q reference. SPM motor using Ferrite PMs. In the $2p = 8$ pole machine 15 deg mechanical degrees correspond to 60 deg electrical degrees

The results under overlaod conditions are:

Average Maxwell Torque = 116 Nm
Average d-q torque = 115.8 Nm
Torque ripple = 9.10 %

The harmonic analysis has been done for Maxwell torque and it is reported in Fig. 1.11. Another time the main contribute to torque ripple is given by the 12$^{\text{th}}$ harmonic. At the same overload conditions its amplitude is 2.72 times lower than the case with NdFeB PMs. Instead the average Maxwell torque is about 2.33 times lower than the previous case. This consideration explains why the torque ripple is better. The cause of torque ripple decreases in fact more than the average torque. The other harmonics also decrease
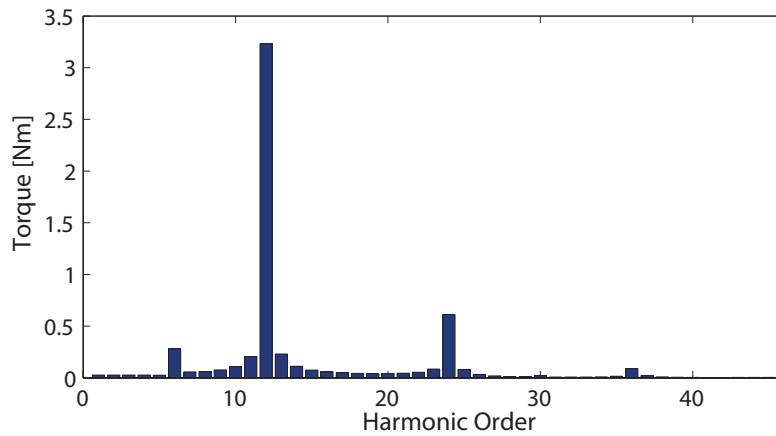
and support this torque performance improvement.

Figure 1.11: Torque ripple harmonic analysis of 8 poles SPM motor using Ferrite PMs at overload conditions. The fundamental is not considered in this harmonic order
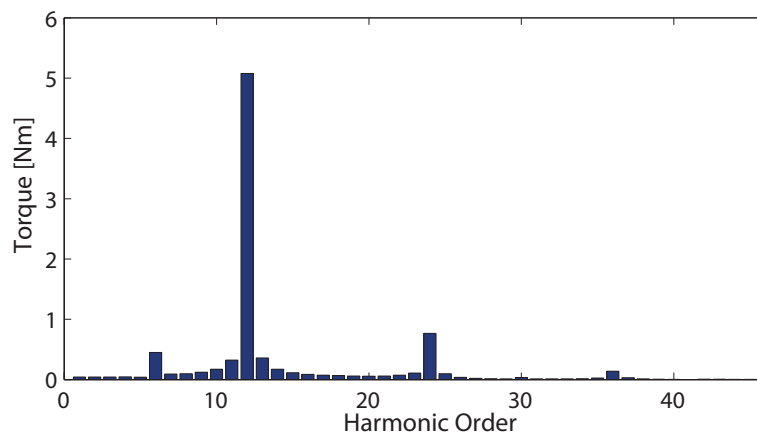
1.4 Considerations

From the results above, the motor using NdFeB PMs exhibits an average torque higher than the motor using Ferrite PMs one. This is verified for both nominal and overload conditions. These results are justified because of the ratio between the H_c of the two PMs. In particular:

- Nominal conditions:

$$\frac{T_{NdFeB}}{T_{Ferrite}} = \frac{165}{70.7} = 2.33 \tag{1.46}$$

- Overload conditions:

$$\frac{T_{NdFeB}}{T_{Ferrite}} = \frac{270.6}{116} = 2.33 \tag{1.47}$$

- H_c ratio:

$$\frac{H_{cNdFeB}}{H_{cFerrite}} = \frac{578.125}{250} = 2.31 \tag{1.48}$$

In fact these ratios obtained present the same values. As far as the average torque is concerned, it is expressed as:

$$T_{dq} = \frac{3}{2} \cdot p \cdot [\Lambda_{mg} \cdot I_q - (L_d - L_q) \cdot I_q \cdot I_d] \tag{1.49}$$

where in the SPM motors the second term is pratically equal to zero, being $Ld \simeq Lq$. Then, the torque difference is due to the difference in the PMs flux linkage.

About the ripple, both motors with NdFeB PM and Ferrite PM present a lower value in overload conditions than in nominal ones. In the first motor the torque ripple is slightly higher.

The last aspect to be considered is the demagnetization of PMs. From the field map of flux density, in overload conditions Ferrite PM results to be irreversibily degmatized because in some regions the flux density in the direction of magnetization is lower than $B_{knee} = 0.1 \ T$. This is the operating limit of the Ferrite PM at 120 C.

This comparison between two different types of PM underlines that in SPM motors is mandatory to use NdFeB PMs instead of Ferrite PMs. Even if rare-earth PMs prices are higher, their use allows to reach an higher average torque with the same geometrical terms and peak current into stator slots. Although from these simulations it is evident that SPM motor with Ferrite PMs must operate at a lower current level to avoid the PMs demagnetization, the analysis is useful to compare its performance with those of the PMARel motor configurations in the following chapters.

Chapter 2

PMARel motor with distributed winding

This chapter deals with of the analysis of a DW PMARel motor. A reference geometry is defined, according to the SPM motor geometry of the previous chapter. In particular, the focus is on the rotor geometry without modifying the stator. Similarly, the same nominal and overload conditions are considered. The initial geometrical data are reported in Table 2.1. The development will be concentrated on the rotor flux barriers and the PMs shape and position. The whole study will be based on rotor configuration with three barriers, which usually guarantees satisfactory performance in terms of both average torque and ripple.

Table 2.1: PMARel motor geometrical data

Symbol	Value	Unit	Stator
D_e	189	$[mm]$	Rotor diameter
D_f	110/130	$[mm]$	Rotor inner diameter
			Common data
$2p$	8	-	Poles number
L_{stk}	145	$[mm]$	Stack length
g	0.5	$[mm]$	Air–gap thickness

2.1 Rotor configurations

The aim is that to obtained the best compromise between both maximum average torque and minimum torque ripple. In this part different solutions are described.

2.1.1 Barrier angles obtained from a 16 poles PMARel motor

At first the study was focused in particular on both barriers shape and end angles, choosing a PMs configuration not optimazed. In this way it was possible to understand the effect of these geometrical parameters on the average torque and the torque ripple.

The first angles combination adopted has been obtained from a 16 poles PMARel motor optimized for what concerns the torque ripple. The original rotor geometrical data related to the PMs and the barrier angles have been doubled. This is because in this case the poles number is half. In this way it was possible to understand if a law scale could be apply to the problem. So the parameters used are reported in Table 2.2:

Table 2.2: First solution for the barrier angles

16 poles angles			Barriers angles adopted		
Symbol	Value	Unit	Symbol	Value	Unit
θ_{b1}	2.75	$[deg]$	θ_{b1}	5.50	$[deg]$
θ_{b2}	4.60	$[deg]$	θ_{b2}	9.20	$[deg]$
θ_{b3}	9.05	$[deg]$	θ_{b3}	18.1	$[deg]$

The PMs shape adopted is reported in Table 2.3:

Table 2.3: PMs parameters

	Radius [mm]	Height [mm]	Width [mm]	Ribs [mm]
PM 1	91.50	3.5	11.0	0.4
PM 2	83.20	5.0	21.5	0.5
PM 3	72.63	7.0	38.0	0.7

where PM 1 is the PM close to the air-gap, PM 2 is the intermediate one and PM 3 is the PM close to the the inner rotor diameter. In this first case the value of the inner rotor diameter has been fixed equal to 130 mm.

At the beginning the attention has been focused only on nominal conditions to have an idea of torque ripple.The current angle considered has been the one related to MTPA condition and in this case it was equal to $\alpha_{ie} = 55 \ deg$. The results obtained are shown in Fig. 2.1 and from this behaviour it is possible to find out that:

Average Maxwell Torque = 142.8 Nm
Average d-q torque = 138.7 Nm
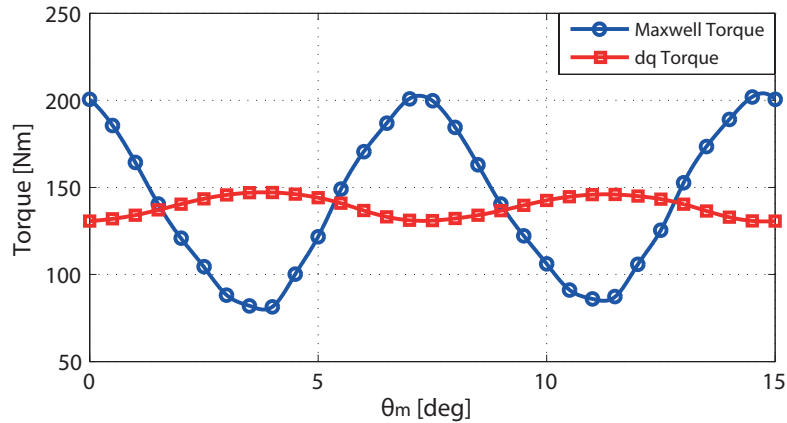Torque ripple = 84.42 %

Figure 2.1: Torque value for different mechanical angles calculated through Maxwell stress tensor and d-q reference at nominal conditions. 48/8 PMARel motor with the geometrical data obtained from a 16 poles PMARel motor

From the results obtained it's clear that this is not a good solution both for average torque and torque ripple. It's easy to see that a law scale isn't possible. So other solutions must be investigated. It has been done also the harmonic analysis of the torque behaviour and it's shown in Fig. 2.2:
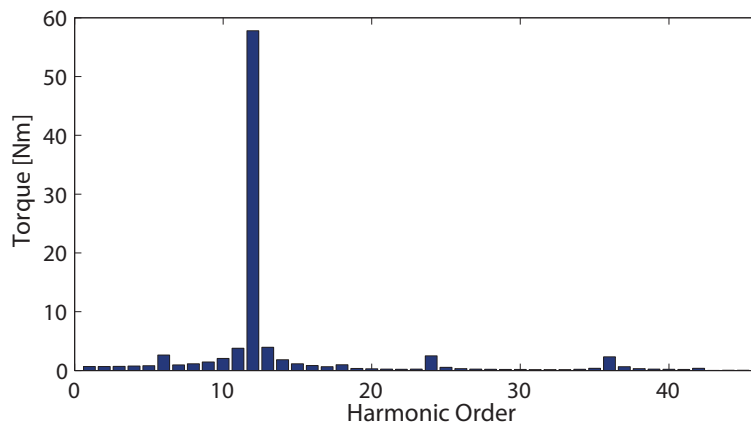
Figure 2.2: Torque ripple harmonic analysis of 48/8 PMARel motor with barrier angles obtained from 16 poles motor. The fundamental is not considered in this order

It's clear how the torque ripple is mainly due to the 12th harmonic. In Fig. 2.2 there are two periods in 60 electrical degrees. The effect of the harmonic of 6th, 24th and 36th order is quite irrilevant and could be noticed in the different peak values of Maxwell torque.

2.1.2 Different configuration of barrier angles

The new configuration has been achieved modifying the previous case. In the second solution the barrier angles and both PMs shape and position into the rotor have been changed. All this has been done to have a lower magnetic saturation in the rotor. According to this, the barrier angles has been increased. The distances between the extremities of the

barriers have been made more uniform. The new angles which have been adopted are reported in Table 2.4:

Table 2.4: Second solution for the barrier angles

Angles values		
Symbol	**Value**	**Unit**
θ_{b1}	7.00	[deg]
θ_{b2}	14.3	[deg]
θ_{b3}	21.5	[deg]

The changes adopted for the PMs have been done to have a better iron saturation between the barriers compared with the first solution. This without changing too much the M.M.F related to the rotor PMs which interacts with the one generated by the stator currents. This interaction has influence on torque ripple and it's important to analyze the influence of the barrier angles on it. After those considerations the new PMs configuration used is reported in Table 2.5:

Table 2.5: PMs parameters

	Radius [mm]	**Height [mm]**	**Width [mm]**	**Ribs [mm]**
PM 1	91.85	2.5	16.0	0.4
PM 2	84.00	3.5	27.0	0.5
PM 3	72.83	6.5	38.0	0.7

The inner diameter has been fixed again equal to $D_f = 130\ mm$ and the simulation has been done only at nominal conditions. The current angle considered has been the one related to MTPA conditions and in this case it was equal to $\alpha_{ie} = 58\ deg$. The results are shown in Fig. 2.3 and from this behaviour it is possible to find out that:

Average Maxwell Torque = 159.1 Nm
Average d-q torque = 159.5 Nm
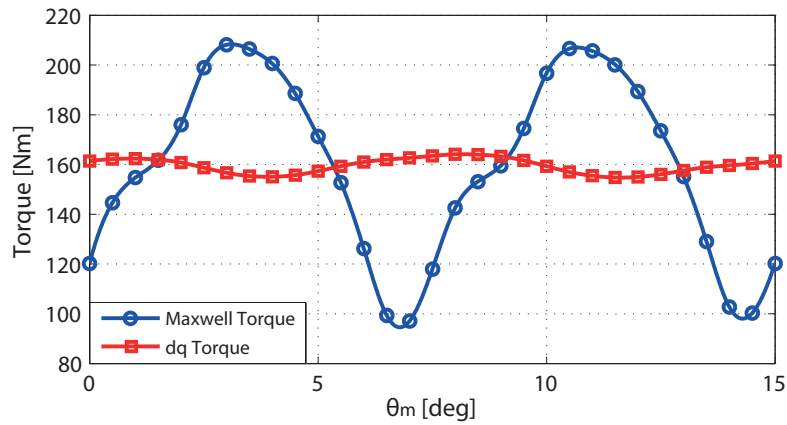Torque ripple = 69.80 %

Figure 2.3: Torque value for different mechanical angles calculated through Maxwell stress tensor and d-q reference at nominal conditions. 48/8 PMARel motor from the second design

The new parameters used gave us better results both in terms of average torque and torque ripple. This isn't enough considering that the torque ripple is too much high. In Fig. 2.4 the harmonic order is shown:
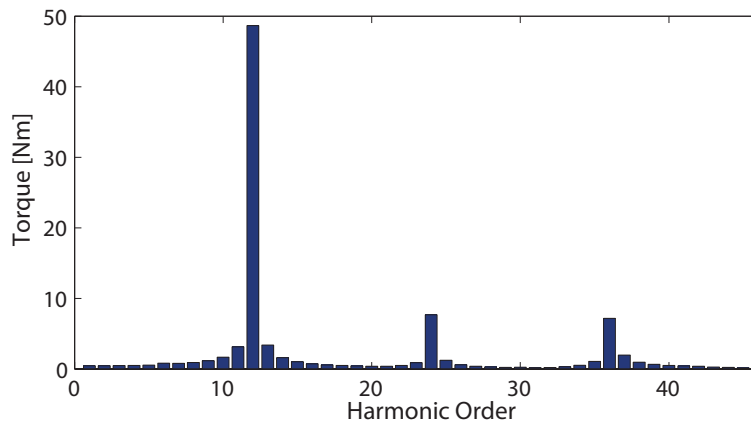
Figure 2.4: Torque ripple harmonic analysis of 48/8 PMARel motor from the second design

In comparison with the previous case, it must be underlined how the amplitudes of the harmonic of 12th order is decreased, while the 24th and 36th harmonics effect has more influence. This is evident if the attention is focused around 1.5 *deg* and 9 *deg* mechanical degrees, where in Maxwell torque two steps appear. This effect is combined with the one described in Sect.2.1.1. All this justify the improvement obtained in torque ripple.

2.1.3   Barrier angles analytically obtained

The third solution analyzed is inspired by *Vagati* theory [3]. It's known that an actual stator with n_s slots per pole-pairs adds several leakage contributions and also introduces belt and slot harmonics. Those last ones generate torque ripple by interaction with the rotor reaction. Now, considering only the slot spatial harmonics they are of $(h \cdot n_s \pm 1)$ order, where h is any positive integer. So the aim is that to design a rotor geometry which is devoted to introduce rotor spatial harmonics which are as much as possible different from the stator ones. In fact in this way there's not interaction between them. Besides, considering that the rotor magnetic potential is a staircase distribution (whose steps correspond to the rotor ribs) these ribs should be uniformly distributed. So we can define a number n_r of equivalent rotor slots per pole-pairs and in this way rotor harmonics of $(k \cdot n_r \pm 1)$ order are introduced,where also k is any positive integer.
So the best strategy is to chose n_r as much as possible near to n_s, but excluding n_s and $n_s \pm 2$, which would lead to direct interaction of stator and rotor harmonics. It's suggested as solution the following expression:

$$n_r = n_s \pm 4$$

In particular $n_r = n_s + 4$ generally leads to a lower ripple, even if $n_r = n_s - 4$ may be preferred for simplicity especially when n_s is large. In our case, we want to create a rotor with three barriers. We couldn't chose the last one possibilty because in this way we could draw only two of them. In the end, after this considerations, knowing that $n_s = 12$ the expression permits us to say that:

$$n_r = 12 + 4 = 16$$

In this case we obtain an incomplete structure because the first couple of rotor slots near to Q-axis must be ignored. It's all represented in Fig. 2.5:
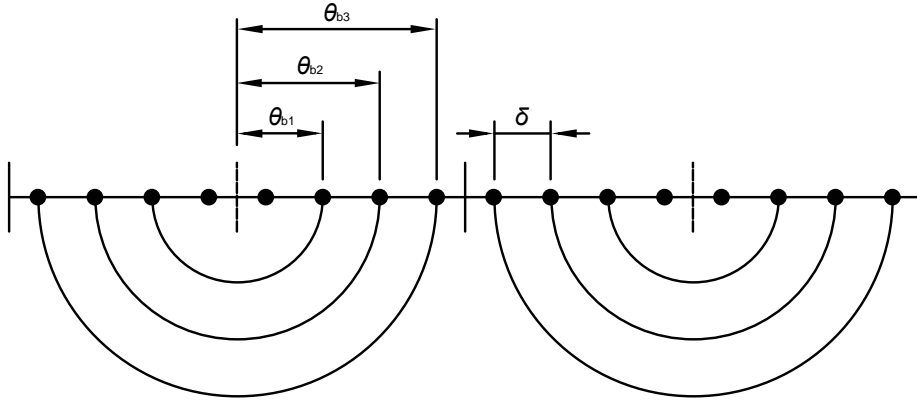

Figure 2.5: Representation of analytical angles when $n_r = 16$.

The new angles adopted, expressed in mechanical degrees, are calculated in this way:

$$\delta = \frac{360}{n_r \cdot 2p} = \frac{360}{16 \cdot 4} = 5.6 \ deg$$

$$\theta_{b1} = 1.5 \cdot \delta = 8.4 \ deg$$

$$\theta_{b2} = 2.5 \cdot \delta = 14.0 \ deg$$

$$\theta_{b3} = 3.5 \cdot \delta = 19.7 \ deg$$

It's also important to specify why haven't been chosen other rotor configurations. They could be obtained from the number of stator slots per pole-pairs. When the solution considered is:

$$n_r = n_s \pm 6$$

also in this case the only possibility to obtain a three barriers configuration is when $n_r = n_s + 6$. The result is equal to $n_r = 18$. As far as electrical degrees are concerned, this means that $\delta = 20 \ deg$. Remembering that $n_s = 12$, the stator slot pitch in electrical degrees is equal to 30 deg. So it's clear how this angles combination between stator and rotor it's not optimal. In fact, it produces a strong harmonic interaction with the effect to increase the torque ripple. In conclusion this configuration has not to be taken into consideration and it is reported in Fig. 2.6.
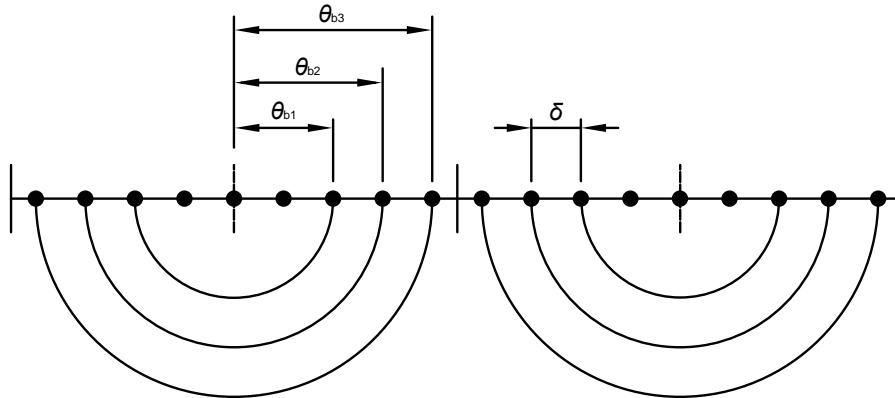
Figure 2.6: Representation of analytical angles when $n_r = 18$

At last, if n_r is gradually increased, it's evident how the rotor configuration references to the four barriers per pole. This could be seen when:

$$n_r = n_s + 10$$

When $n_r = 22$, in addition to the imaginary rotor slots placed on the Q axis, two couples of slots are ignored. This because one of them should be used to create the fourth barrier as it is shown in Fig. 2.7.
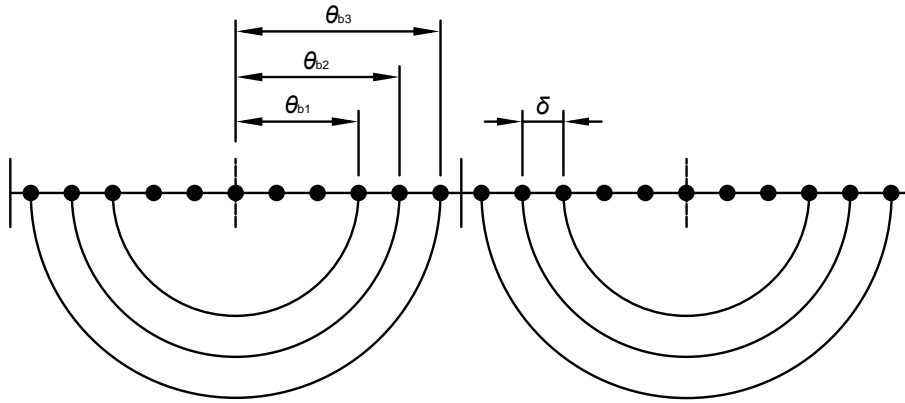
Figure 2.7: Representation of analytical angles when $n_r = 22$

It's possible to understand how the best analytic solution is the first one discussed at the beginning of this section.

Also for what concerns the geometry of PMs some changes has been done. The heights have been increased because PMs had tendency to degmatize themselves. To make this possible there were the necessity to decrease the inner rotor diameter from 130 mm to 110 mm. Also their position into the rotor has been changed as it's possible to see from the different radii. The PMs parameters are reported in Table 2.6:

Table 2.6: PMs parameters

	Radius [mm]	Height [mm]	Width [mm]	Ribs [mm]
PM 1	89.30	4.0	16.0	0.4
PM 2	78.93	6.0	27.0	0.5
PM 3	65.00	8.0	38.0	0.7

The current angle considered has been the one related to MTPA conditions and in this case it has been equal to $\alpha_{ie} = 58 \ deg$. After that, considering that the simulation has been done only at nominal conditions, the results are shown in Fig. 2.8 and from this behaviour it is possible to find out that:

Average Maxwell Torque = 167.3 Nm
Average d-q torque = 167.2 Nm
Torque ripple = 35.44 %

Figure 2.8: Torque value for different mechanical angles calculated through Maxwell stress tensor and d-q reference at nominal conditions. 48/8 PMARel motor analytically designed

The torque ripple is quite half then before and the average torque with the new PMs configuration is slightly increased. As aspected, the results have been improved. In Fig. 2.9 it is clear how the effect of 12th harmonic is halved and this is mirrored in torque ripple. The presence of the 24th and 36th harmonic is always visible from the torque behaviour where there are two steps at 3 and 10.5 mechanical degrees, while the peak values are again different one from each other.
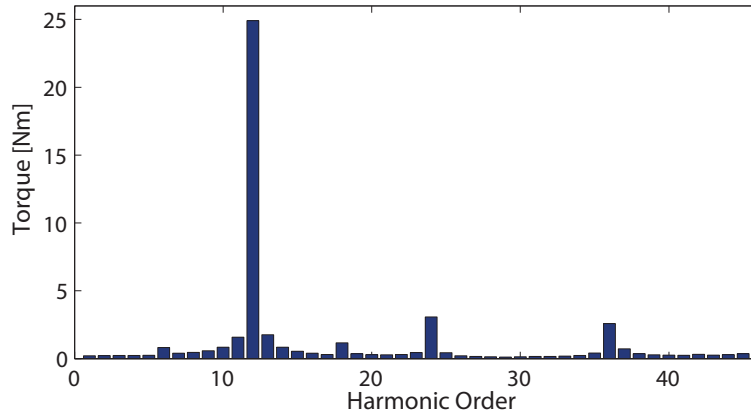
Figure 2.9: Torque ripple harmonic analysis of 48/8 PMARel motor analytically designed

2.1.4 Improvement of barrier angles analytically obtained

Focusing the attention on the interbarrier pitch a new analytical design approach created by *Vagati* [4] could be considered to improve the torque performance. In particular it has been advised a different interbarrier pitch depending on n_r values. If it's verified the following equation:

$$n_r = 4 \cdot n + 2$$

where n is the number of rotor flux barriers per pole, it is advised to use a constant and equal rotor slot pitch along the whole periphery of the rotor. While if it's satisfied the following constraint:

$$n_r > 4 \cdot n + 2$$

it's more advisable to use a larger value of the angle between the smallest layer and the Q-axis, keeping constant and equal the other pitches. So given that we are in the second case because $16 > 14$. To further improve the motor, it has been decided to produce some variations on the geometries both of the barrier angles and the PMs shape and position. In particular the same θ_{b1} has been used and the others two angles calculated as in Sect.2.1.3 have been adopted. So the new values are reported in Table 2.7:

Table 2.7: Barrier angles analytically improved

Angles values		
Symbol	Value	Unit
θ_{b1}	9.80	$[deg]$
θ_{b2}	14.1	$[deg]$
θ_{b3}	19.7	$[deg]$

Instead the PMs have been designed with a lower thickness without changing their position into the rotor. This with the aim to increase the section of the iron between the barriers because previously it was too much saturated.

Their new geometrical data are reported in Table 2.8:

Table 2.8: PMs parameters

	Radius [mm]	Height [mm]	Width [mm]	Ribs [mm]
PM 1	89.67	3.0	14.4	0.4
PM 2	81.83	4.0	28.0	0.4
PM 3	68.96	7.0	37.8	0.4

Also their lenghts have been changed. The current angle which has been simulated was the one related to MTPA conditions and in this case it has been equal to $\alpha_{ie} = 56 \ deg$. The new results obtained are shown in Fig. 2.10 and from this behaviour it is possible to find out that:

Average Maxwell Torque = 173.5 Nm
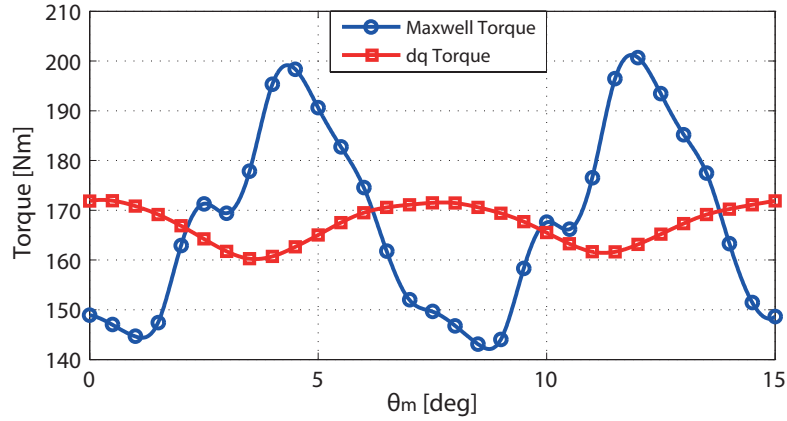Average d-q torque = 171.4 Nm
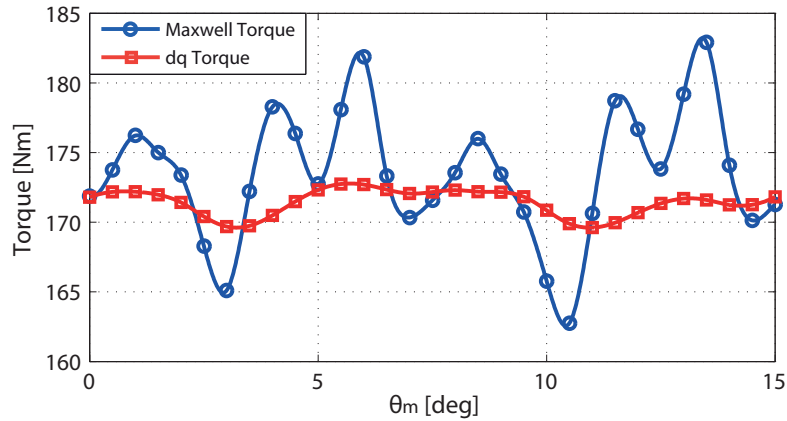Torque ripple = 11.62 %

Figure 2.10: Torque value for different mechanical angles calculated through Maxwell stress tensor and d-q reference at nominal conditions. 48/8 PMARel motor improving the one analytically designed

With this solution both the average torque and torque ripple have been improved. The analysis has been focused only on nominal conditions without considering the overload ones. The PMs thickness must be increased because of their tendency to degmatize. The reason of this remarkable improvement in torque ripple and average torque also must be investigated through the harmonic analysis which is reported in Fig. 2.11:
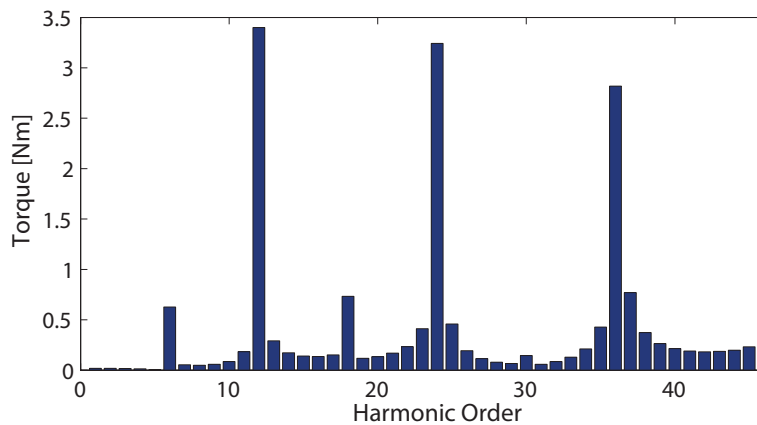
Figure 2.11: Torque ripple harmonic analysis of 48/8 PMARel motor improving the barrier angles analytically improved

In this case the effect of 12th harmonic is comparable to the ones of the harmonic of 24th and 36th order. The harmonic contribution with higher order is clearly increased. In fact, also if it is left the presence of two main periods, the Maxwell torque behaviour is much more variable with tendency to increase the number of periods in the same mechanical gap. It must be observed how the reduction of all harmonics amplitude is related to a torque ripple reduction.

2.1.5   Optimization

The last attempt which has been done to try to go under the 10% of torque ripple has been the optimization.

Differential Evolution (DE) is the method employed to optimize the solution about practical problems which have objective functions that are non- differentiable, non-continuous, non-linear, noisy, flat, multi-dimensional or have many local minima and constraints. This is possible through many iteractions to try to find approximate solutions to them. This kind of method is commonly known as metaheuristic as it makes few or no assumptions about the problem being optimized and can search very large spaces of candidate solutions. However, metaheuristics such as DE do not guarantee an optimal solution is ever found. This alghoritm is based on the theory shortly explained by *Fusar* [5]. The considerations adopted to obtain the problem solution are shown below. At the beginning a fourteen parameters vector has been defined. Each one is related to the rotor pole geometry and is different from a motor to another. Besides, at the beginning of the optimization for each parameter a range of variations has been defined. As far as the extremities of each interval are concerned, they have been fixed on the basis of the kind of parameter, the knowledge obtained during the previous steps seen in this chapter and on the theoretical considerations. The set of these fourteen parameters is the following:

- k_{air} $\Rightarrow$ it is the ratio between the air thickness into the rotor along the Q-axis (supposing that the PMs are not inset into the flux barriers and so that the motor could be considered a pure reluctance one) and the total thickness of the circular sector of the rotor. This parameter ranges between 0 and 1. In the optimization it has been ranged between 0.3 and 0.7. In this way the iron between the flux barriers saturates very well, without reaching too much high or too much low values of saturation;

- θ_{b1} $\Rightarrow$ it is the angle related to the flux barrier close to the air-gap. It is referred to the angular opening between the Q-axis (through the center of the rotor pole) and the flux barrier end. The extremities of the interval have been decided considering the previous results obtained during the development of the rotor. So it has been fixed between 7 *deg* and 10 *deg* mechanical degrees;

- θ_{b2} $\Rightarrow$ it is the angle related to the intermediate flux barrier. It is referred to the angular opening between the Q-axis and the flux barrier end. The extremities of the interval have been decided considering the previous results. So it has been fixed between 12.5 *deg* and 15.5 *deg* mechanical degrees;

- θ_{b3} $\Rightarrow$ it is the angle related to the flux barrier most distant from the air-gap. It is referred to the angular opening between the Q-axis and the flux barrier end. The extremities of the interval have been again decided considering the previous results. So it has been fixed between 17.5 *deg* and 20.5 *deg* mechanical degrees;

- R_{PM1} $\Rightarrow$ it is related to the centering radius into the rotor of the PM which is part of the first flux barriers. The extremities of the interval have been fixed between 86 *mm* and 91 *mm*;

- w_1 $\Rightarrow$ it is related to the width of the PM which is part of the first rotor flux barrier. The extremities of the interval have been fixed between 14 *mm* and 20 *mm*;

- $h_1 \Rightarrow$ it is related to the height of the PM which is part of the first rotor flux barrier. The extremities of the interval have been fixed between 3.5 mm and 5 mm;

- $R_{PM2} \Rightarrow$ it is related to the centring radius into the rotor of the PM which is part of the intermediate flux barriers. The extremities of the interval have been fixed between 77 mm and 82 mm ;

- $w_2 \Rightarrow$ it is related to the width of the PM which is part of the second rotor flux barrier. The extremities of the interval have been fixed between 25 mm and 33 mm;

- $h_2 \Rightarrow$ it is related to the height of the PM which is part of the second rotor flux barrier. The extremities of the interval have been fixed between 5.5 mm and 7 mm;

- $R_{PM3} \Rightarrow$ it is related to the centring radius into the rotor of the PM which is part of the flux barriers most distant from the air-gap. The extremities of the interval have been fixed between 60 mm and 67 mm;

- $w_3 \Rightarrow$ it is related to the width of the PM which is part of the third rotor flux barrier. The extremities of the interval have been fixed between 35 mm and 45 mm;

- $h_3 \Rightarrow$ it is related to the height of the PM which is part of the third rotor flux barrier. The extremities of the interval have been fixed between 7.5 mm and 12 mm;

- $rib \Rightarrow$ it is related to the ribs thickness situated between the end of the flux bariers and the external diameter of the rotor. Their value has been defined to obtain their complete saturation so that they could be considered equal to the air as far as concerned the magnetic properties. This parameter must be included between 0.4 mm and 0.8 mm;

After the geometrical constraints have been defined, for each one of the parameters it must be fixed also the number of generations and the number of motors which composed each one of them. The total number of motors being equal, it has been better to split in a very high number of generations. In this way the alghoritm as tendency to converge most quickly than the case when there are a few generations. 300 different motors have been splitted in 30 generations each one of 10 motors. The mutation and cross-over ratios have been fixed equal respectively to 0.7 and 0.9. The results obtained are reported in Fig. 2.12:
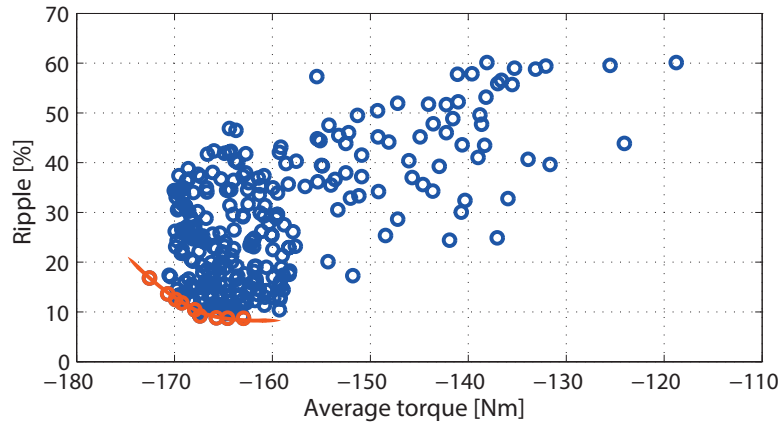
Figure 2.12: Pareto front.

From these results it has been possible to obtain the Pareto front (highlighted in red). All the motors belonging to it have the same validity from a theoretical point of view. The final decision related to the choise of the motor must be done by the motor designer who must evaluate the best in terms both of torque ripple and average torque. In the specific case developed in this chapter the one which had the best combination had the values reported in Table 2.9 for what concerns the barrier angles, while in Table 2.10 are reported the PMs geometry.

Table 2.9: Optimization solution for different barrier angles

Angles values second optimization		
Symbol	Value	Unit
θ_{b1}	8.3	$[deg]$
θ_{b2}	13.7	$[deg]$
θ_{b3}	19.5	$[deg]$

Table 2.10: PMs parameters from optimization

	Radius [mm]	Height [mm]	Width [mm]	Ribs [mm]
PM 1	90.35	4.7	16.5	0.5
PM 2	82.23	5.5	25.8	0.5
PM 3	69.30	9.0	37.6	0.5

The current angle considered was the one related to MTPA conditions and in this case it has been equal to $\alpha_{ie} = 58 \ deg$. The results are represented in Fig. 2.13:
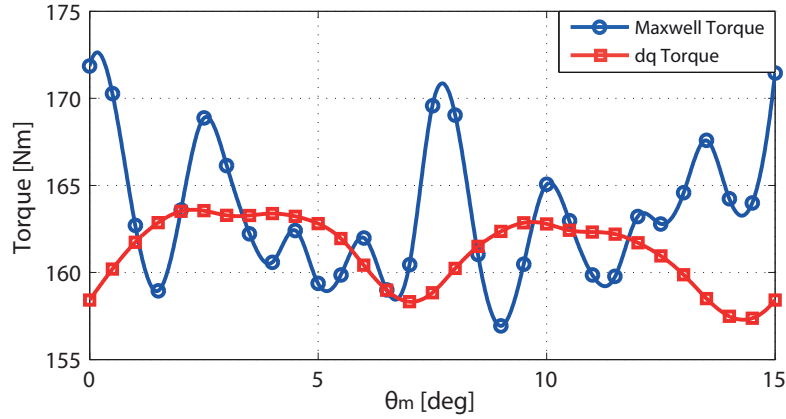
Figure 2.13: Torque value for different mechanical angles calculated through Maxwell stress tensor and d-q reference at nominal conditions. It is referred to the 48/8 PMARel motor obtained from DE optimization.

and from this behavior it is possible to find out that:

Average Maxwell Torque = 163.6 Nm
Average d-q torque = 161.2 Nm
Torque ripple = 9.12 %

Through this last attempt has been obtained an interesting torque ripple also if part of the average torque has been sacrified. Due to the iron saturation between the barriers, the radius and the shape of each PM have been modified. After to have tried different solutions, the best one has been used on the barrier angles discussed in Sect.2.1.4 and the data related to PMs are reported in Table 2.11. All that was done without greatly modifying the optimization result.

Table 2.11: PMs parameters modified with respect to the optimization

	Radius [mm]	Height [mm]	Width [mm]	Ribs [mm]
PM 1	90.48	4.5	16.5	0.5
PM 2	81.00	5.5	26.0	0.5
PM 3	68.10	9.0	37.8	0.5

The current angle considered has been related to the MTPA condition: in this case it $\alpha_{ie} = 58\ deg$. In this way the result becomes as shown in Fig. 2.14 and from this behaviour it is possible to find out that:

Average Maxwell Torque = 170.3 Nm
Average d-q torque = 168.2 Nm
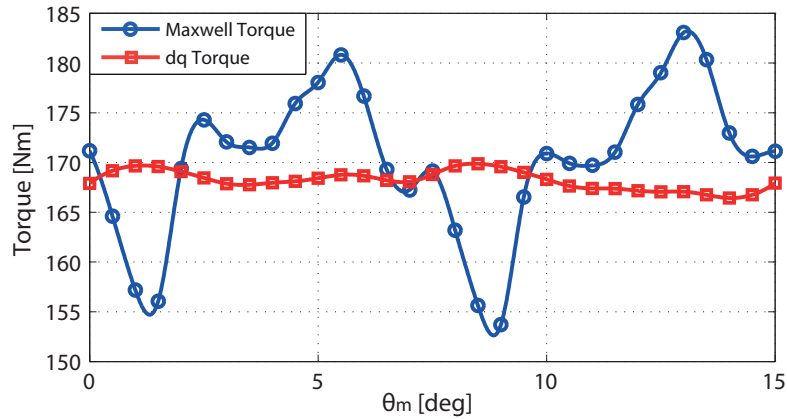Torque ripple = 17.24 %

Figure 2.14: Torque value for different mechanical angles calculated through Maxwell stress tensor and d-q reference at nominal conditions. It is referred to the 48/8 PMARel motor obtained from DE optimization slightly modified

The torque ripple has been increased becoming worse than in 2.1.4. Instead the average torque has been improved. The harmonic content is shown in Fig. 2.15:
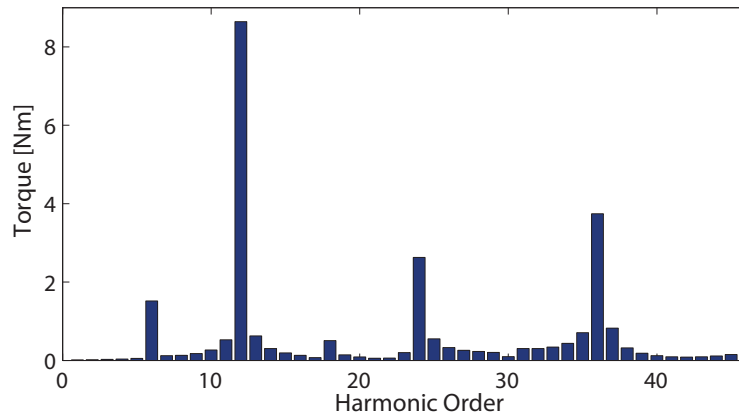
Figure 2.15: Torque ripple harmonic analysis of 48/8 PMARel motor with barrier angles obtained from the optimization slightly improved

It is possible to understand that this torque ripple worsening is due to the increase of amplitude of the 12th harmonic. At the end of all these different cases put under analysis we can reasumed them in Table 2.12. It's possible to see that the best rotor configuration has been described in Sect.2.1.4 .

Table 2.12: Comparison of the results obtained from different rotor configurations of a 48/8 PMARel motor

	Average Maxwell Torque [N·m]	Average d-q Torque [N·m]	Ripple [%]
1st **design Sect.2.1.1**	142.8	138.7	84.42
2nd **design Sect.2.1.2**	159.1	159.5	69.80
Analytical Sect.2.1.3	167.3	167.2	35.44
Improvement Sect.2.1.4	173.5	171.4	11.62
Optimization Sect.2.1.5	170.3	168.2	17.24

2.2 Analysis of the best rotor configuration at overload conditions

In this paragraph the attention has been focused on the performance of the best rotor configuration at overload conditions. It corresponds to $I_{slot} = 1140\ A$ into the slot and to a speed equal to $n = 123\ rpm$. It has been considered the worst situation i.e. when the current vector presents an angle equal to $\alpha_{ie} = 90\ deg$. In this case the flux due to the stator currents is completely opposed to the flux related to the PMs. The motor analyzed in Sect. 2.1.4 when it has been done working in these conditions has PMs tendency to degmatize, in particular the intermediate one. This is because they are too much thin and stressed, when they're exposed to the linkage flux due to the current stator slots. This PMs behaviour could also be noticed at overload conditions as shown in Fig. 2.16 where in particular an angle of the second PM has been degmatized.
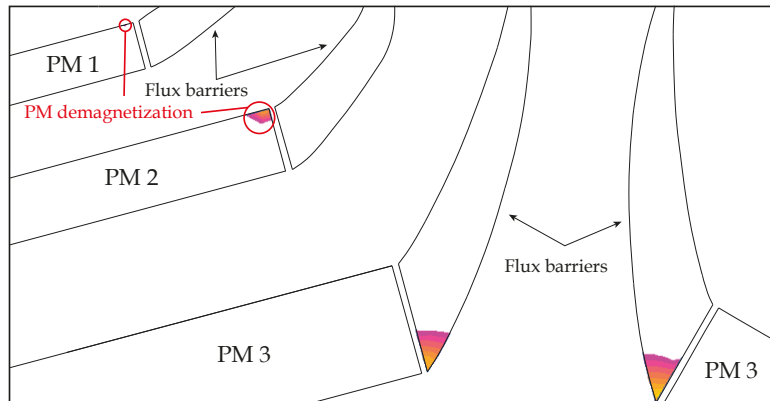
Figure 2.16: View of PM degmagnetization at overload conditions with the geometry described in 2.1.4.

To solve this problem there are two possibilities. The first one is based on a different PMs geometry, where all the sharp edges have been changed introducing a curvature for each one of them. This choice brings the flux lines to be smoother than before without concentrated themselves against PMs angles. As a consequence, PMs degmagnetization

is avoided. The second way is based on the increase of the thickness of each PM. This in fact guarantees an higher PMs flux which opposes to that due to the stator slots current avoiding PMs degmagnetization. This last solution has been preferred to the first one because in this way PMs don't degmatize even in the worst situation that is when $\alpha_{ie} = 90 \, deg$ as explained before. In fact the curvatures could solve the problem only at overload conditions analyzed, but not when all the linkage flux due to the stator slots current is opposed. So PMs heights and radii have been modified as shown in Table 2.13

Table 2.13: PMs parameters

	Radius [mm]	Height [mm]	Width [mm]	Ribs [mm]
PM 1	89.48	4.0	14.4	0.4
PM 2	79.83	7.0	28.0	0.4
PM 3	65.93	9.0	37.8	0.4

The barrier angles haven't been changed. Because of this improvement we must again analyse the motor also at nominal conditions.

At the beginning it has been done a simulation to obtain a torque ripple band which goes from $0 \, deg$ to $90 \, deg$ related to the current vector. From the results it has been possible to observe how the torque ripple has been remained almost the same (in absolute value) whether or not the electrical angle. Instead in per cent it has been tendency to decrease from $0 \, deg$ to $63 \, deg$ because of the aveage torque increasing. Then it starts to increase again due to the average torque drop as shown in Fig. 2.17.
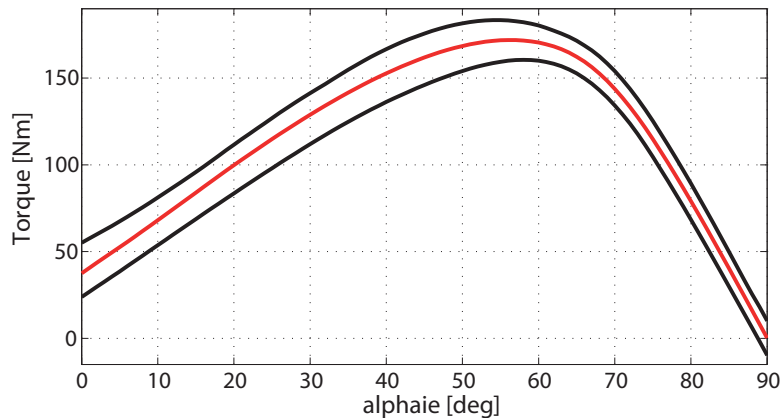

Figure 2.17: Torque value for different current vector angles at nominal conditions

In particular the red line is related to the average Maxwell torque while the two black lines are respectively related to the maximum and minimum values of Maxwell torque. In this way has been defined the ripple band. Later other two simulations have been done, the first at nominal conditions while the second one at overload conditions. Both of them fixing the current angle for different rotor mechanical positions. The current angle has been related to MTPA condition. In the first case it has been found being equal to $\alpha_{ie} = 57 \, deg$, while in the second one to $\alpha_{ie} = 62 \, deg$. The performance in both situations

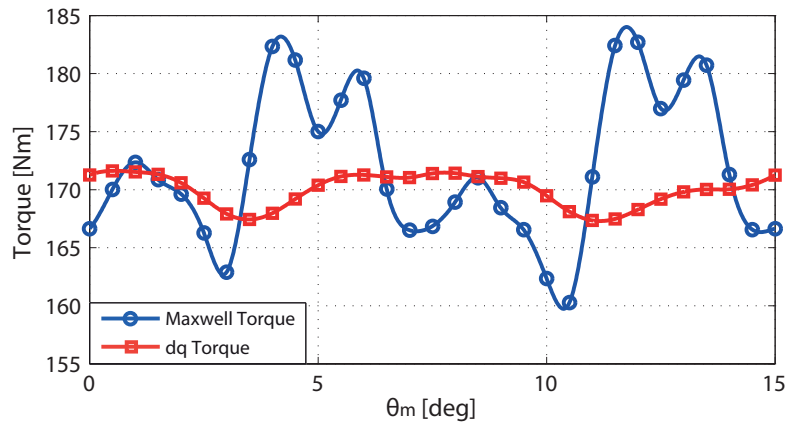are reported in Fig. 2.18 and in Fig. 2.19 respectively:

Figure 2.18: Torque values for different mechanical angles calculated through Maxwell stress tensor and d-q reference at nominal conditions. 48/8 PMARel motor

and from this behaviour it is possible to find out that:

Average Maxwell Torque = 171.8 Nm
Average d-q torque = 170.0 Nm
Torque ripple = 13.05 %

Figure 2.19: Torque value for different mechanical angles calculated through Maxwell stress tensor and d-q reference at overload conditions. 48/8 PMARel motor

while from this behaviour it is possible to find out that:

Average Maxwell Torque = 300.4 Nm
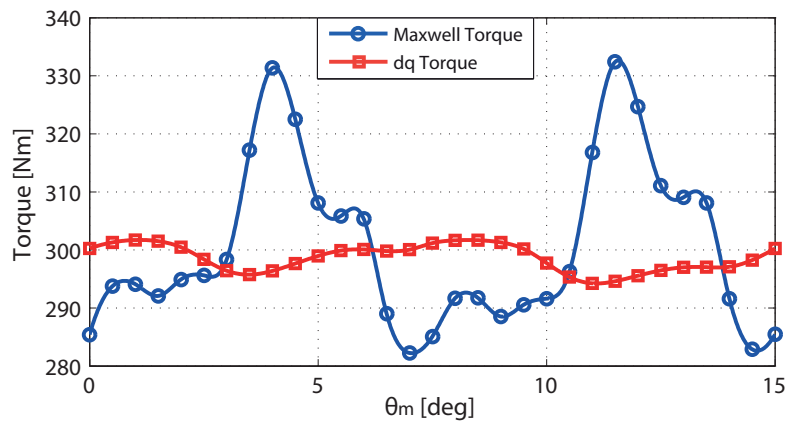Average d-q torque = 298.7 Nm
Torque ripple = 16.69 %

Finally we have obtained a motor that perfectly works in both nominal and overload conditions, without problem of PMs demagnetization. Fig. 2.20 shows the final shape of
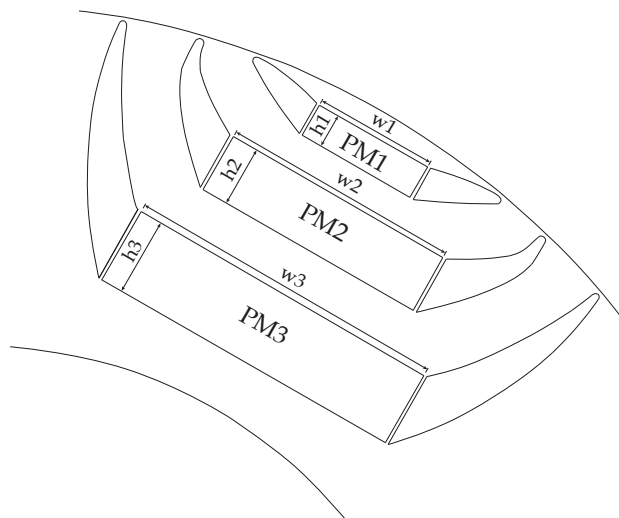
a rotor pole.

Figure 2.20: Reference three barriers section of a rotor pole.

The iron saturation between the rotor flux barriers could be lower even if it reaches an acceptable value. The final solution adopted gives us the possibility to have a better average torque if compared tho the SPM motor with PMs in NdFeB especially about the maximum torque. It's also important to say that the torque ripple is slightly increased. This is because, acting on rotor PMs configuration, probably the M.M.F of the rotor has been slightly changed, advancing his interaction with the stator one. As far as the harmonic analysis is concerned in nominal conditions it is possible to do the same considerations of Sect.2.1.4. Instead it is particularly interesting to consider the harmonic spectrum at overload conditions which is shown in Fig. 2.21. It's clear how the amplitudes of the main harmonics that contribute to the torque ripple have been increased significantly. This because of the higher iron saturation among the flux barriers due to the higher density current into the slots.
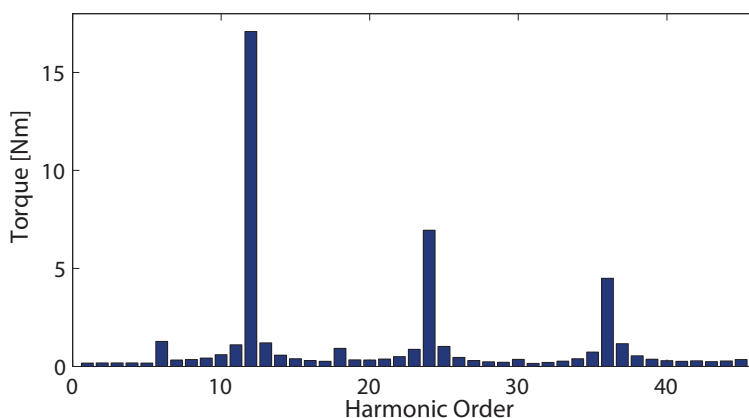

Figure 2.21: Torque ripple harmonic analysis of the reference 48/8 PMARel motor at overload conditions

Any considerations about the torque amount related to the PMs and the reluctance could

be done. To decompose the torque in these two parts must be remembered that:

$$T = \frac{3}{2} \cdot p \cdot [\Lambda_{mg} \cdot I_d + (L_d - L_q) \cdot I_d \cdot I_q] \tag{2.1}$$

From this expression it could be noticed that two different simulations could be done without modifying the current module but only the I_d sign. It results is that also the reluctance torque changes its sign. In particular the torque values obtained from the two simulations are:

-
$$T_1(I_q > 0) = T_{PM} + T_{REL} \tag{2.2}$$

-
$$T_2(I_q < 0) = T_{PM} - T_{REL} \tag{2.3}$$

In the end, combining T_1 with T_2 it is possible to show that:

-
$$T_{PM} = \frac{T_1 + T_2}{2} \tag{2.4}$$

-
$$T_{REL} = \frac{T_1 - T_2}{2} \tag{2.5}$$

As shown in Fig. 2.22 the contribute due to the PMs torque is lower than the one due to the reluctance torque.
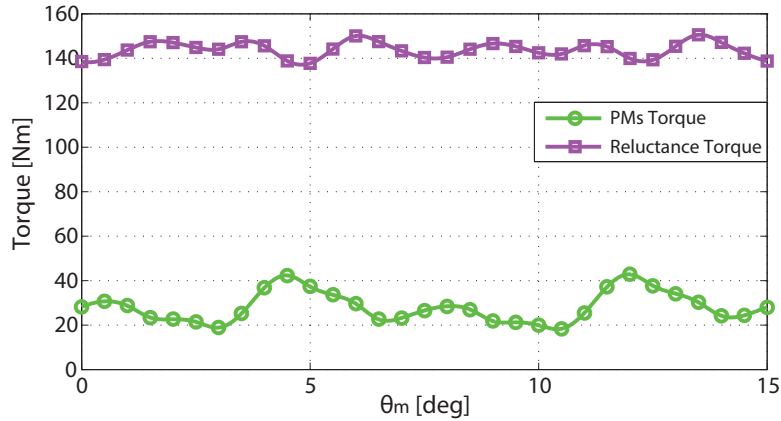
Figure 2.22: PMs torque and reluctance torque values for different mechanical angles related to Maxwell torque shown in Fig. 2.18. Reference 48/8 PMARel motor

The Maxwell torque has been analyzed basing the considerations on the behaviour of these two components. As it was aspected, it's clear how the maximums and the minimums of the Maxwell torque correspond to those of PMs torque at the same rotor position. The secondary maximums are linked to the reluctance torque. It could also be observed how the behaviour of Maxwell torque is more influenced by the PMs than by the reluctance. From the analysis of the behaviour of these two amounts it is possible to find out that:

Average PMs Torque = 28.1 Nm
PMs torque ripple = 14.23 %

Average REL torque = 143.7 Nm
Reluctance torque ripple = 7.48 %

As far as the torque ripple is concerned in nominal conditions, from these results it's evident that the PMs behaviour is more variable than the reluctance one. The Maxwell average torque is mostly composed by the reluctance torque, while the torque ripple is mostly influenced by the PMs torque.

This could be considered the reference DW PMAREL motor. Table 2.14 reports the comparison between this DW PMARel motor and the SPM motor analyzed in Chap.1.

Table 2.14: DW PMARel motor and SPM motor performance

Nominal Conditions		
	SPM motor with PM in NdFeB	**DW PMARel motor with PM in Ferrite**
MxW Avg Torque [N·m]	165	171.8
d-q Avg Torque [N·m]	164.9	170
Ripple [%]	12.44	13.05
Overload Conditions		
	SPM motor with PM in NdFeB	**DW PMARel motor with PM in Ferrite**
MxW Avg Torque [N·m]	270.6	300.4
d-q Avg Torque [N·m]	270.2	298.7
Ripple [%]	10.65	16.69

2.3 DW PMARel motor with industrial stator lamination

The following step that has been done was to substitute the stator lamination custom-tailored with a commercial one. The lamination considered is used for asynchronous machines. This is because we wanted to see if it was possible to reduce the production cost without modifying the performance. The new stator geometry is reported in Table 2.15:

Table 2.15: Industrial stator geometrical data

Symbol	Value	Unit	Stator
D_r	290	$[mm]$	External diameter
D_f	190	$[mm]$	Stator inner diameter
Q_s	48	-	Slot number
w_t	6.76	$[mm]$	Tooth width
w_{so}	3.15	$[mm]$	Slot opening width
h_{so}	0.75	$[mm]$	Slot opening height
h_s	25.3	$[mm]$	Slot height

The external stator diameter has been fixed. So it has been decreased from 300 mm to 290 mm. This is possible because of the high number of poles which entails that the flux divides itself in a greater number of paths than in an induction motor. Moreover the slot height is shorter than the one of the initial stator lamination. For this reason a reduction of D_r is convenient also for what concerns a better exploitation of the back iron from the point of view of the flux density.

Two simulations have been done, both in nominal conditions but with different stator slot currents. The first one has been done always with $I_{slot} = 694.6$ A and $n = 159$ rpm. While the second has been done considering the current density equal to 6 A/mm^2. The cross-section area of the slot has been reduced from nearly 205 mm^2 to almost 179 mm^2. So, fixing a $k_{fill} = 0.4$ it's possible to calculate it as:

$$I_{slotcomm} = \sqrt{2} \cdot A_{slot} \cdot k_{fill} \cdot \widehat{J}_{slot} = \sqrt{2} \cdot 175.9 \cdot 0.4 \cdot 6 = 597.4 \ [A]$$

The simulation has given back the results represented in Fig. 2.23 and Fig. 2.24. The current angles which has been considered is related to MTPA conditions. In the first case it has been equal to $\alpha_{ie} = 57$ deg and in the second one to $\alpha_{ie} = 55$ deg.

Figure 2.23: Torque value for different mechanical angles calculated through Maxwell stress tensor and d-q reference at nominal conditions with $I_{slot} = 694.6\ A$

and from this behaviour it is possible find out that:

Average Maxwell Torque = 168.8 Nm
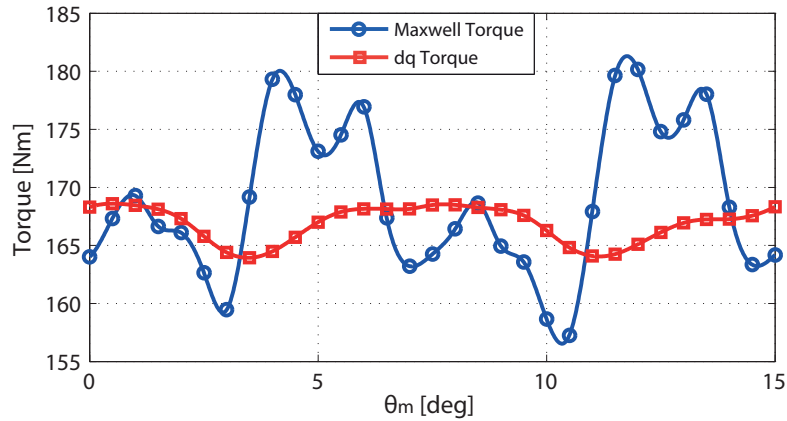Average d-q torque = 166.9 Nm
Torque ripple = 13.55 %

Figure 2.24: Torque value for different mechanical angles calculated through Maxwell stress tensor and d-q reference at nominal conditions with $I_{slot} = 597.4\ A$

while from this behaviour it is possible find out that:

Average Maxwell Torque = 140.2 Nm
Average d-q torque = 138.4 Nm
Torque ripple = 13.78 %

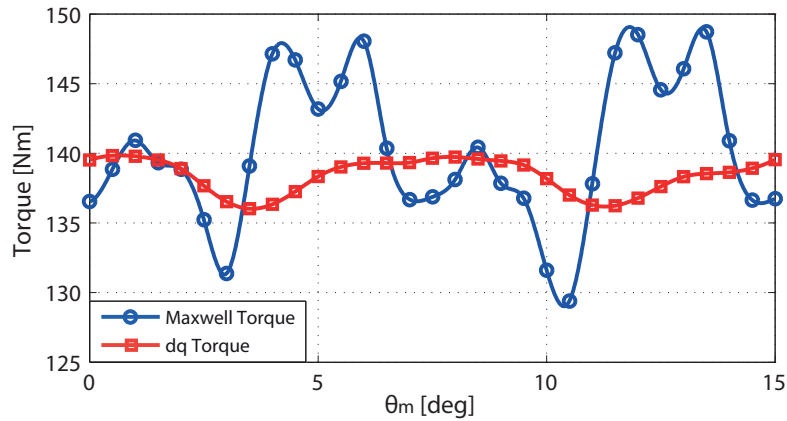In conclusion it could be noticed how the average torque is lower in the second case. It's obvious considering the important difference of current into the stator slots. It's also important to underline how the torque ripple remains almost the same and so this is due

to the Maxwell torque harmonic content which is not changed as a consequence of the changes of the stator. It could be deduced that the stator M.M.F in the air-gap doesn't change and so also its interaction with the rotor M.M.F doesn't change. The saturation in the iron between the barriers changes only of $0.1\ T$ from the first to the second nominal condition considered. So it's advised to work with $I_{slot} = 694.6\ A$. In this way the torque performance are again remarkable even if, with higher value of Joule losses into the stator slots copper due to the smaller section, we are going to worsen the efficiency.

Chapter 3

Reference fractional slot PMARel motors

In this chapter will be considered different FCSW PMARel motor configurations. The interest in this kind of motor is explained by *Bianchi* and *Barcaro* in [6]. This represents an interesting step in the development of a PMARel motor that could substitute an SPM one. In fact, despite a strong non linear behviour and a complex design, this kind of motor is a proper solution among PM machines owing to its interesting peculiarities, i.e., higher torque in flux-weakening operation, higher fault tolerance, and ability to adopt low-cost PMs. A second trend in designing PM machines concerns the adoption of fractional-slot (FS) nonoverlapped coil windings, which reduce the end winding lenght and consequently the Joule losses and the cost. Therefore, the adoption of an IPM machine with an FS winding aims to combine both advantages: high torque and efficiency in a wide operating region. However, the combination of an anisotropic rotor and an FS winding stator causes some problems. The iteraction between the magnetomotive force harmonics due to the stator current and the rotor anisotropy causes a very high torque ripple. This is the main problem to solve about this type of motors. In particular four different configurations have been analyzed and for each one of them at the beginning have been done a first sizing and analysis to have an idea of the results both of average torque and torque ripple. The configurations analyzed have been:

- 9 stator slots and 8 poles;

- 12 stator slots and 8 poles;

- 12 stator slots and 10 poles;

- 15 stator slots and 10 poles.

To have the possibility to compare the performance of all of them with the previous motors has been decided to size them keeping constant the geometric constraints introduced in Chap.1. The external and internal stator diameter have been kept constant. In this way the comparison with the DW PMARel motor take into consideration only the effects related to the different kind of winding.

3.1   Configuration with 9 stator slots and 8 poles

3.1.1   Motor design

The sizing must be based on some geometrical constraints and other specifications reported in Table 3.3:

Table 3.1: 9/8 PMARel geometrical specifications

Symbol	Value	Unit	Geometrical constraints
D_e	290	$[mm]$	External stator diameter
D	190	$[mm]$	Internal stator diameter
L_{stk}	145	$[mm]$	Stack length
			Other specifications
Q_s	9	-	Slots number
$2p$	8	-	Poles number
g	0.5	$[mm]$	Air–gap thickness
n	159	$[rpm]$	Motor speed at nominal conditions
T_N	165	$[Nm]$	Nominal torque

At the beginning the stator has been designed. It has been supposed that the sizing must be done for a SPM motor because in this way it has been possible to have a reference flux value. So, in this case from the BH curve of NdFeB PM at 120 C it's fixed that:

$$\frac{B_{g0}}{B_r} \simeq 0.83 \tag{3.1}$$

It's known that $B_r = 1.1\ T$ and from (3.1) could be obtained:

$$B_{g0} \simeq 0.83 \cdot B_r = 0.83 \cdot 1.1 = 0.913\ [T] \tag{3.2}$$

Always from the NdFeB BH curve, considering that the magnetic field is proportional to the induction, it's fixed $H_{g0} = -160\ kA/m$. Also the working point limit of the magnetic field has been fixed, and in particular it corresponds to $H_{knee} = -571.875\ kA/m$. The difference between these two values represents the available range of magnetic field on which the PMs work:

$$H_{g0} - H_{knee} = -160 + 571.875 \simeq 412\ [kA/m] \tag{3.3}$$

Deciding to work at nominal conditions with a $H_{gN} = 170\ kA/m$, the peak induction into the air-gap at nominal conditions could be calculated as:

$$\Delta H_s = H_{g0} - H_{gN} = -160 + 170 = 10\ [kA/m] \tag{3.4}$$

$$\Delta B_s \simeq 0.015\ [T] \tag{3.5}$$

and so:

$$B_g = B_{g0} - \Delta B_s = 0.913 - 0.015 = 0.898\ [T] \tag{3.6}$$

As far as the slot pitch is concerned it is estimated through the De Jong expression. It has been considered the internal stator diameter increased of the thickness due to the opening stator slots and the link between the lower vertexes of the slot and the opening slot. So it has been estimated that $D = 194$ mm. The slot pitch could be expressed as reported by *Bianchi* in [1]:

$$p_s \simeq 1.6 \cdot \sqrt{\frac{D}{p}} = 1.6 \cdot \sqrt{\frac{194}{4}} = 67.72 \ [mm] \tag{3.7}$$

Estimating that $B_t = 1.85$ T the tooth width results:

$$w_t = \frac{B_{g0} + \Delta B_s}{B_t} \cdot p_s \cdot K_{pack} = \frac{0.913 + 0.015}{1.85} \cdot 67.72 \cdot 0.96 = 32.62 \ [mm] \tag{3.8}$$

So, the slot width will be equal to:

$$w_s = p_s - w_t = 67.72 - 32.62 = 35.1 \ [mm] \tag{3.9}$$

Assuming that $J_s = 6$ A/mm^2, it could be possible to define the geometry of the conductors. The mechanical speed and the nominal power are expressed like:

$$\omega_m = n \cdot \frac{2 \cdot \pi}{60} = 159 \cdot \frac{2 \cdot \pi}{60} = 16.65 \ [rad/s] \tag{3.10}$$

$$P_N = T_N \cdot \omega_m = 165 \cdot 16.65 = 2747 \ [W] \tag{3.11}$$

Fixing $cos\varphi = 0.9$, $\eta = 0.73$ % and $E = 210$ V the current root mean square [rms] value is:

$$I = \frac{P_N}{3 \cdot E \cdot cos\varphi \cdot \eta} = \frac{2747}{3 \cdot 210 \cdot 0.9 \cdot 0.73} = 5.38 \ [A] \tag{3.12}$$

So the cross-section area of the single conductor is calculated as:

$$S_c = \frac{I}{J_s} = \frac{5.38}{6} = 0.9 \ [mm^2] \tag{3.13}$$

and as a consequence the conductor diameter could be analytically defined and then rounded off to a commercial value. So :

$$d_c = \sqrt{\frac{4 \cdot S_c}{\pi}} = \sqrt{\frac{4 \cdot 0.9}{\pi}} = 1.07 \Rightarrow 1.06 \ [mm^2] \tag{3.14}$$

Considering this diameter, the opening slot is defined in terms both of width and height. They are fixed equal to:

$$\omega_{so} = 3.15 \ [mm] \qquad\qquad h_{so} = 0.75 \ [mm] \tag{3.15}$$

As far as the flux is concerned it is defined as:

$$\phi = B_g \cdot \frac{D_{re} \cdot Lstk}{p} = 0.898 \cdot \frac{0.19 \cdot 0.145}{4} = 6.18 \ [mWb] \tag{3.16}$$

The total conductors is the next parameter which must be defined. Fixing the winding factor equal to $K_w = 1$, the frequency is expressed as:

$$f = \frac{n \cdot p}{60} = \frac{159 \cdot 4}{60} = 10.6 \; [Hz] \tag{3.17}$$

and so:

$$N_s = \frac{E}{\frac{\pi}{\sqrt{2}} \cdot f \cdot K_w \cdot \phi} = \frac{210}{\frac{\pi}{\sqrt{2}} \cdot 10.6 \cdot 1 \cdot 6.18 \cdot 10^{-3}} = 1443 \tag{3.18}$$

Having defined both stator slots number and the number of total conductors it is possible calculating the total conductors into a slot. The choice is that to have a two parallel paths winding ($n_{pp} = 2$) and so:

$$n_{cs} = \frac{3 \cdot N_s}{Q_s} = \frac{3 \cdot 1443}{9} = 481 \div 482 \tag{3.19}$$

Two choises have been possible about the winding configuration. It could be single layer or double layer. It has been chosen that it must be double layer and for this reason an even number of conductor in series must be considered. Considering $n_{cs} = 482$ the total number of conductors must be calculated again:

$$N_s = \frac{n_{cs} \cdot Q_s}{m} = \frac{482 \cdot 9}{3} = 1446 \tag{3.20}$$

The number of conductors in parallel is also defined as:

$$n_c = n_{cs} \cdot n_{pp} = 482 \cdot 2 = 964 \tag{3.21}$$

As a consequence, the section-area of each one must be halved. So:

$$S_{ceq} = \frac{S_c}{n_{pp}} = \frac{0.9}{2} = 0.45 \; [mm^2] \tag{3.22}$$

Finally the total cross-section area related to the conductors into a slot is:

$$S_{Cuslot} = n_c \cdot S_c = 964 \cdot 0.45 = 433.8 \; [mm^2] \tag{3.23}$$

Supposing a $k_{fill} = 0.4$ the total slot cross-section area is:

$$S_{slot} = \frac{S_{Cuslot}}{k_{fill}} = \frac{433.8}{0.4} \simeq 1085 \; [mm^2] \tag{3.24}$$

The slot height could be evaluated as:

$$h_s = \frac{Q_s}{2 \cdot \pi} \cdot \left\{ \sqrt{\left[\omega_s^2 + \frac{4 \cdot \pi}{Q_s} \cdot S_{slot} \right]} - \omega_s \right\}$$
$$= \frac{9}{2 \cdot \pi} \cdot \left\{ \sqrt{\left[35.1^2 + \frac{4 \cdot \pi}{9} \cdot 1085 \right]} - 35.1 \right\} = 24.8 \simeq 30 \; [mm] \tag{3.25}$$

The slot height has been increased because in this way the teeth shape will be more straight and the back-iron height will be the same as in the case of the DW PMARel motor. To complete the sizing of the slot the external slot width must be defined as:

$$\omega_{se} = \frac{\pi \cdot (D + 2 \cdot h_s)}{Q_s} - \omega_t = \frac{\pi \cdot (190 + 2 \cdot 30)}{9} - 32.62 = 44.27 \; [mm] \tag{3.26}$$

As far as the back iron height is concerned it could be expressed as:

$$h_{bi} = \frac{D_e - D - 2 \cdot h_s}{2} = \frac{290 - 190 - 2 \cdot 30}{2} = 20 \; [mm] \qquad (3.27)$$

The winding factor k_w (assumed during the sizing) must be now correctly defined considering that the winding is a fractional-slot double layer one. The pitch factor and the distribution factor couldn't be calculated through the expressions used in the first chapter because those had validity only for the distributed winding. So they have been obtained through *Winding* software:

- Distribution factor:

$$K_d = 0.960 \qquad (3.28)$$

- Chording factor:

$$K_p = 0.985 \qquad (3.29)$$

- Winding factor:

$$K_w = K_d \cdot K_p = 0.96 \cdot 0.985 = 0.945 \qquad (3.30)$$

Through the star of slots method it is possible to define the winding slot matrix which will be used in the simulations. It is reported hereafter:

ka = [1 -1 0.5 0 0 0 0 0 -0.5];

kb = [0 0 -0.5 1 -1 0.5 0 0 0];

kc = [0 0 0 0 0 -0.5 1 -1 0.5];

The rotor has been considered the same of that used for the DW PMARel motor. To achieve, the motor geometry is reported in Fig. 3.1, and Table 3.2 shows the geometrical parameters:
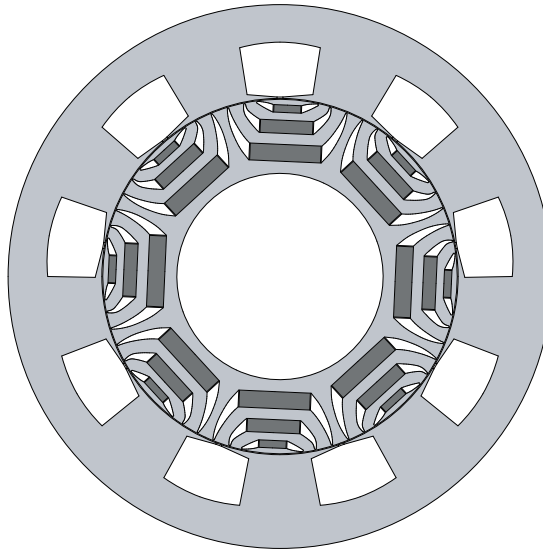

Figure 3.1: 9/8 PMARel section area

Table 3.2: 9/8 PMARel geometrical data

Symbol	Value	Unit	Stator
D_e	290	[mm]	Ext. diameter
D_i	190	[mm]	Inner diameter
Q_s	9	-	Slot number
w_t	32.62	[mm]	Tooth width
w_{so}	3.15	[mm]	Slot opening width
h_s	30	[mm]	Slot height
S_{slot}	1085	[mm^2]	Slot area
			Common data
$2p$	8	-	Poles number
L_{stk}	145	[mm]	Stack length
g	0.5	[mm]	Air-gap thickness
			Rotor
D_r	189	[mm]	Diameter
R_{PM1}	89.48	[mm]	1st PM radius
h_1	4	[mm]	1st PM height
w_1	14.4	[mm]	1st PM width
R_{PM2}	79.83	[mm]	2nd PM radius
h_2	7	[mm]	2nd PM height
w_2	28	[mm]	2nd PM width
R_{PM3}	65.93	[mm]	3rd PM radius
h_3	9	[mm]	3rd PM height
w_3	37.8	[mm]	3rd PM width
r	0.4	[mm]	Ribs thickness

3.1.2   Simulations

The motor analysis has been done directly through the finite element method. It has been simulated only at nominal conditions. Following the same steps adopted in Chap. 1 and in Chap. 2 at the beginning must be defined the peak current into the stator slots. Considering a current equal to $I = 5.38\ A$ through each series conductor, the total peak current into each slot could be computed as:

$$\widehat{I}_{slot} = I \cdot n_{cs} \cdot \sqrt{2} = 5.38 \cdot 482 \cdot \sqrt{2} = 3667\ [A] \Rightarrow 3627\ [A] \tag{3.31}$$

It has been decreased a little trying to strenghten the effect due to the slot height rounding up to 30 [mm] during the sizing. As a consequence, the back iron thickness has been increased with the aim to reduce the back iron saturation. The reduction of the peak current has the aim to balance out this effect. The slot current density could be considered again equal to $J_s = 6\ A/mm^2$. The motor has been done working at MTPA conditions and the current angle related is equal to $\alpha_{ie} = 37\ deg$. The torque behaviour has been considered. In particular the motor torque has been analyzed from 0 deg to 15 deg mechanical degrees i.e. 60 deg electrical degrees. The Maxwell torque has been compared again with the d-q torque. The results are shown in Fig.3.2 and from this behaviour it has been obtained

that:

Average Maxwell Torque = 106.5 Nm
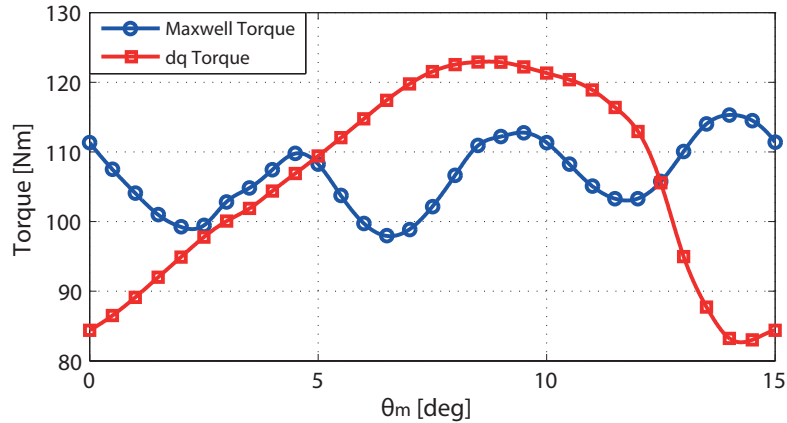Average d-q torque = 105.6 Nm
Torque ripple = 16.29 %

Figure 3.2: Torque value for different mechanical angles calculated through Maxwell stress tensor and d-q reference at nominal conditions. PMARel motor with 9 stator slots and 8 poles

It is clear how the nominal average torque supposed during the sizing ($T_N = 165 \ Nm$) was optimisitc. In fact the average torque reached from the FEM analysis is almost the 36 % lower. In terms of torque ripple the result is very interesting because it is comparable with the one related to the DW PMARel motor. The attention could be focused on the harmonic analysis of the torque behaviour which is shown in Fig.3.3.
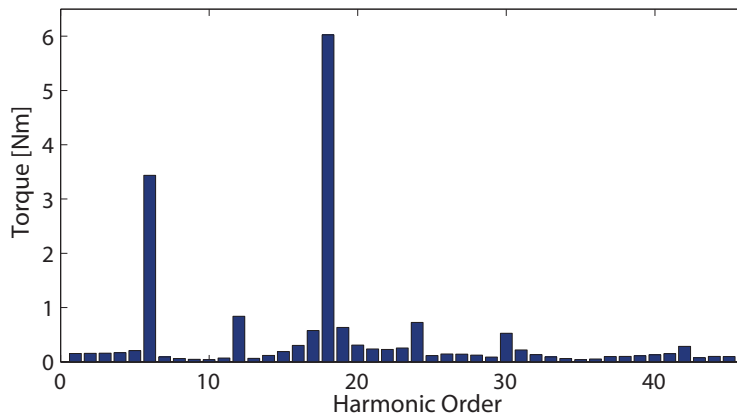

Figure 3.3: Torque ripple harmonic analysis of a PMARel motor with 9 stator slots and 8 poles

The main harmonic which has the greater influence on the torque ripple is the 18th one. It could be seen in Fig.3.2 because the Maxwell torque presents three periods in 60 *deg* electrical degrees. This means that in 360 *deg* electrical degrees there are 18 periods which

highlight the presence of this harmonic order. Besides it is important to notice how the maximum have different values among them. The same could be said for the minimum. This could be due to the harmonics of 6th, 12th, 24th and 30th order which also contribute to the torque ripple.

A consideration must be done about the tooth and back iron saturation. It has been seen how they saturate to the same level equal to 1.7 T. Usually the back iron must reach a lower induction (around $1.5 \div 1.6$ T). This deals with the consideration about the peak current done at the beginning of this paragraph and it is clear that maybe the back iron thickness could be increased again to support a saturation reduction. It must be remembered that at overload conditions the back iron could saturate too much. Probably some devices could be done to solve this. However the problem won't be engaged because the attention will be focused at nominal conditions. As far as the PMs are concerned, they do not exhibit problems about degmagnetization.

In the end it has been done an analysis about the two torque components: the first related to the reluctance while the second one related to the PMs. The results are shown in Fig.3.4:
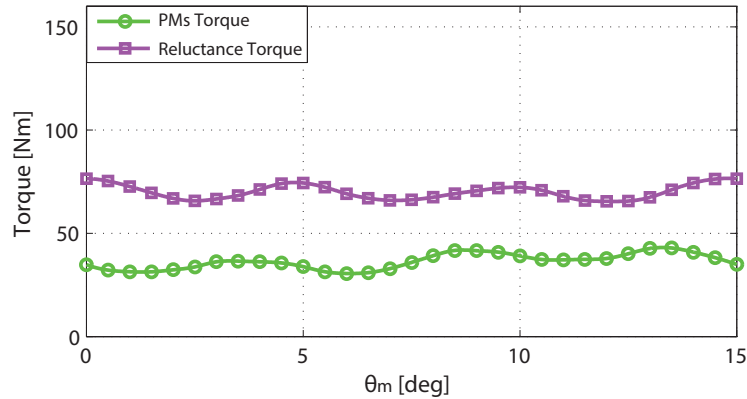

Figure 3.4: PMs torque and reluctance torque values for different mechanical angles related to Maxwell torque shown in Fig.3.2. PMARel motor with 9 stator slots and 8 poles

From the analysis of the behaviour of these two amounts it results:

Average PMs Torque = 36.4 Nm
PMs torque ripple = 11.59 %

Average REL torque = 70.2 Nm
Reluctance torque ripple = 10.34 %

It must be highlighted that the average torque loss is due to the reduction of the reluctance torque. In particular it is halved if it is compared to the DW PMARel motor. The PMs torque is increased of about 30 %. The PMs and reluctance torque ripple are comparable also if the first one is a few higher. The maximums and the minimums if the Maxwell torque correspond to those ones of PMs torque at the same rotor position. The secondary maximums are linked to the reluctance torque.

3.2 Configuration with 12 stator slots and 8 poles

3.2.1 Motor design

The sizing method is the same used in Sect.3.1.1. The geometrical constraints and other specifications have been reported in Table 3.3:

Table 3.3: 12/8 PMARel geometrical specifications

Symbol	Value	Unit	Geometrical constraints
D_e	290	[mm]	External stator diameter
D	190	[mm]	Internal stator diameter
L_{stk}	145	[mm]	Stack length
			Other specifications
Q_s	12	-	Slots number
$2p$	8	-	Poles number
g	0.5	[mm]	Air–gap thickness
n	159	[rpm]	Motor speed at nominal conditions
T_N	165	[Nm]	Nominal torque

From the BH curve of NdFeB PM at 120 C it's fixed that:

$$\frac{B_{g0}}{B_r} \simeq 0.87 \tag{3.32}$$

It's known that $B_r = 1.1\ T$ and from (3.1) could be obtained:

$$B_{g0} \simeq 0.87 \cdot B_r = 0.83 \cdot 1.1 = 0.961\ [T] \tag{3.33}$$

Always from the NdFeB BH curve, considering that the magnetic field is proportional to the induction, it's fixed $H_{g0} = -145\ kA/m$. Also the working point limit of the magnetic field is fixed, and in particular it corresponds to $H_{knee} = -571.875\ kA/m$. The difference between these two values represents the available range of magnetic field on which the PMs work:

$$H_{g0} - H_{knee} = -145 + 571.875 \simeq 427\ [kA/m] \tag{3.34}$$

Deciding to work at nominal conditions with a $H_{gN} = 165\ kA/m$, the peak induction into the air-gap at nominal conditions could be calculated as:

$$\Delta H_s = H_{g0} - H_{gN} = -145 + 165 = 20\ [kA/m] \tag{3.35}$$

$$\Delta B_s \simeq 0.032\ [T] \tag{3.36}$$

and so:

$$B_g = B_{g0} - \Delta B_s = 0.961 - 0.032 = 0.898\ [T] \tag{3.37}$$

As far as the slot pitch is concerned it is exstimated through the De Jong expression. It has been considered the internal stator diameter increased of the thickness due to the

opening stator slots and the link between the lower vertexes of the slot and the opening slot. So it has been estimated that $D = 195\ mm$. The slot pitch could be expressed as reported by *Bianchi* in [1]:

$$p_s \simeq 1.6 \cdot \sqrt{\frac{D}{p}} = 1.6 \cdot \sqrt{\frac{195}{4}} = 51.05\ [mm] \tag{3.38}$$

Exstimating that $B_t = 1.7\ T$ the tooth width could be now expressed as:

$$w_t = \frac{B_{g0} + \Delta B_s}{B_t} \cdot p_s \cdot k_{pack} = \frac{0.961 + 0.032}{1.7} \cdot 51.05 \cdot 0.96 = 27.7\ [mm] \tag{3.39}$$

So, the slot width will be equal to:

$$w_s = p_s - w_t = 51.05 - 27.7 = 23.35\ [mm] \tag{3.40}$$

Assuming that $J_s = 6\ A/mm^2$, it could be possible to define the geometry of the conductors. The mechanical speed and the nominal power are expressed like:

$$\omega_m = n \cdot \frac{2 \cdot \pi}{60} = 159 \cdot \frac{2 \cdot \pi}{60} = 16.65\ [rad/s] \tag{3.41}$$

$$P_N = T_N \cdot \omega_m = 165 \cdot 16.65 = 2747\ [W] \tag{3.42}$$

Fixing $cos\varphi = 0.9$, $\eta = 0.73\ \%$ and $E = 210\ V$ the current root mean square [rms] value is:

$$I = \frac{P_N}{3 \cdot E \cdot cos\varphi \cdot \eta} = \frac{2747}{3 \cdot 210 \cdot 0.9 \cdot 0.73} = 5.38\ [A] \tag{3.43}$$

So the cross-section area of the single conductor is calculated as:

$$S_c = \frac{I}{J_s} = \frac{5.38}{6} = 0.9\ [mm^2] \tag{3.44}$$

and as a consequence the conductor diameter could be analytically defined and then rounded off to a commercial value. So :

$$d_c = \sqrt{\frac{4 \cdot S_c}{\pi}} = \sqrt{\frac{4 \cdot 0.9}{\pi}} = 1.07 \Rightarrow 1.06\ [mm^2] \tag{3.45}$$

Considering this diameter, the opening slot is defined in terms both of width and height. They are fixed equal to:

$$\omega_{so} = 3.15\ [mm] \qquad\qquad h_{so} = 0.75\ [mm] \tag{3.46}$$

As far as the flux is concerned it is defined as:

$$\phi = B_g \cdot \frac{D_{re} \cdot Lstk}{p} = 0.898 \cdot \frac{0.19 \cdot 0.145}{4} = 6.18\ [mWb] \tag{3.47}$$

The total conductors is the next parameter which must be defined. Fixing the winding factor equal to $K_w = 1$, the frequency is expressed as:

$$f = \frac{n \cdot p}{60} = \frac{159 \cdot 4}{60} = 10.6 \ [Hz] \tag{3.48}$$

and so:

$$N_s = \frac{E}{\frac{\pi}{\sqrt{2}} \cdot f \cdot K_w \cdot \phi} = \frac{210}{\frac{\pi}{\sqrt{2}} \cdot 10.6 \cdot 1 \cdot 6.18 \cdot 10^{-3}} = 1443 \tag{3.49}$$

Having defined both stator slots number and the number of total conductors it is possible to calculate the total conductors into a slot. The choice is that to have a two parallel paths winding ($n_{pp} = 2$) and so:

$$n_{cs} = \frac{3 \cdot N_s}{Q_s} = \frac{3 \cdot 1443}{12} = 360 \div 361 \tag{3.50}$$

Two choises are possible about the winding configuration. It could be single layer or double layer. A double layer is selected and for this reason the number of conductor in series must be considered even. Considering $n_{cs} = 360$ the total number of conductors must be calculated again:

$$N_s = \frac{n_{cs} \cdot Q_s}{m} = \frac{360 \cdot 12}{3} = 1444 \tag{3.51}$$

The number of conductors in parallel has also been defined as:

$$n_c = n_{cs} \cdot n_{pp} = 360 \cdot 2 = 720 \tag{3.52}$$

As a consequence, the section-area of each one must be halved. So:

$$S_{ceq} = \frac{S_c}{n_{pp}} = \frac{0.9}{2} = 0.45 \ [mm^2] \tag{3.53}$$

Finally the total cross-section area related to the conductors into a slot as:

$$S_{Cuslot} = n_c \cdot S_c = 720 \cdot 0.45 = 324 \ [mm^2] \tag{3.54}$$

and assuming that $k_{fill} = 0.4$, the total slot cross-section area results:

$$S_{slot} = \frac{S_{Cuslot}}{k_{fill}} = \frac{324}{0.4} \simeq 810 \ [mm^2] \tag{3.55}$$

The slot height could be evaluated as:

$$
\begin{aligned}
h_s &= \frac{Q_s}{2 \cdot \pi} \cdot \left\{ \sqrt{\left[\omega_s^2 + \frac{4 \cdot \pi}{Q_s} \cdot S_{slot} \right]} - \omega_s \right\} \\
&= \frac{12}{2 \cdot \pi} \cdot \left\{ \sqrt{\left[23.35^2 + \frac{4 \cdot \pi}{12} \cdot 810 \right]} - 23.35 \right\} = 26.67 \simeq 30 \ [mm]
\end{aligned}
\tag{3.56}
$$

The slot height has been increased because in this way the teeth shape will be more straight and the back-iron height will be the same as in the case of the DW PMARel motor. To complete the sizing of the slot the external slot width must be defined as:

$$\omega_{se} = \frac{\pi \cdot (D + 2 \cdot h_s)}{Q_s} - \omega_t = \frac{\pi \cdot (190 + 2 \cdot 30)}{12} - 27.7 = 37.75 \ [mm] \tag{3.57}$$

As far as the back iron height is concerned it could be expressed as:

$$h_{bi} = \frac{D_e - D - 2 \cdot h_s}{2} = \frac{290 - 190 - 2 \cdot 30}{2} = 20 \ [mm] \tag{3.58}$$

The winding factor k_w (assumed during the sizing) must be now correctly defined considering that the winding is a fractional-slot double layer one. The pitch factor and the distribution factor couldn't be calculated through the expressions used in the first chapter because those had validity only for the distributed winding. So they have been obtained through *Winding* software:

- Distribution factor:

$$K_d = 1 \tag{3.59}$$

- Chording factor:

$$K_p = 0.866 \tag{3.60}$$

- Winding factor:

$$K_w = K_d \cdot K_p = 1 \cdot 0.866 = 0.866 \tag{3.61}$$

Through the star of slots method it is possible to define the winding slot matrix which will be used in the simulations. It is reported hereafter:

ka = [0.5 -0.5 0 0.5 -0.5 0 0.5 -0.5 0 0.5 -0.5 0];

kb = [0 0.5 -0.5 0 0.5 -0.5 0 0.5 -0.5 0 0.5 -0.5];

kc = [-0.5 0 0.5 -0.5 0 0.5 -0.5 0 0.5 -0.5 0 0.5];

The rotor has been considered the same of that used for the DW PMARel motor. To achieve, the motor geometry is reported in Fig. 3.5, and Table 3.4 shows the geometrical parameters:
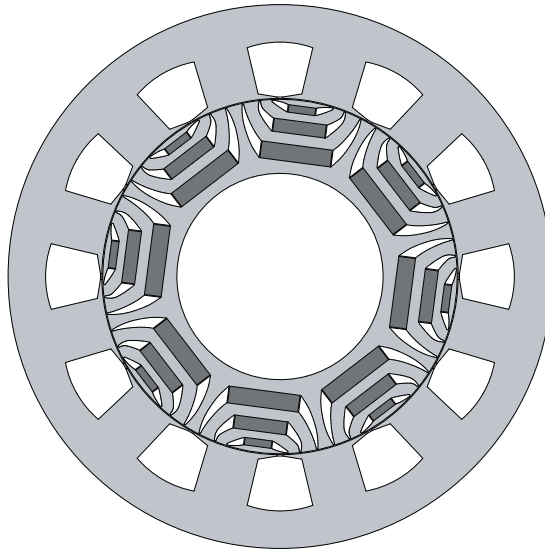

Figure 3.5: 12/8 PMARel section area

Table 3.4: 12/8 PMARel geometrical data

Symbol	Value	Unit	Stator
D_e	290	[mm]	Ext. diameter
D_i	190	[mm]	Inner diameter
Q_s	12	-	Slot number
w_t	27.7	[mm]	Tooth width
w_{so}	3.15	[mm]	Slot opening width
h_s	30	[mm]	Slot height
S_{slot}	810	[mm^2]	Slot area
			Common data
$2p$	8	-	Poles number
L_{stk}	145	[mm]	Stack length
g	0.5	[mm]	Air-gap thickness
			Rotor
D_r	189	[mm]	Diameter
R_{PM1}	89.48	[mm]	1st PM radius
h_1	4	[mm]	1st PM height
w_1	14.4	[mm]	1st PM width
R_{PM2}	79.83	[mm]	2nd PM radius
h_2	7	[mm]	2nd PM height
w_2	28	[mm]	2nd PM width
R_{PM3}	65.93	[mm]	3rd PM radius
h_3	9	[mm]	3rd PM height
w_3	37.8	[mm]	3rd PM width
r	0.4	[mm]	Ribs thickness

3.2.2   Simulations

Also in this case the analysis has been carried out at nominal conditions using the finite element method. The peak current into the stator slots has been expressed as in (3.31). In fact, always considering that each series conductor is passed through by $I = 5.38\ A$ and that $n_{cs} = 360$:

$$\widehat{I}_{slot} = I \cdot n_{cs} \cdot \sqrt{2} = 5.38 \cdot 360 \cdot \sqrt{2} = 2739\ [A] \tag{3.62}$$

Also if as in Sect.3.1 the slot height has been rounded up to 30 mm, the peak current into each stator slot hasn't been decreased because of its lower level which will less saturate the back iron. The motor has been done working at MTPA conditions and the current angle related is equal to $\alpha_{ie} = 50\ deg$. The torque behaviour has been analyzed again from 0 deg to 15 deg mechanical degrees and both Maxwell torque and d-q torque have been considered. The results which have been reached are shown in Fig.3.6 and it results:

Average Maxwell Torque = 122.6 Nm
Average d-q torque = 121.3 Nm
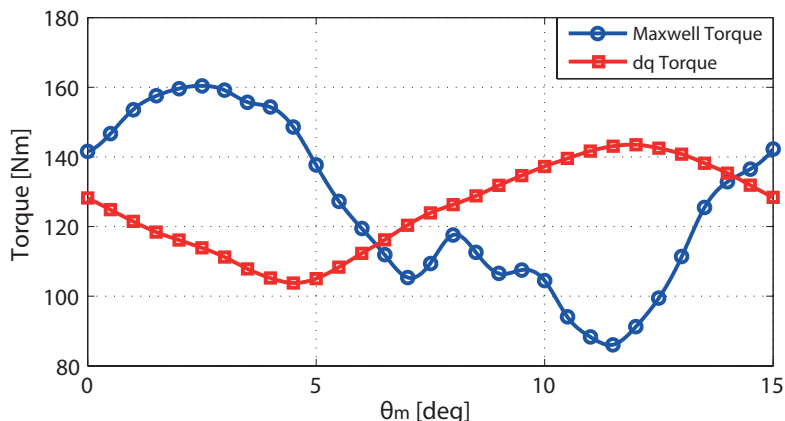Torque ripple = 56.95 %

Figure 3.6: Torque value for different mechanical angles calculated through Maxwell stress tensor and d-q reference at nominal conditions. PMARel motor with 12 stator slots and 8 poles.

It could be observed that the average torque is better than the 9/8 PMARel motor configuration. It is again lower than the one supposed at the beginning of the sizing about the 26 %. If compared with the configuration described in Sect.3.1 the improvement in terms of average torque is linked to a worst torque ripple. This is the main problem of this kind of configuration and in the following chapters will be seen some techniques adopted to decrease this parameter. The attention could be focused on the harmonic analysis of the torque behaviour which is shown in Fig.3.7:
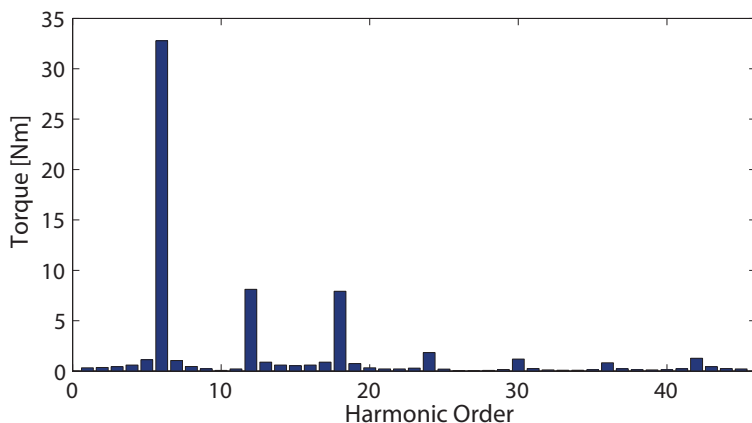
Figure 3.7: Torque ripple harmonic analysis of a PMARel motor with 12 stator slots and 8 poles

The harmonic order highlights the presence of the same harmonics considered in Sect.3.1.

In particular the main one in this case is the 6th. Its amplitude is very high. There are also the 12th and the 18th harmonics. This is clear from the torque behaviour which is shown in Fig.3.6 where could be observed the presence of two periods in 60 *deg* mechanical degrees. This is related to the 12th harmonic. Between 7 *deg* and 9 *deg* there is the tendency by torque behaviour to add a third period and this is due to the 18th one.

Other considerations about the iron stator saturation must be done. The tooth reach a saturation equal to 1.6 *T* while the back iron reaches a saturation equal to 1.4 *T*. The thickness of both of them could be decreased and this means that the slot cross-section area could be increased. If the density current into the slots is kept constant this deals with an improvement of peak current. As a consequence, also the average torque will reach an higher value, but due to the higher iron saturation probably this will be linked also to an improvement of torque ripple. At overload conditions the motor sized will work better than the one with the tooth and the back iron properly sized for the operation at nominal conditions. The PMs haven't problems about degmagnetization.

At last it an analysis has been done to determine the two torque components: the first related to the reluctance while the second one related to the PMs. The results are shown in Fig.3.8:
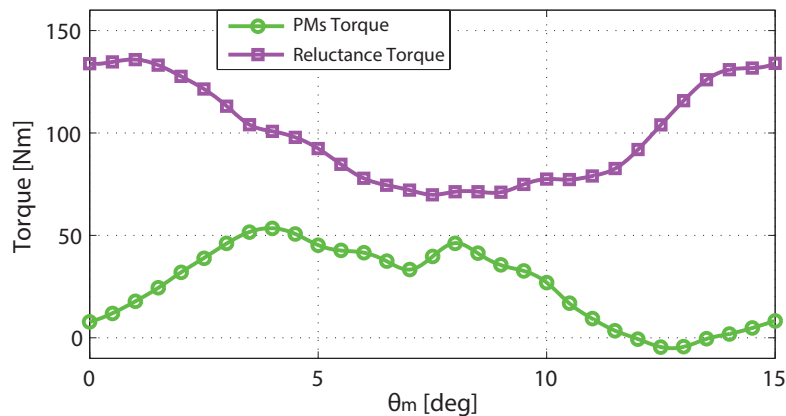

Figure 3.8: PMs torque and reluctance torque values for different mechanical angles related to Maxwell torque shown in Fig.3.6. PMARel motor with 12 stator slots and 8 poles

From the analysis of the behaviour of these two amounts it results:

Average PMs Torque = 25.5 Nm
PMs torque ripple = 39.99 %

Average REL torque = 100.4 Nm
Reluctance torque ripple = 53.81 %

It must be highlighted that the average torque drop is due to the reduction of the reluctance torque. It is evident how the PMs torque between 11 *deg* and 14 *deg* mechanical degrees is opposed to the reluctance one. This means that it doesn't contribute to the average torque supporting its reduction.

In particular, the reluctance torque is equal to 70 % if it is compared to the DW PMARel

motor, while the PMs one is equal to 91 %. The PMs torque ripple is lower than the one related to the reluctance torque. Overall it's clear how the maximums and the minimums of the Maxwell torque deal with the ones of PMs torque at the same rotor position. The secondary maximums are linked to the reluctance torque.

3.3 Configuration with 12 stator slots and 10 poles

3.3.1 Motor design

The sizing method is the same used in Sect.3.2.1. The geometrical constraints and other specifications have been reported in Table 3.5:

Table 3.5: 12/10 PMARel geometrical specifications

Symbol	Value	Unit	Geometrical constraints
D_e	290	[mm]	External stator diameter
D	190	[mm]	Internal stator diameter
L_{stk}	145	[mm]	Stack length
			Other specifications
Q_s	12	-	Slots number
$2p$	10	-	Poles number
g	0.5	[mm]	Air–gap thickness
n	159	[rpm]	Motor speed at nominal conditions
T_N	165	[Nm]	Nominal torque

As far as the stator is concerned, it is the same which has been sized in Sect.3.2.1. The winding is different and the winding factor results to be different. Also the pitch factor and the distribution factor will be different. They have been obtained through *Winding* software:

- Distribution factor:

$$K_d = 0.966 \tag{3.63}$$

- Chording factor:

$$K_p = 0.966 \tag{3.64}$$

- Winding factor:

$$K_w = K_d \cdot K_p = 1 \cdot 0.866 = 0.933 \tag{3.65}$$

Through the star of slots method it is possible to define the winding slot matrix which will be used in the simulations. It is reported hereafter:

ka = [1 -0.5 0 0 0 0.5 -1 0.5 0 0 0 -0.5];

kb = [0 0.5 -1 0.5 0 0 0 -0.5 1 -0.5 0 0];

kc = [0 0 0 -0.5 1 -0.5 0 0 0 0.5 -1 0.5];

The rotor sizing has been done with the aims to design a simple rotor configuration which has also a similar PMs shape respect the 8 poles rotor following again the *Vagati* theory [3]. The PMs have been defined with the same thicknesses and average radii which were adopted in the 8 poles configuration. Their widths have been reduced because of the higher poles number. This the external and internal rotor diameter being equal to the 8 poles

configurations. The ribs have been kept equal to the 8 poles rotor. The PMs geometry has been reported in Table 3.6:

Table 3.6: PMs parameters

	Radius [mm]	Height [mm]	Width [mm]	Ribs [mm]
PM 1	89.48	4.0	11.4	0.4
PM 2	79.83	7.0	22.4	0.4
PM 3	65.93	9.0	30.2	0.4

The last parameters to consider are the flux barrier angles. It has been decided to design a rotor with equally spaced imaginary rotor slots. This to obtain a simple and symmetrical rotor structure. The analytical method previously seen in Sect.2.1.3 has been used again. It must be adapted because it has validity only in the case of distributed windings. The mechanical angle related to a rotor pole could be expressed as:

$$\theta_{pole} = \frac{360}{2 \cdot p} = \frac{360}{10} = 36 \ [deg] \tag{3.66}$$

To define the three barrier angles has been fixed that $n_r = 14$ in a pair pole. This because 12 of them correspond to the position of the flux barriers extremities, while 2 have been placed along the Q-axis. It's all represented in Fig. 3.9:
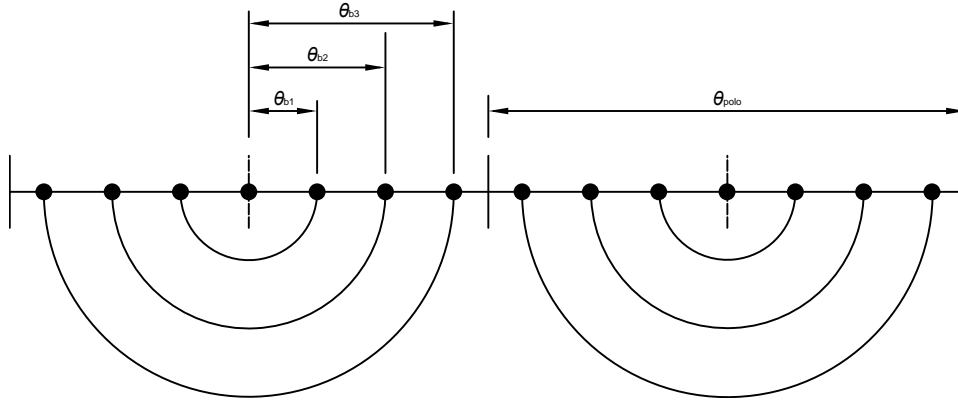
Figure 3.9: Representation of analytical angles of a 10 poles rotor

In particular the θ_{pole} has been divided in 7 regular parts because in this way the angle between the Q-axis and the first flux-barriers is the same of those beween two consecutive flux barriers. It results:

$$\theta_{b1} = \frac{\theta_{pole}}{7} = 5.14 \ [deg]$$

$$\theta_{b2} = \theta_{b1} \cdot 2 = 10.3 \ [deg]$$

$$\theta_{b3} = \theta_{b1} \cdot 3 = 15.4 \ [deg]$$

To achieve, the motor geometry is reported in Fig. 3.10, and Table 3.7 shows the geometrical parameters:

Table 3.7: 12/10 PMARel geometrical data

Symbol	Value	Unit	Stator
D_e	290	$[mm]$	Ext. diameter
D_i	190	$[mm]$	Inner diameter
Q_s	12	-	Slot number
w_t	27.7	$[mm]$	Tooth width
w_{so}	3.15	$[mm]$	Slot opening width
h_s	30	$[mm]$	Slot height
S_{slot}	810	$[mm^2]$	Slot area
			Common data
$2p$	10	-	Poles number
L_{stk}	145	$[mm]$	Stack length
g	0.5	$[mm]$	Air-gap thickness
			Rotor
D_r	189	$[mm]$	Diameter
R_{PM1}	89.48	$[mm]$	1st PM radius
h_1	4	$[mm]$	1st PM height
w_1	11.4	$[mm]$	1st PM width
R_{PM2}	79.83	$[mm]$	2nd PM radius
h_2	7	$[mm]$	2nd PM height
w_2	22.4	$[mm]$	2nd PM width
R_{PM3}	65.93	$[mm]$	3rd PM radius
h_3	9	$[mm]$	3rd PM height
w_3	30.2	$[mm]$	3rd PM width
r	0.4	$[mm]$	Ribs thickness

Figure 3.10: 12/10 PMARel section area

3.3.2   Simulations

The motor analysis also in this case has been based on finite element method at nominal conditions. From the sizing it is known that $I = 5.38\ A$ is the current which passes through each series conductor and that $n_{cs} = 360$. The peak current into the slot could be expressed as:

$$\widehat{I}_{slot} = I \cdot n_{cs} \cdot \sqrt{2} = 5.38 \cdot 360 \cdot \sqrt{2} = 2739\ [A] \tag{3.67}$$

Since the stator chosen is the same used in Sect.3.2, also the peak current is the same. The motor has been done working at MTPA conditions and the current angle results to be $\alpha_{ie} = 53\ deg$. The rotor in this configuration has 10 poles. This means that also the range of mechanical angle to consider must change. According with the (1.42), the motor simulation must be carried out from 0 deg to 12 deg mechanical degrees and both Maxwell torque and d-q torque have been considered. The results which have been reached are shown in Fig.3.11 and from this behaviour it results:

Average Maxwell Torque = 103.5 Nm
Average d-q torque = 102.8 Nm
Torque ripple = 23.73 %
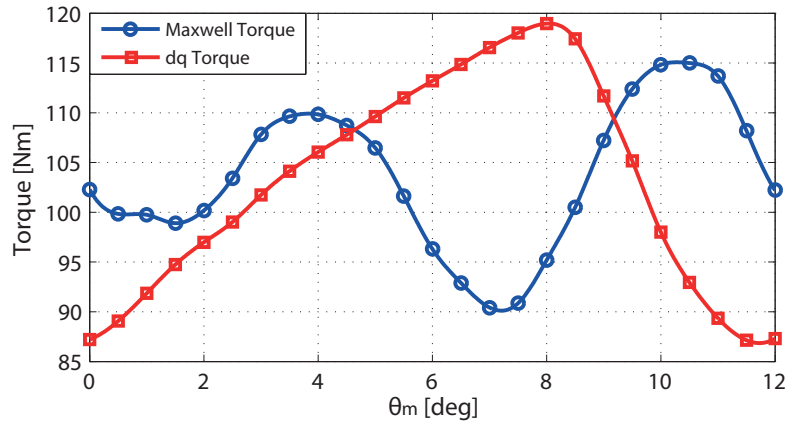
Figure 3.11: Torque value for different mechanical angles calculated through Maxwell stress tensor and d-q reference at nominal conditions. PMARel motor with 12 stator slots and 10 poles

It is clear how the average torque is similar to the one obtained with the configuration studied in Sect.3.1, while the torque ripple is worsen. Compared with the average torque supposed at the beginning of the sizing the one computed from the simulation is about 37 % lower. From the harmonic analysis of the torque behaviour the harmonic order could be defined. It is shown in Fig.3.12:
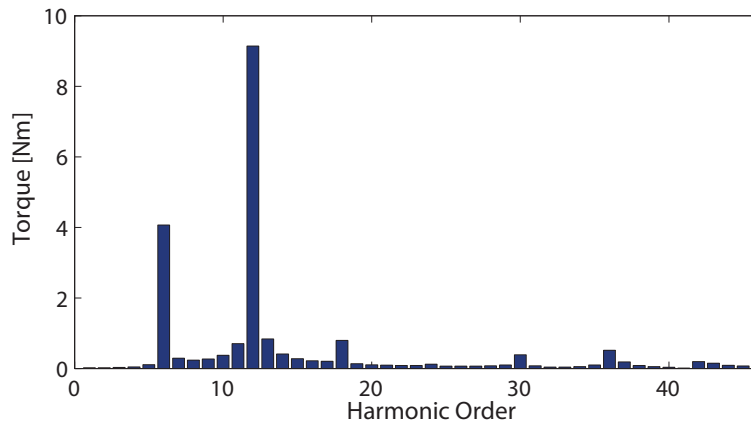
Figure 3.12: Torque ripple harmonic analysis of a PMARel motor with 12 stator slots and 10 poles

The harmonic order highlights the presence of the same harmonics considered in Sect.3.1. In particular the main one in this case is the 12$^{\text{th}}$ and there are also harmonics of 6$^{\text{th}}$ and 18$^{\text{th}}$ order. From the torque behaviour shown in Fig.3.6, could be observed the presence of two periods in 60 *deg* mechanical degrees. This is related to the 12$^{\text{th}}$ harmonic. The maximums have different values among them. The same could be said for the minimums. This could be due to the harmonics of 6$^{\text{th}}$, 18$^{\text{th}}$, 30$^{\text{th}}$ and 36$^{\text{th}}$ order which also contribute to the torque ripple.

As far as the stator tooth and back iron are concerned, they reached satisfactory induction values. In particular the tooth reaches an induction equal to 1.8 T while the back iron equal to 1.67 T. The PMs do not exhibit problems about degmagnetization.

The two torque components are segregated due to the reluctance and due to the PMs. The results are shown in Fig.3.13:
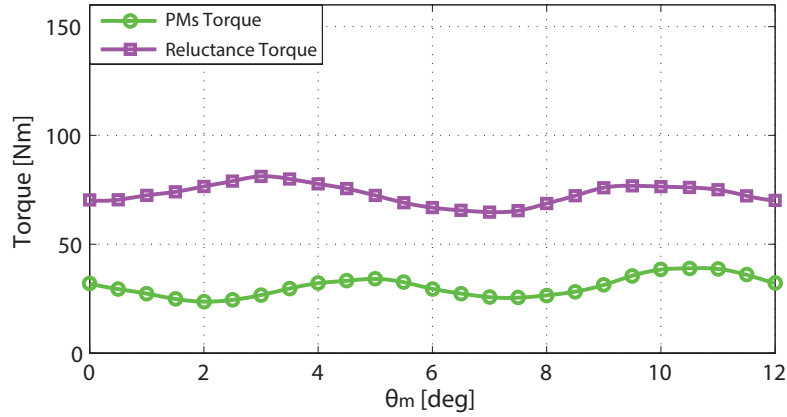

Figure 3.13: PMs torque and reluctance torque values for different mechanical angles related to Maxwell torque shown in Fig.3.11. PMARel motor with 12 stator slots and 10 poles

From the analysis of the behaviour of these two amounts it results:

Average PMs Torque = 30.5 Nm
PMs torque ripple = 14.79 %

Average REL torque = 73 Nm
Reluctance torque ripple = 15.87 %

From an accurate observation it is possible to do similar considerations about Sect.3.1. In particular the reluctance torque is equal to 50 % if it is compared to the DW PMARel moto, while the PMs one is increased about 9 %. The PMs and reluctance torque ripple are comparable. The reluctance torque ripple is a few higher than the PMs one.

3.4 Configuration with 15 stator slots and 10 poles

3.4.1 Motor design

In the end also for the last motor configuration the sizing method is the same used in 3.1.1. The geometrical constraints and other specifications have been reported in Table 3.8:

Table 3.8: 15/10 PMARel geometrical specifications

Symbol	Value	Unit	Geometrical constraints
D_e	290	[mm]	External stator diameter
D	190	[mm]	Internal stator diameter
L_{stk}	145	[mm]	Stack length
			Other specifications
Q_s	15	-	Slots number
$2p$	10	-	Poles number
g	0.5	[mm]	Air–gap thickness
n	159	[rpm]	Motor speed at nominal conditions
T_N	165	[Nm]	Nominal torque

From the BH curve of NdFeB PM at 120 C it's fixed that:

$$\frac{B_{g0}}{B_r} \simeq 0.83 \tag{3.68}$$

It's known that $B_r = 1.1\ T$ and from 3.1 could be obtained:

$$B_{g0} \simeq 0.83 \cdot B_r = 0.83 \cdot 1.1 = 0.913\ [T] \tag{3.69}$$

Always from the NdFeB BH curve, considering that the magnetic field is proportional to the induction, it's fixed $H_{g0} = -160\ kA/m$. Also the working point limit of the magnetic field is fixed, and in particular it corresponds to $H_{knee} = -571.875\ kA/m$. The difference between these two values represents the available range of magnetic field on which the PMs work:

$$H_{g0} - H_{knee} = -160 + 571.875 \simeq 412\ [kA/m] \tag{3.70}$$

Deciding to work at nominal conditions with a $H_{gN} = 170\ kA/m$, the peak induction into the air-gap at nominal conditions could be calculated as:

$$\Delta H_s = H_{g0} - H_{gN} = -160 + 170 = 10\ [kA/m] \tag{3.71}$$

$$\Delta B_s \simeq 0.015\ [T] \tag{3.72}$$

and so:

$$B_g = B_{g0} - \Delta B_s = 0.913 - 0.015 = 0.898\ [T] \tag{3.73}$$

As far as the slot pitch is concerned it is estimated through the De Jong expression. It has been considered the internal stator diameter, increased of the thickness due to the

opening stator slots and the link between the lower vertexes of the slot and the opening slot. So it has been exstimated that $D = 198.6 \ mm$. The slot pitch could be expressed as reported by *Bianchi* in [1]:

$$p_s = \frac{\pi \cdot D}{Q_s} = \frac{\pi \cdot 198.6}{15} = 41.59 \ [mm] \tag{3.74}$$

Estimating that $B_t = 1.8 \ T$ the tooth width could be now expressed as:

$$w_t = \frac{B_{g0} + \Delta B_s}{B_t} \cdot p_s \cdot k_{pack} = \frac{0.913 + 0.015}{1.8} \cdot 41.59 \cdot 0.96 = 20.59 \ [mm] \tag{3.75}$$

So, the slot width will be equal to:

$$w_s = p_s - w_t = 41.59 - 20.59 = 21 \ [mm] \tag{3.76}$$

Assuming that $J_s = 6 \ A/mm^2$, it could be possible to define the geometry of the conductors. The mechanical speed and the nominal power are expressed like:

$$\omega_m = n \cdot \frac{2 \cdot \pi}{60} = 159 \cdot \frac{2 \cdot \pi}{60} = 16.65 \ [rad/s] \tag{3.77}$$

$$P_N = T_N \cdot \omega_m = 165 \cdot 16.65 = 2747 \ [W] \tag{3.78}$$

Fixing $cos\varphi = 0.9$, $\eta = 0.73 \ \%$ and $E = 210 \ V$ the current root mean square [rms] value is:

$$I = \frac{P_N}{3 \cdot E \cdot cos\varphi \cdot \eta} = \frac{2747}{3 \cdot 210 \cdot 0.9 \cdot 0.73} = 5.38 \ [A] \tag{3.79}$$

So the cross-section area of the single conductor is calculated as:

$$S_c = \frac{I}{J_s} = \frac{5.38}{6} = 0.9 \ [mm^2] \tag{3.80}$$

and as a consequence the conductor diameter could be analytically defined and then rounded off to a commercial value. So :

$$d_c = \sqrt{\frac{4 \cdot S_c}{\pi}} = \sqrt{\frac{4 \cdot 0.9}{\pi}} = 1.07 \Rightarrow 1.06 \ [mm^2] \tag{3.81}$$

Considering this diameter the opening slot is defined in terms both of width and height. They are fixed equal to:

$$\omega_{so} = 3.15 \ [mm] \qquad\qquad h_{so} = 0.75 \ [mm] \tag{3.82}$$

As far as the flux is concerned it is defined as:

$$\phi = B_g \cdot \frac{D_{re} \cdot Lstk}{p} \ = 0.898 \cdot \frac{0.19 \cdot 0.145}{4} = 6.18 \ [mWb] \tag{3.83}$$

The total conductors is the next parameter which must be defined. Fixing the winding factor equal to $K_w = 1$, the frequency is expressed as:

$$f = \frac{n \cdot p}{60} = \frac{159 \cdot 4}{60} = 10.6 \ [Hz] \tag{3.84}$$

and so:

$$N_s = \frac{E}{\frac{\pi}{\sqrt{2}} \cdot f \cdot K_w \cdot \phi} = \frac{210}{\frac{\pi}{\sqrt{2}} \cdot 10.6 \cdot 1 \cdot 6.18 \cdot 10^{-3}} = 1443 \qquad (3.85)$$

Having defined both stator slots number and the number of total conductors it is possible to calculate the total conductors into a slot. The choice is that to have a two parallel paths winding ($n_{pp} = 2$) and so:

$$n_{cs} = \frac{3 \cdot N_s}{Q_s} = \frac{3 \cdot 1443}{15} = 289 \div 290 \qquad (3.86)$$

Two choices are possible about the winding configuration. It could be single layer or double layer. A double layer is selected and for this reason the number of conductor in series must be even. Considering $n_{cs} = 482$ the total number of conductors must be calculated again:

$$N_s = \frac{n_{cs} \cdot Q_s}{m} = \frac{290 \cdot 15}{3} = 1450 \qquad (3.87)$$

The number of conductors in parallel has also been defined as:

$$n_c = n_{cs} \cdot n_{pp} = 482 \cdot 2 = 580 \qquad (3.88)$$

As a consequence, the section-area of each one must be halved. So:

$$S_{ceq} = \frac{S_c}{n_{pp}} = \frac{0.9}{2} = 0.45 \; [mm^2] \qquad (3.89)$$

Finally the total cross-section area related to the conductors into a slot is:

$$S_{Cuslot} = n_c \cdot S_c = 580 \cdot 0.45 = 261 \; [mm^2] \qquad (3.90)$$

and supposing a $k_{fill} = 0.4$ the total slot cross-section area results:

$$S_{slot} = \frac{S_{Cuslot}}{k_{fill}} = \frac{261}{0.4} = 652.5 \; [mm^2] \qquad (3.91)$$

The slot height could be evaluated as:

$$\begin{aligned} h_s &= \frac{Q_s}{2 \cdot \pi} \cdot \left\{ \sqrt{\left[\omega_s^2 + \frac{4 \cdot \pi}{Q_s} \cdot S_{slot} \right]} - \omega_s \right\} \\ &= \frac{15}{2 \cdot \pi} \cdot \left\{ \sqrt{\left[21^2 + \frac{4 \cdot \pi}{15} \cdot 652.5 \right]} - 21 \right\} = 24.9 \simeq 30 \; [mm] \end{aligned} \qquad (3.92)$$

The slot height has been increased because in this way the teeth shape will be more straight and the back-iron height will be the same as in the case of the DW PMARel motor. To complete the sizing of the slot the external slot width must be defined as:

$$\omega_{se} = \frac{\pi \cdot (D + 2 \cdot h_s)}{Q_s} - \omega_t = \frac{\pi \cdot (190 + 2 \cdot 30)}{15} - 20.59 = 31.77 \; [mm] \qquad (3.93)$$

As far as the back iron height is concerned it could be expressed as:

$$h_{bi} = \frac{D_e - D - 2 \cdot h_s}{2} = \frac{290 - 190 - 2 \cdot 30}{2} = 20 \ [mm] \tag{3.94}$$

The winding factor k_w (assumed during the sizing) must be now correctly defined considering that the winding is a fractional-slot double layer one. The pitch factor and the distribution factor couldn't be calculated through the expressions used in the first chapter because those had validity only for the distributed winding. So they have been obtained through $Winding$ software:

- Distribution factor:

$$K_d = 1 \tag{3.95}$$

- Chording factor:

$$K_p = 0.866 \tag{3.96}$$

- Winding factor:

$$K_w = K_d \cdot K_p = 1 \cdot 0.866 = 0.866 \tag{3.97}$$

Through the star of slots method it is possible to define the winding slot matrix which will be used in the simulations. It is reported hereafter:

ka = [+0.5 -0.5 0 +0.5 -0.5 0 +0.5 -0.5 0 +0.5 -0.5 0 +0.5 -0.5 0];

kb = [0 +0.5 -0.5 0 +0.5 -0.5 0 +0.5 -0.5 0 +0.5 -0.5 0 +0.5 -0.5];

kc = [-0.5 0 +0.5 -0.5 0 +0.5 -0.5 0 +0.5 -0.5 0 +0.5 -0.5 0 +0.5];

The rotor has been considered the same of that used for the DW PMARel motor. To achieve, the motor geometry is reported in Fig. 3.14, and Table 3.9 shows the geometrical parameters:
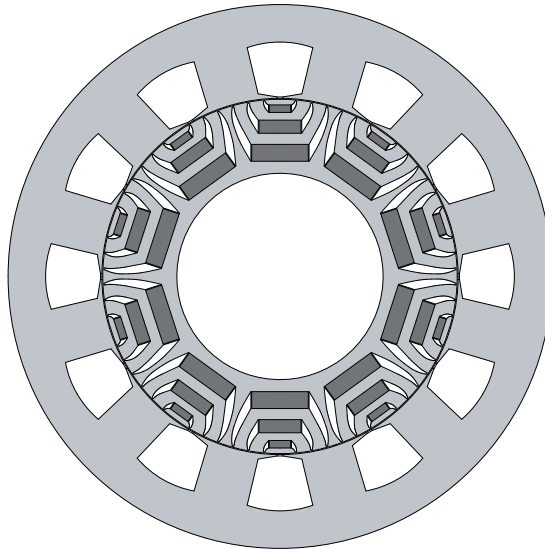
Figure 3.14: 15/10 PMARel section area

Table 3.9: 15/10 PMARel geometrical data

Symbol	Value	Unit	Stator
D_e	290	$[mm]$	Ext. diameter
D_i	190	$[mm]$	Inner diameter
Q_s	15	-	Slot number
w_t	20.59	$[mm]$	Tooth width
w_{so}	3.15	$[mm]$	Slot opening width
h_s	30	$[mm]$	Slot height
S_{slot}	652	$[mm^2]$	Slot area
			Common data
$2p$	10	-	Poles number
L_{stk}	145	$[mm]$	Stack length
g	0.5	$[mm]$	Air-gap thickness
			Rotor
D_r	189	$[mm]$	Diameter
R_{PM1}	89.48	$[mm]$	1st PM radius
h_1	4	$[mm]$	1st PM height
w_1	11.4	$[mm]$	1st PM width
R_{PM2}	79.83	$[mm]$	2nd PM radius
h_2	7	$[mm]$	2nd PM height
w_2	22.4	$[mm]$	2nd PM width
R_{PM3}	65.93	$[mm]$	3rd PM radius
h_3	9	$[mm]$	3rd PM height
w_3	30.2	$[mm]$	3rd PM width
r	0.4	$[mm]$	Ribs thickness

3.4.2 Simulations

Also for this last motor configuration have been followed the same steps during the simulations. Remembering that $I = 5.38\ A$ and $n_{cs} = 290$, the peak currentt could be computed as:

$$\widehat{I}_{slot} = I \cdot n_{cs} \cdot \sqrt{2} = 5.38 \cdot 290 \cdot \sqrt{2} \simeq 2207\ [A] \tag{3.98}$$

The motor has been done working at MTPA conditions and the current angle results to be $\alpha_{ie} = 50\ deg$ electrical degrees. The torque behaviour has been analyzed from $0\ deg$ to $12\ deg$ mechanical degrees and both Maxwell torque and d-q torque have been considered. The results are shown in Fig.3.15 and from this behaviour it results:

Average Maxwell Torque = 113 Nm
Average d-q torque = 111.1 Nm
Torque ripple = 63.48 %
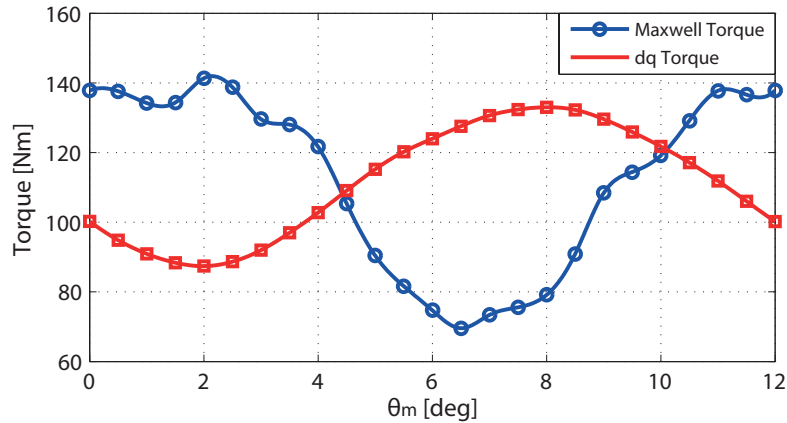
Figure 3.15: Torque value for different mechanical angles calculated through Maxwell stress tensor and d-q reference at nominal conditions. PMARel motor with 15 stator slots and 10 poles

It must be highlighted how the results are similar to those ones related to Sect.3.3. This is because both those motors belong to the reference configuration 3-slots/ 2-poles. The losses in terms of average torque respect the one supposed at the beginning of the sizing are about 32 %. An harmonic analysis has been done to have a deeper point of view about the torque behaviour. The results are shown in Fig.3.16:
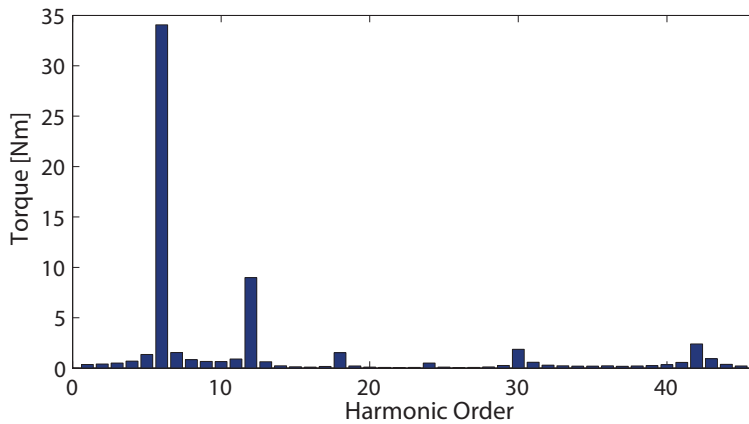
Figure 3.16: Torque ripple harmonic analysis of a PMARel motor with 15 stator slots and 10 poles

The harmonic that greatly influences on the torque behaviour is the 6$^{\text{th}}$. This could be observed also in Fig.3.15 where is represented the presence of one period in 60 *deg* mechanical degrees. Consequently this means that in 360 *deg* mechanical degrees there will be 6 periods. The Maxwell torque is a little distorted from the sinusoidal shape and this is due to the presence of the harmonics of 12$^{\text{th}}$, 18$^{\text{th}}$, 30$^{\text{th}}$ and 42$^{\text{th}}$ order.

Some considerations must be done about the back iron. Infact this doesn't properly saturate, reaching an induction of 1.2 T. This happens because during the sizing, the back iron thickness has been increased. The PMs haven't problems about degmagnetization.

The two torque components have been segregated due to the reluctance and due to the

PMs. The results are shown in Fig.3.17 and from the analysis of the behaviours of these two amounts it is possible to find out that:

Average PMs Torque = 28.8 Nm
PMs torque ripple = 14.39 %

Average REL torque = 84.3 Nm
Reluctance torque ripple = 60.29%
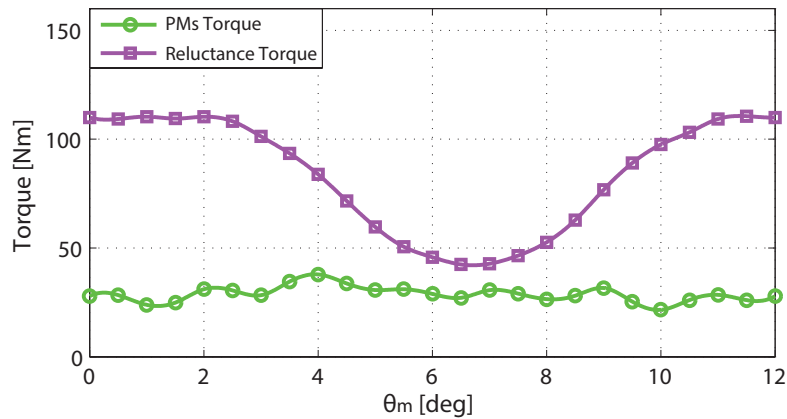
Figure 3.17: PMs torque and reluctance torque values for different mechanical angles related to Maxwell torque shown in Fig.3.15. PMARel motor with 15 stator slots and 10 poles

From an accurate observation it is possible to say that the reluctance torque is equal to 59 % if it is compared to the DW PMARel motor, while the PMs one remains almost the same. Besides, in contrast with all the other cases, the PMs torque ripple is considerably lower than the one related to the reluctance torque. This because at 7 *deg* mechanical degrees there is a marked reluctance torque minimum. Overall it's clear how the maximums and the minimums of the Maxwell torque agree with the ones of PMs torque at the same rotor position. The secondary maximums are linked to the reluctance torque.

3.5   Final considerations

A comparison is carried out among these different motor configurations:

- the results obtained are summarized in Tab.3.10

Table 3.10: Comparison among the different configurations of FCSW PMARel motor analyzed in terms both of torque performance

	9/8 (t=1)	12/8 (t=4)	12/10 (t=1)	15/10 (t=5)
Avg Torque [Nm]	106.5	122.6	103.5	113
Torque Ripple [%]	16.29	56.95	23.73	63.48
PMs Torque [Nm]	36.4	25.5	30.5	28.8
Reluctance Torque [Nm]	70.2	100.4	73	84.3

The attention must be focused on the motor periodicity which is computed as:

$$t = M.C.D\{Q_s, p\} \tag{3.99}$$

It is clear how the average torque and the torque ripple are lower in motors with periodicity equal to $t = 1$, while with higher periodicity they increase. In particular, the torque ripple increases more than the average torque. The 12/8 and 15/10 motors belong also to the same motors group. Both of them have as basic configuration the 3-slots/2-poles one. This is the reason that why they have comparable performance;

- From the harmonic analysis, it has been highlighted the presence of the same harmonic order. The torque ripple is always due to the multiples of the 6$^{\text{th}}$ harmonic. What changes was the main one. In fact in Sect.3.1 (9/8 PMARel motor) has more influence the 18$^{\text{th}}$ harmonic, in Sect.3.2 (12/8 PMARel motor) and Sect.3.4 (15/10 PMARel motor) the 6$^{\text{th}}$ harmonic while in Sect.3.3 (12/10 PMARel motor) the 12$^{\text{th}}$ one. It is again evident the similarity between the two motors with the same basic configuration slot/pole = 3/2;

- as far as the average torque is concerned, in all the configurations the reduction respect to the DW PMARel motor has been due to the high reduction of the reluctance torque component. The PMs torque component exhibits similar behaviour indipendently from the motor configuration. Only in Sect.3.2 (12/8 PMARel motor) the configuration exhibits an unexpected evolution.

Chapter 4

Tooth cut

The comparison between the DW PMARel motor and the FCSW PMARel motors has shown the difference in terms of average torque and the reason why this happens. The torque ripple problem is increased in the FCSW motors because of a concentrated M.M.F wave. The stator M.M.F. harmonics interact with the rotor anisotropic geometry. In the following chapter a technique is proposed to reduce this problem. In particular it will be seen how a change of the stator tooth shape could influence the torque ripple.

4.1 Problem opening

The first change which has been done in all the FCSW PMARel motors has been to define a different shape of the stator tooth. The reason of this deals with the observation of the torque contribution of each pole to the average torque. In particular, it must be highlighted that there are poles which induce a torque contrary to the motor rotation wise. They act as a brake, reducing the average torque. Focusing the attention on the flux lines related to each pole it has been studied how they are at the bottom of this phenomenon. It could be seen also in Fig.4.1: in some poles, when the flux lines cross the air-gap and go within the teeth shoe, they are bended so that they push in the wrong direction.
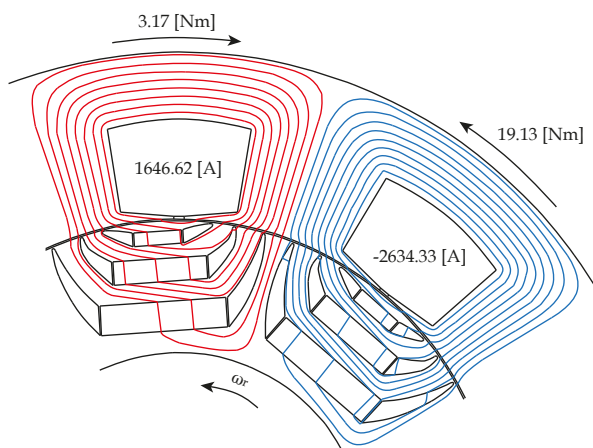
Figure 4.1: Detail related to different torque behaviours of two consecutive poles in a fractional-slot PMARel motors with 9 slots/ 8 poles configuration. The pole which has been highlighted with the red flux lines has an anomalous torque contribute.

The pole with the red flux lines generates a torque opposed to the one of the pole with the blue flux lines. This is due to the poles tendency to reach the position with lower reluctance to support a better flow of the flux lines. This is explained by the Hopkinson law as follow:

$$N \cdot I = \Re \cdot \phi \tag{4.1}$$

where $N \cdot I$ is the magnetic voltage, $\Re$ the reluctance and ϕ the flux. In particular in the motors which have been analyzed the magnetic voltage must be considered always fixed and so, if the reluctance is reduced, then the flux increases.

In order to decrease this behaviour, different kinds of tooth cut have been analyzed to understand which could be the best one in terms of improvement on torque performance. This technique influences the $L_d - L_q$ difference and the air-gap thickness and as a consequence also the torque performance. Anyway, if in some rotor mechanical positions this solution solves the problem, in others it produces higher ripple.

4.2   Configuration with 9 stator slots and 8 poles

At first, let us investigate the 9 slots/ 8 poles. Three different kinds of tooth cut have been considered:

- the first one exhibits a cut on the right side of the tooth. In particular it has been decided to cut the height related to the opening slot ($h_{so} = 0.75 \ mm$), by reducing it of a value $h_{cut} = 0.4 \ mm$. Besides the angular sector chosen has been the one between the symmetrical stator slot axis and the symmetrical axis of the tooth. In this configuration it is:

$$\gamma_{cut} = \frac{360}{2 \cdot Q_s} = \frac{360}{2 \cdot 9} = 20 \ [deg] \tag{4.2}$$

and the shape adopted has been that of an arch as it is shown in Fig.4.2:
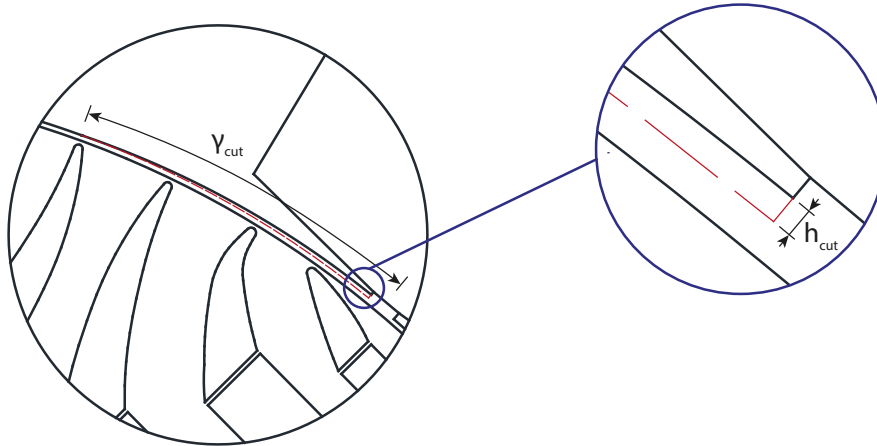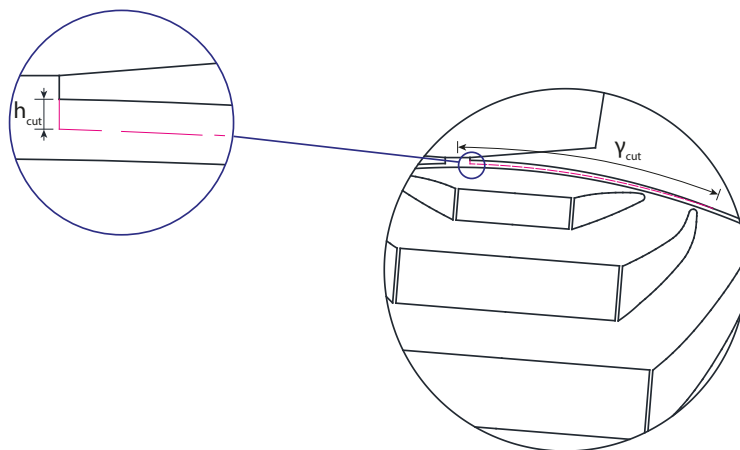

Figure 4.2: Detail related to the teeth cut on the right side. The dash red line shows the reference teeth shape, while the black line is related to the final shape of the teeth shoe

It must be considered that this solution jeopardised the machine symmetry so that it is not optimized to operate in both clockwise and anticlockwise directions, but only in one of them.

From the simulations it has been seen that, also if this is a minimal change in the machine geometry, the current angle related to the MTPA operating point changes a lot. In fact it moves from $\alpha_{ie} = 37\ deg$ to $\alpha_{ie} = 47\ deg$. The peak current remains the same, simulating the new motor for a 15 deg mechanical degrees variation, the results reported in Fig.4.3 have been obtained. Also if there are no more symmetries the range of mechanical degrees simulated could be again considered equal to 15 deg because the teeth cut doesn't introduce strong changes in this sense.
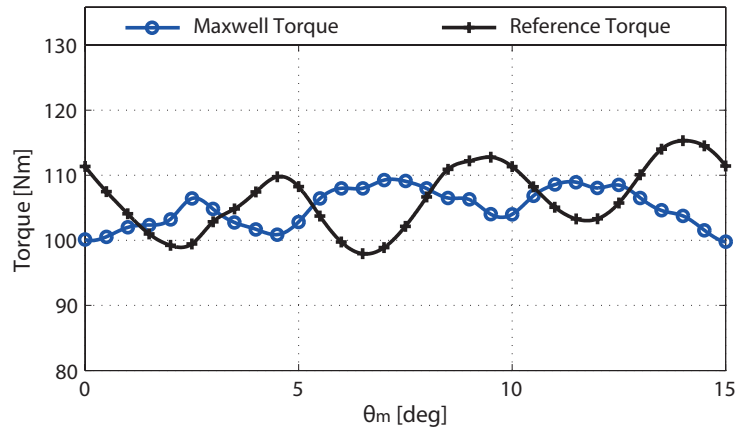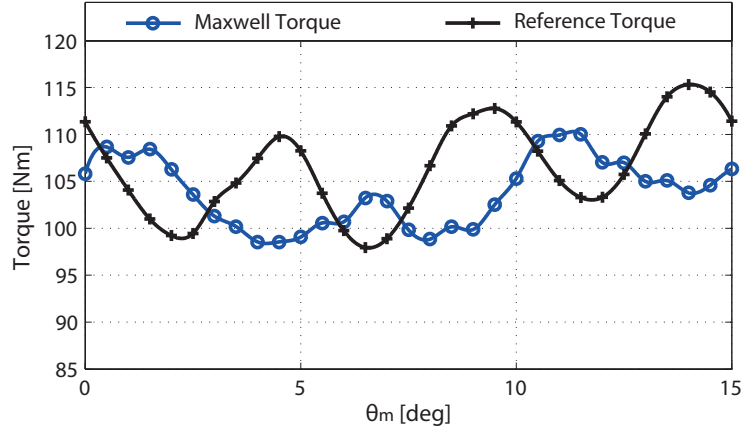

Figure 4.3: Torque value for different mechanical angles calculated through Maxwell stress tensor at nominal conditions. It is compared to the Maxwell torque of the reference PMARel motor. PMARel motor with 9 stator slots and 8 poles after the tooth cut technique.

It results:

Average Maxwell Torque = 105 Nm

Average d-q torque = 105.2 Nm

Torque ripple = 9.03 %

Both average torque and torque ripple decrease if compared with the reference PMARel motor with the same configuration. In particular, the torque ripple is quite halved, while the average torque decreases slightly. This last one effect is due to the larger air-gap introduced and to the $L_d - L_q$ difference which characteristic is shown in Fig.4.4:
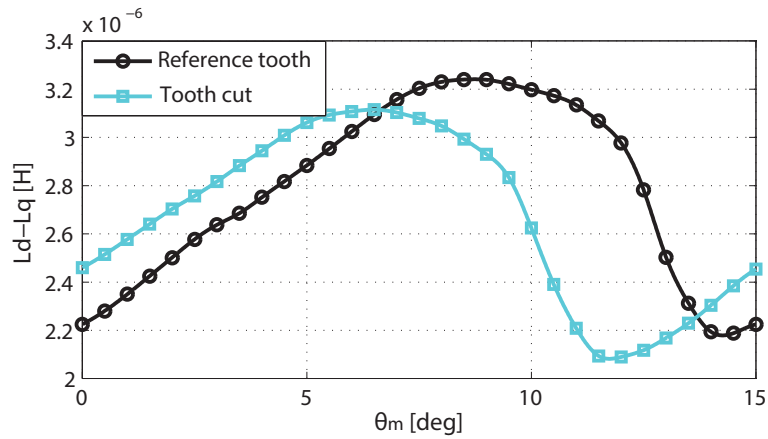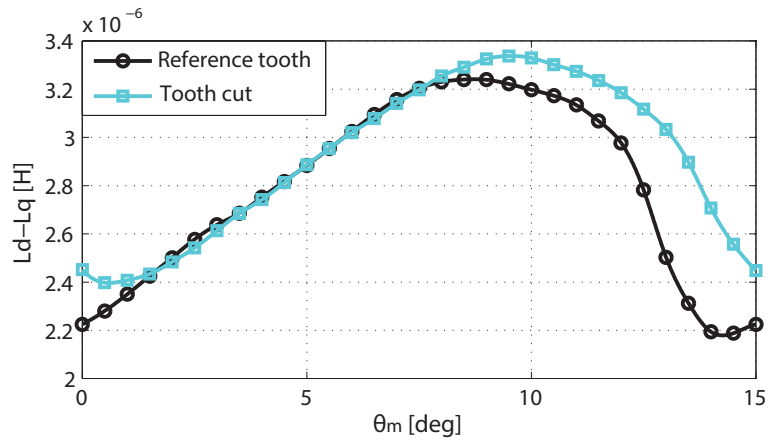
Figure 4.4: Difference between the inductance of D-axis and Q-axis for different mechanical angles at nominal conditions. It is compared the behaviour related to the reference teeth shape with the one related to the teeth cut. PMARel motor with 9 stator slots and 8 poles.

From the comparison with the reference PMARel motor it is clear that with the new tooth geometry it has been changed the magnetic circuit properties and in particular the inductances related to D-axis and Q-axis. As a consequence, their difference has been reduced between 6.5 deg and 13.5 deg mechanical degrees influencing the reluctance torque. It is evident how the two behaviour could be considered out of phase of about 2.5 deg mechanical degrees. Besides the Maxwell torque behaviour seems to be out of phase of about 2 deg mechanical degrees if compared with the reference one.

• the second kind of cut presents has been done on the left side of the tooth. A cut height and an angular sector have been chosen as done before. The shape adopted has been again that of an arch and it is all shown in Fig.4.5:
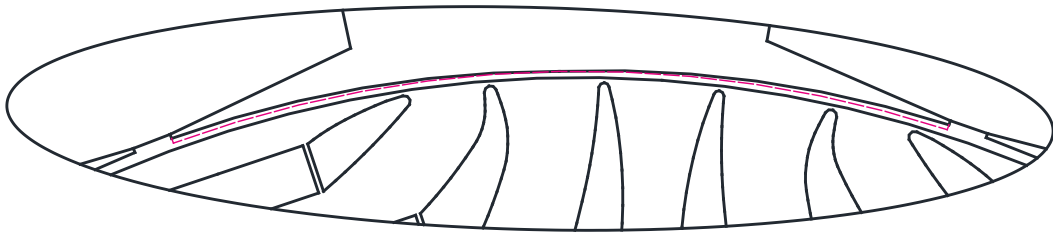

Figure 4.5: Detail related to the teeth cut on the left side. The dash red line shows the reference teeth shape, while the black line is related to the final shape of the teeth shoe

Also in this case the symmetry of the motor has been jeopardized with a small

change on the tooth shoes shape. Again for this reason the PMARel motor could be simulated for a 15 *deg* mechanical degrees variation. The current angle related to the MTPA operating point changes. It moves from $\alpha_{ie} = 37\ deg$ to $\alpha_{ie} = 32\ deg$. The peak current into the slots is kept to be constant. The results are shown in Fig.4.6:
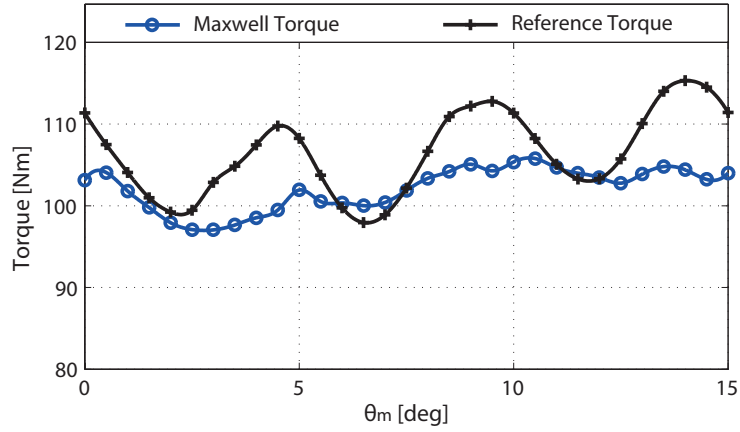

Figure 4.6: Torque value for different mechanical angles calculated through Maxwell stress tensor and at nominal conditions. It is compared to the Maxwell torque of the reference PMARel. PMARel motor with 9 stator slots and 8 poles after the tooth cut technique.

It results:

Average Maxwell Torque = 103.9 Nm

Average d-q torque = 103.1 Nm

Torque ripple = 11.04 %

It is clear how the torque ripple decreases again if compared to the reference PMARel motor with the same configuration. The average torque is lower than when the tooth cut has been done on the right side. This is due to the $L_d - L_q$ difference which has been shown in Fig.4.7 and whose effect must be summed to the one due to the higher air-gap introduced.

From the comparison of the two behaviours it could be seen how the $L_d - L_q$ difference in the motor with the teeth cut on the left is higher than the one related to the reference PMARel motor with the same configuration. This means that the average torque must be increased, but the increase of the air-gap balances the inductances effect decreasing again the average torque.
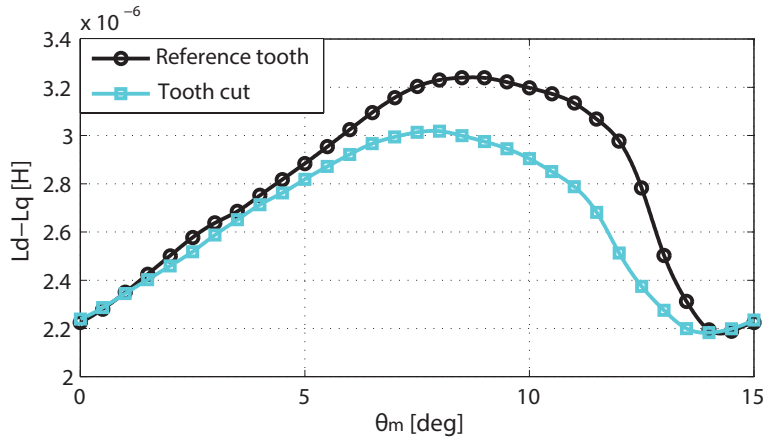
Figure 4.7: Difference between the inductance of D-axis and Q-axis for different mechanical angles at nominal conditions. It is compared the behaviour related to the reference teeth shape with the one related to the teeth cut. PMARel motor with 9 stator slots and 8 poles.

- the last kind of tooth cut was the union of the two analyzed before. This has been done because in this way the symmetry of the motor will remain without going to limit its rotation wise. In fact, both anticlockwise and clockwise will be again possible. The shape adopted has been reported in Fig.4.8:

Figure 4.8: Detail related to the teeth cut on the both sides. The dash red line shows the reference teeth shape, while the black line is related to the final shape of the teeth shoe

The peak current into the slots doesn't change and its current angle related to the MTPA operating point moves from $\alpha_{ie} = 37 \ deg$ to $\alpha_{ie} = 39 \ deg$. Since the symmetry has been kept the motor could be simulated for a 15 deg mechanical degrees variation. The results that have been computed are shown in Fig.4.9. From the elaboration of the values highlighted in this torque behaviour it is possible to obtain:

Average Maxwell Torque = 102 Nm

Average d-q torque = 101.7 Nm

Torque ripple = 8.56 %

Figure 4.9: Torque value for different mechanical angles calculated through Maxwell stress tensor and d-q reference at nominal conditions. It is compared to the Maxwell torque of the reference PMARel motor. PMARel motor with 9 stator slots and 8 poles after the tooth cut technique.

This solution yields the lowest torque ripple because it reaches the lower value among the three computed. However it must be considered that the average torque is also the lower one and compared to the reference PMARel motor, it is about 4 % lower. It could be an acceptable loss if it is considered the conservation of the symmetry and the good torque ripple reached. The reason of this torque reduction must be valued through the $L_d - L_q$ difference which behaviour is reported in Fig.4.10:

Figure 4.10: Difference between the inductance of D-axis and Q-axis for different mechanical angles at nominal conditions. It is compared the behaviour related to the reference teeth shape with the one related to the symmetrical teeth cut. PMARel motor with 9 stator slots and 8 poles.

The characteristic related to the teeth cut is always lower than the one referred to the reference PMARel motor with the same configuration. As a consequence the reluctance torque is decreased and this effect, if it is summed to the one due to the higher air-gap, leads to the lowest average torque among the three cases that have been analyzed. This is increased also because the $L_d - L_q$ difference, if compared with

the same parameter in the other kinds of tooth cut, is never higher than the one of the reference PMARel motor. A deep harmonic analysis of the torque behaviour must be done to understand on which component of the harmonic order this technique has influence. In Fig.4.11 has been shown the comparison between the harmonics related to the reference PMARel motor and the one on which has been applied the tooth cut. It is clear that the 18th harmonic is strongly decreased and that also the harmonic of 24th and 30th order have lower influence on torque ripple. This is the reason of the improvement of the torque ripple performance, supported also by the value related to the harmonic of 6th and 12th order which remain almost the same.
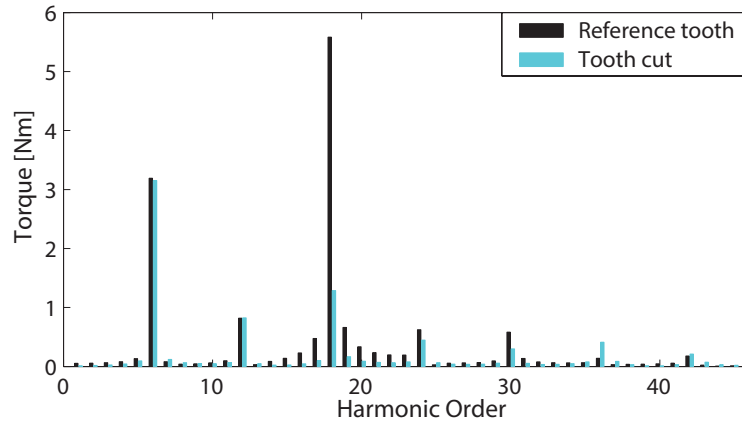
Figure 4.11: Harmonic order comparison between the reference PMARel motor and the PMARel motor with the tooth cut. Both having 9 stator slots and 8 poles.

To better understand the origin of this harmonic reduction about the torque ripple it has been decided to analyse the harmonic spectrum of the stator M.M.F. This last one is on the base of the harmonic pollution due to the excitation. So, focusing the attention on this aspect it could be understood on which harmonics the tooth cut acts. To do so, the motor has been simulated in linear conditions with the relative permeability of the iron fixed equal to $\mu_r = 7000$ and the rotor composed only by iron without any barriers and PMs. In this way in the air-gap there is the only presence of the M.M.F. due to the stator currents. The same has been done for the reference PMARel motor with the same configuration and the comparison between the two harmonic spectrums is shown in Fig.4.12.

It is worth to notice that this technique influences the amplitude of the slot harmonics. They are the harmonics on which the winding arrangement has no effect and could be calculated according to the following relationship:

$$\nu_{sh} = k \cdot Q_s \pm p \tag{4.3}$$

where k is an integral number, Q_s is the stator slots number and p is the pair-poles number. Since $Q_s = 9$, $p = 4$ and $k = 0, 1, 2, ...$ it is:

$$\nu_{sh} = 4, 5, 13, 14, 22, 23, 31, 32, 40, 41... \tag{4.4}$$

which are exactly the M.M.F harmonics that have reduced their amplitudes. This deals with the torque ripple reduction and partially explains it. In fact it must be

considered also the effect due by the iteraction of the other harmonics related to the stator winding with the rotor anisotropic geometry.
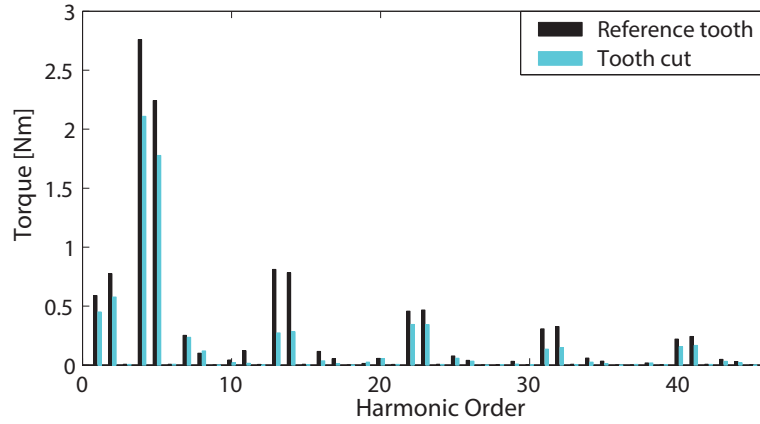

Figure 4.12: Stator M.M.F harmonic order comparison between the reference PMARel motor and the PMARel motor with the tooth cut. Both having 9 stator slots and 8 poles.

To conclude, this last one will be the new geometry applied to all the other FCSW PMARel motor o torque performance.

4.3   Configuration with 12 stator slots and 8 poles

Also in this configuration the tooth shape introduced is the symmetrical one. It has been decided again to chose a cut height related to the opening ($h_{so} = 0.75\ mm$), by reducing it of a value $h_{cut} = 0.4\ mm$. The angular sector chosen has been the one between the stator slot axis of symmetry and the tooth one. In this way both the anticlockwise and the clockwise are available. The stator slots cross-section area doesn't change and so the peak current remains the same. Instead the current angle related to the MTPA operating point moves from $\alpha_{ie} = 37\ deg$ to $\alpha_{ie} = 48\ deg$. The motor has been simulated for a range of mechanical degrees equal to 15 deg and the results which have been computed are shown in Fig.4.13.
It results:

Average Maxwell Torque = 115.5 Nm
Average d-q torque = 114.3 Nm
Torque ripple = 60.02 %
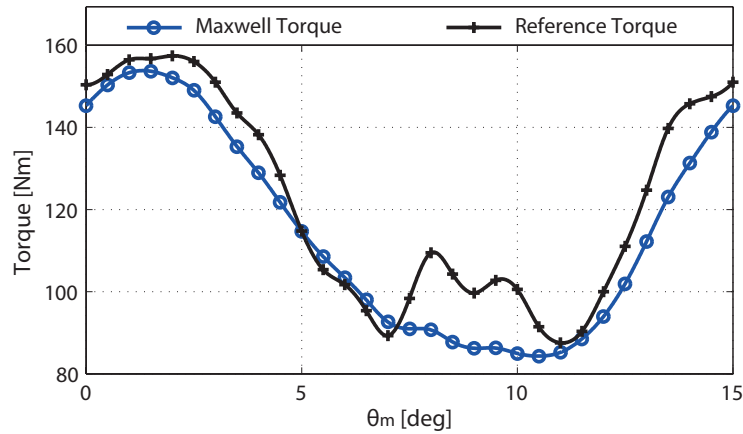
Figure 4.13: Torque value for different mechanical angles calculated through Maxwell stress tensor and d-q reference at nominal conditions. They are compared to the Maxwell torque of the reference PMARel motor. PMARel motor with 12 stator slots and 8 poles after the tooth cut technique

If compared with the reference PMARel motor with the same configuration it could be seen how the torque performance is worst than before. The average torque has been decreased while the torque ripple is increased about the 4 %. The reason of this must be studied focusing the attention on the $L_d - L_q$ difference which has been reported in Fig.4.14:
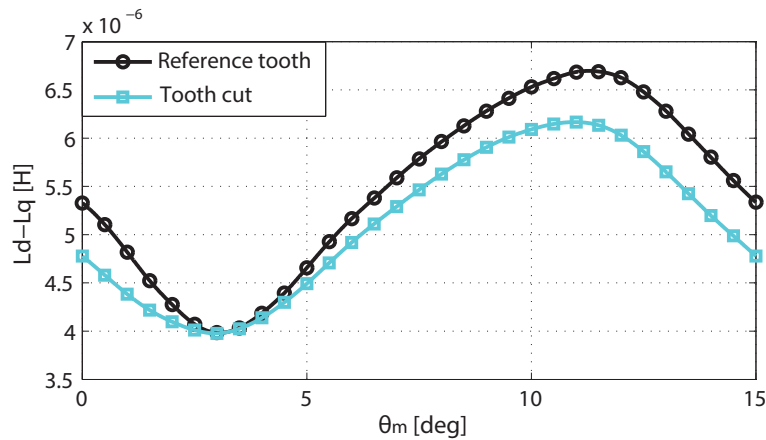
Figure 4.14: Difference between the inductance of D-axis and Q-axis for different mechanical angles at nominal conditions. It is compared the behaviour related to the reference teeth shape with the one related to the symmetrical teeth cut. PMARel motor with 12 stator slots and 8 poles

The behaviour due to the tooth cut reaches lower values of inductances respect to the one related to the reference PMARel motor. Besides, if to this effect is summed the one due to the higher air-gap thickness, this explains why the average torque is lower of about the 6 %. As far as the torque ripple is concerned, the swinging which were presented between 7 deg and 11 deg mechanical degrees are deleted. In this way the characteristic is more gradual. The minimum and the maximum change. In particular the minimum has a greater value than the reference PMARel motor, while the maximum has a lower value.

This explains why the torque ripple is a few increased. To better understand the influence of this technique on the torque ripple it must be observed the harmonic order which has been reported in Fig.4.15.
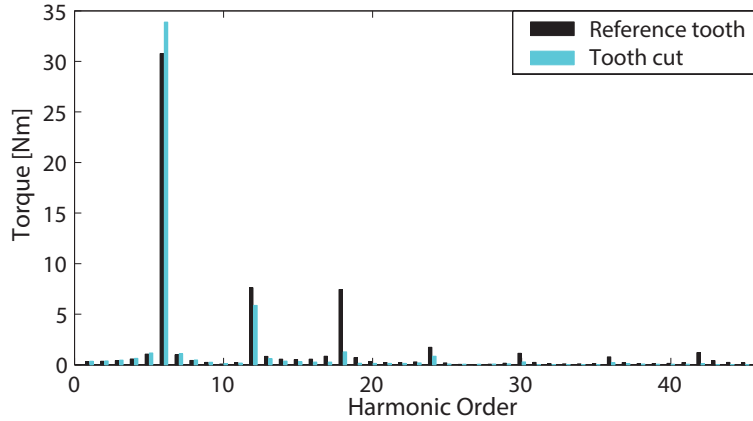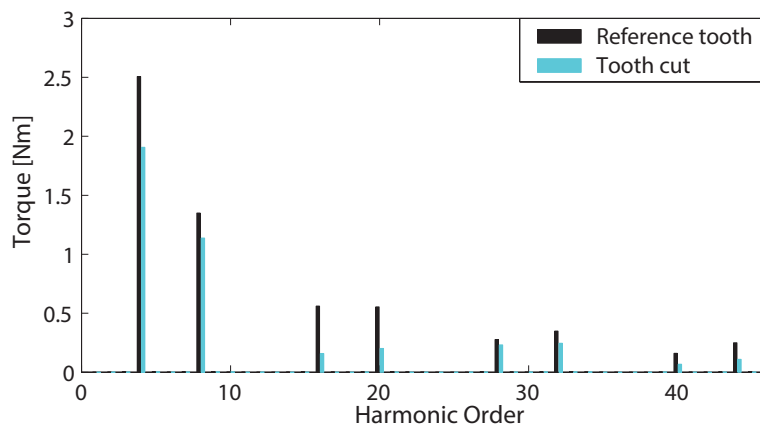

Figure 4.15: Harmonic order comparison between the reference PMARel motor and the PMARel motor with the tooth cut. Both having 12 stator slots and 8 poles

From the comparison of the harmonic orders related to the reference PMARel motor and the one with the tooth cut it must be done some considerations. The new technique has a good effect on the secondary harmonics as the 12th, 18th and 24th. There is an improvement of the torque ripple, but the 6th harmonic (which is the main one) increases up to delete the previous benefit. The tooth cut technique has the main effect on the 18th harmonic. As in Sect.4.2 a deeper harmonic analysis has been done about the stator M.M.F.

Always in linear condition, fixing that $\mu_r = 7000$ and considering the rotor made up completely by the Terni iron has been computed from simulations the harmonic spectrum of the machine before and after the tooth cut technique. The results are shown in Fig.4.16:

Figure 4.16: Stator M.M.F harmonic order comparison between the reference PMARel motor and the PMARel motor with the tooth cut. Both having 12 stator slots and 8 poles

Also in this kind of FCSW PMARel motor configuration it is clear how this technique acts on the slot harmonics. From (4.3) it could be obtained that:

$$\nu_{sh} = 4, 8, 16, 20, 28, 32, 40, 44... \qquad (4.5)$$

The slot harmonics reduction doesn't deal with the torque ripple which remains almost the same. There are the stator M.M.F. interacting with rotor M.M.F harmonics balancing out the positive effects introduced by the tooth cut. Other solutions must be tried to improve the torque performance of this kind of motor configuration.

4.4   Configuration with 12 stator slots and 10 poles

For this kind of PMARel motor configuration could be done the same geometrical considerations described in Sect.4.3. As far as the peak current is concerned it remains the same, while the current angle related to the MTPA conditions moves from $\alpha_{ie} = 37\ deg$ to $\alpha_{ie} = 48\ deg$. Considering that the number of poles has been changed, deals with (1.42), could be found that the PMARel motor must be simulated for mechanical degrees interval equal to 12 deg. The results are shown in Fig.4.17.
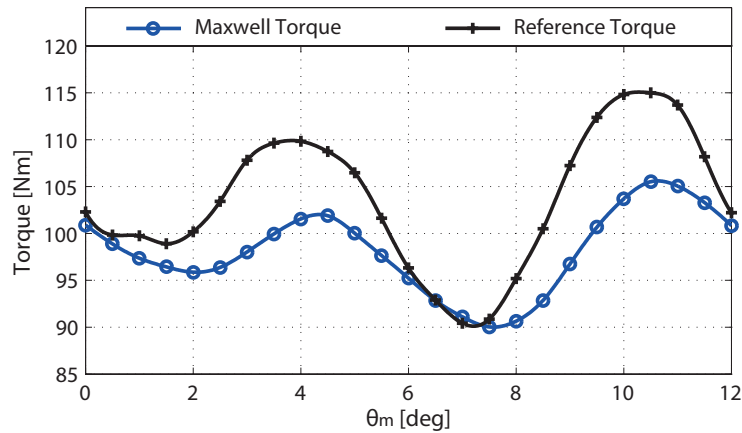
Figure 4.17: Torque value for different mechanical angles calculated through Maxwell stress tensor and at nominal conditions. They are compared to the Maxwell torque of the reference PMARel motor. PMARel motor motor with 12 stator slots and 10 poles after the tooth cut technique

It results:

Average Maxwell Torque = 98.1 Nm
Average d-q torque = 97.6 Nm
Torque ripple = 15.77 %

If compared with the reference PMARel motor with the same configuration it could be seen how the average torque is lower. In particular, this effect deals with all the previous analysis which has been done in Sect.4.2 and in Sect.4.3. In fact this is due again to the sum of the effects related to the higher air-gap thickness and to the $L_d - L_q$ difference as it has been shown in Fig.4.18:
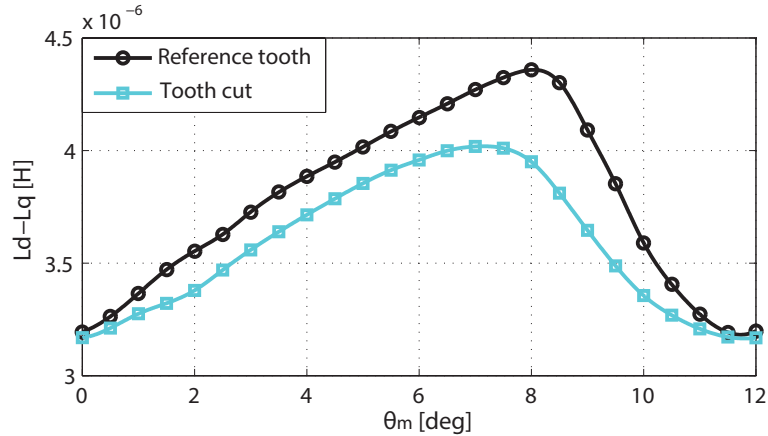

Figure 4.18: Difference between the inductance of D-axis and Q-axis for different mechanical angles at nominal conditions. It is compared the behaviour related to the reference teeth shape with the one related to the symmetrical teeth cut. PMARel motor with 12 stator slots and 10 poles

Also for this motor configuration it is evident how the inductances behaviour related to the PMARel motor with the tooth cut is always lower in amplitude than the reference one. This for all the mechanical interval which has been simulated. This validates the average torque reduction. Instead the torque ripple has been improved due to the Maxwell torque behaviour reported in Fig.4.17 is more flat. The minimum amplitude has been remain almost the same, while the maximum one has been strongly reduced. The reason of this torque behaviour deals with the harmonic analysis which has been done. It is shown in Fig.4.19:
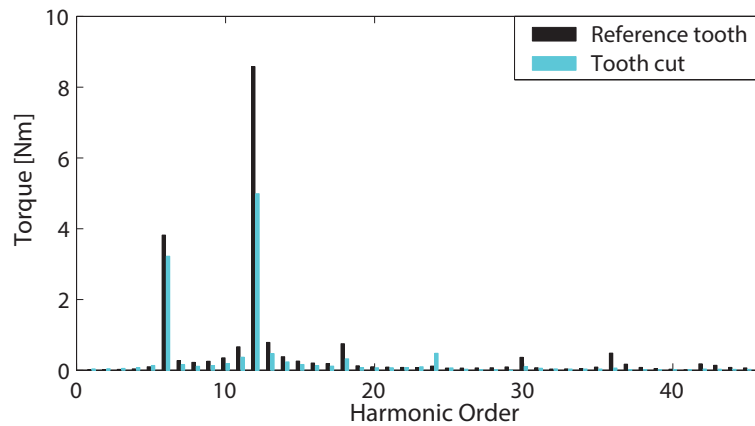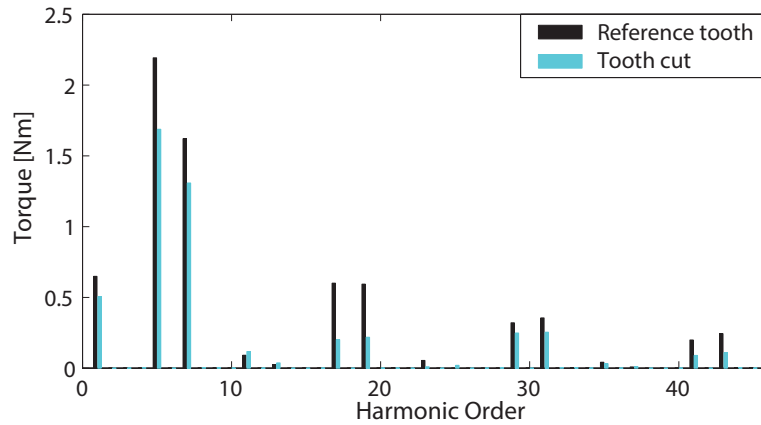

Figure 4.19: Harmonic order comparison between the reference PMARel motor and the PMARel motor with the tooth cut. Both having 12 stator slots and 10 poles

The tooth cut influences the 12$^{\text{th}}$ (which is the main harmonic) and the 6$^{\text{th}}$ one. In particular the first has been quite halved, while the second one has been slightly decreased. As far as the others secondary harmonics are concerned as the harmonic of 18$^{\text{th}}$, 30$^{\text{th}}$ and 36$^{\text{th}}$ order they could be considered deleted. In the reference PMARel motor there wasn't the 24$^{\text{th}}$ harmonic which now must be considered. It have been decided to focus the attention on the stator M.M.F. harmonic spectrum. This to understand if this technique has effects on the harmonics due to the excitation. In particular it has been all done in linear conditions, fixing $\mu_r = 7000$ and considering the rotor made up completely by the Terni iron. The results computed are shown in Fig.4.20:

Figure 4.20: Stator M.M.F harmonic order comparison between the reference PMARel motor and the PMARel motor with the tooth cut. Both having 12 stator slots and 10 poles

Deal with (4.3) and considering that $Q_s = 12$, $p = 5$ and $k = 0, 1, 2...$ could be obtained that:

$$\nu_{sh} = 5, 7, 17, 19, 29, 31, 41, 43... \tag{4.6}$$

which are exactly the stator M.M.F. harmonics that have reduced their amplitudes. This deals with the torque ripple reduction and partially explaines it. In fact, it must be considered also the effect due by the iteration of the other harmonics related to the stator winding with the rotor M.M.F due to the rotor anisotropic geometry.

4.5   Configuration with 15 stator slots and 10 poles

The geometrical changes which have been done are again related to the tooth cut. The peak current has been kept fixed at the same value, while the current angle chosen to work in MTPA conditions moves from $\alpha_{ie} = 37\ deg$ to $\alpha_{ie} = 50\ deg$. As far as the mechanical interval is concerned, it has been fixed equal to 12 deg. This is on the base of the expression (1.42). The results which have been obtained are shown in Fig.4.21:
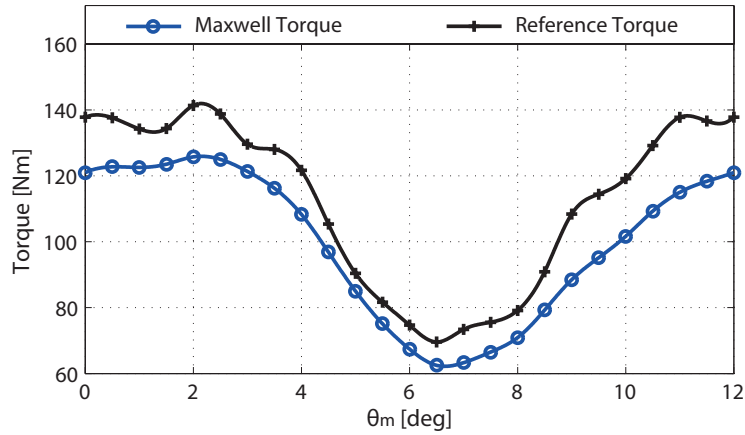
Figure 4.21: Torque value for different mechanical angles calculated through Maxwell stress tensor and at nominal conditions. They are compared to the Maxwell torque of the reference PMARel motor. PMARel motor with 15 stator slots and 10 poles after the tooth cut technique

It results:

Average Maxwell Torque = 100 Nm
Average d-q torque = 98.6 Nm
Torque ripple = 63.21 %

From the comparison between the torque behaviour related to the reference PMARel motor and the one referred to the Maxwell torque of the PMARel motor with the tooth cut it is possible to notice that the two curves are almost the same. They are shifted one from each other. This explains why the torque ripple doesn't change and the average torque decreases. In particular, this last one effect is again due to the $L_d - L_q$ difference. It is possible to see in Fig.4.22 how this parameter is lower than before after the tooth cut. Also the effect due to the air-gap thickness increase deals with the average torque drop.
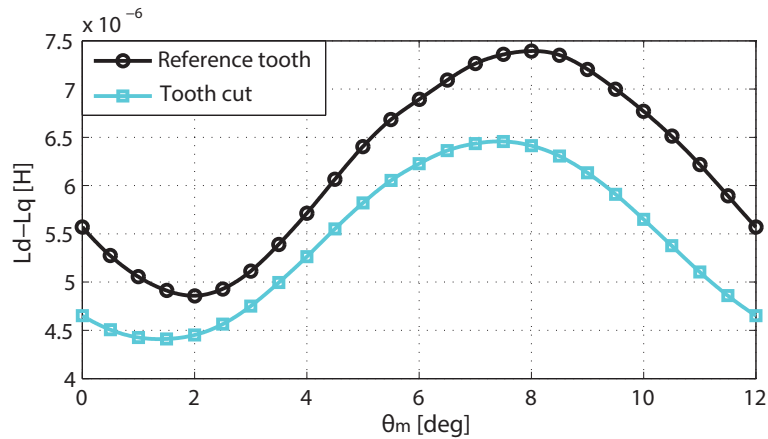
Figure 4.22: Difference between the inductance of D-axis and Q-axis for different mechanical angles at nominal conditions. It is compared the behaviour related to the reference teeth shape with the one related to the symmetrical teeth cut. PMARel motor with 15 stator slots and 10 poles

Finally has been simulated the motor in linear conditions, fixing $\mu_r = 7000$ and considering the rotor made up completely by the Terni iron without barriers and PMs. This to compute the harmonic spectrum of the only stator M.M.F. The results are shown in Fig.4.23:
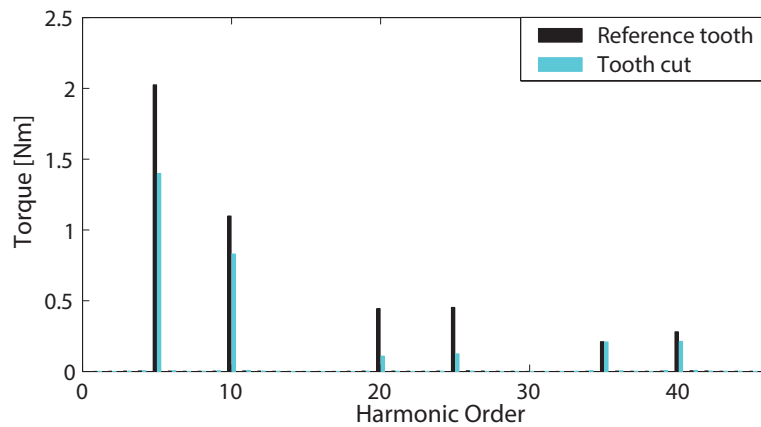
Figure 4.23: Stator M.M.F harmonic order comparison between the reference PMARel motor and the PMARel motor with the tooth cut. Both having 15 stator slots and 10 poles.

Also in this kind of FCSW PMARel motor configuration the tooth cut technique has influence on the slot harmonics. In fact, its effect deals with the solution given by (4.3). Considering that $Q_s = 15$, $p = 5$ and $k = 0, 1, 2...$ it is possible to compute analytcally the slot harmonic order which corresponds to:

$$\nu_{sh} = 5, 10, 20, 25, 35, 40... \tag{4.7}$$

As in Sect.4.3 the slot harmonics reduction doesn't deal with the torque ripple which remains almost the same. This because there are the harmonics due to the winding factor

which interact with the ones of the rotor M.M.F balancing out the positive effects introduced by the tooth cut. Other solutions must be tried to improve the torque performance of this kind of motor configuration.

4.6   Final considerations

At the end of the analysis for all FCSW PMARel motor configurations a comparison it could be done. In particular this is reported in Table.4.1:

Table 4.1: Comparison between reference FCSW PMARel motor configurations and those with the tooth cut

	Maxwell Average Torque [N·m]	Torque Ripple [%]
Reference 9/8	106.5	16.29
9/8 Tooth Cut	102	8.56
Reference 12/8	125.96	59.02
12/8 Tooth Cut	115.5	60.04
Reference 12/10	103.5	23.73
12/10 Tooth Cut	98.1	15.77
Reference 15/10	113.1	63.48
15/10 Tooth Cut	100.8	63.21

Starting from this comparison in terms of torque performance some considerations about this technique could be done:

- among the different kinds of tooth cut the symmetrical cut results to be the best one. In fact, also if it deals with the worst average torque, it must be considered that the torque ripple could be improved or could remain almost the same. Besides the rotation wise isn't limited;

- in all PMARel motors configurations the $L_d - L_q$ difference is decreased by the symmetrical tooth cut and this is at the base of the average torque drop;

- the improvement of torque ripple is reached only for the FCSW PMARel motors configurations with low periodicity (i.e. $t = 1$). In particular it effects on the 18th harmonic;

- for the motors with high periodicity and in particular for those which belong to the 3 slots/ 2 poles family, this technique doesn't lead to any benefits. It only worsens or doesn't influence the average torque;

- in all the cases the tooth cut effects on the main harmonic of the harmonic order;

- if compared with the DW PMARel motor it is clear how some fractional-slot configurations have better torque ripple, but the average torque is lower about $33 \div 43$ % depending on the case;

- it always acts on the slot harmonics of the stator M.M.F independently from the FCSW PMARel motor configuration considered.

Chapter 5

Stator shifting increasing the slot number

After seeing that the *tooth cut technique* could reach some positive results only in fixed configurations, it has been tried to apply a new one which could have a better improvement in terms of torque performance in all the configuration.

5.1 The concept of stator shifting

As far as the FCSW PMARel motors are concerned the main problem to solve is that related to the higher torque ripple and lower average torque than the DW PMARel motors. The concept at the base of stator shifting technique is the harmonic cancellation and it has been introduced by *El-Refaie* in [7]. To reach this result two fractional-slot winding stators will be used belonging to the same slot/pole combination to form a combined machine having ower harmonics, while mantaining the torque producing capability. The two stators are shifted by an electrical angle α, and combined togheter to form the final machine, while the rotor is not changed. During the combination of the two stators, the slots of one stator will be inserted between the slots of the other stator and winding overlaps will occur. The two individual winding configurations presented in the final machine are placed in series with each other, so as to produce the maximum benefit of the final machine as well as to eliminate the possibility of circulating currents. In this way the final machine has a double a number of poles as each individual machine. The notation of the shift angle is indicative of the mechanical shift of the two stators. The shift angle α is defined as the electrical angle of the second shifted stator with respect to the first stator. They are shown in Fig.5.1:
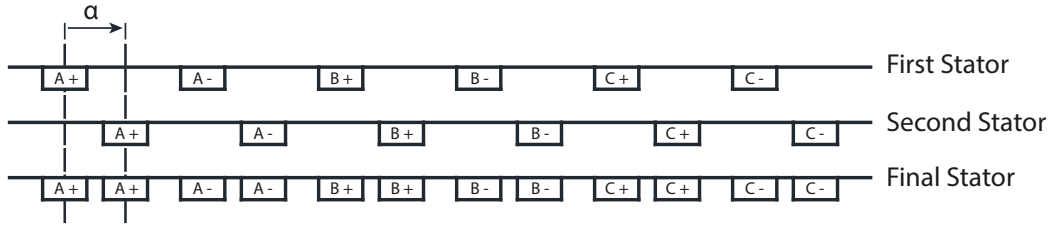
Figure 5.1: View, step by step, about the stator shifting concept. The α angle is due to the n harmonic number which must be deleted to improve the FCSW PMARel motor in terms of torque performance

Since the working harmonic of these FCSW machines is not the fundamental, care is to be taken in identifying the correct harmonic while defining the shift angle. The whole concept of the shift angle is aimed at the reduction of the harmonics in this kind of machines. While the initial design has a tooth winding and it is harmonically rich, the final design is expected to have a lower harmonic content and may not necessarily have a tooth winding. Differentiation with the distributed winding is a key benefit in these types of windings. While the coil pitch in the concentrated windings can be unity, the coil pitch in shifted windings is actually two. On the other hand, distributed windings can have coil pitch of at least three (in a one slot/pole/phase windings), reaching up to six in the widely used two slot/pole/phase windings. In other words, while tooth windings lie at one extreme of the spectrum with extremely short end-windings, and the traditional distributed windings lie at the other extreme with higher coil pitches. The proposed winding technique has coil pitch which will fall in between and hence has shorter end-windings that distributed windings, but longer end-windings than tooth windings.

In terms of stator harmonics the addition of the second stator can be understood as the addition of shifted harmonic to the similar harmonic of the first stator. In this way the synchronous harmonic of the first stator adds only to the synchronous harmonic of the second one. The final winding factor with the inclusion of the shift is explained using an attenuation factor (shift factor/distribution factor), which is a function of the electrical shift angle:

$$k_{final} = k_{initial} \cdot cos\left(\frac{n \cdot \alpha}{2 \cdot p}\right) \tag{5.1}$$

where α is the electrical shift angle for the working harmonic, n is the harmonic number and p is the number of poles in the machine. The variation of the attenuation factor is sinusoidal, which means that if proper shift angle is chosen, it is possible to minimize the winding factor for a particular harmonic. It must be noticed that multiple shift angles can result in similar values for the winding factor for a particular harmonic. It is significant to note that the attenuation factor is generic and can be applied to all slot/pole configurations. It is a powerful handle to reduce the harmonic content in the tooth windings, which can lead to the reduction in losses and improvement in the machine power density. Besides a reduction of the higher harmonics is expected to reduce the saturation effects and thereby improving the machine saliency. This dual effect is expected to have a considerable impact on the power density of the final machine.

In order to provide a meaningful study of the effect of stator shifting, the following design variables were kept constant between the reference PMARel motors and the ones where

will be applied the stator shifting:

- current density (6 A/mm^2);

- rotor structure;

- air-gap thickness;

- outer stator diameter.

The comparison between the motor with and without the stator shifting will be done in terms both of average torque and torque ripple.

The concept of stator shifting can also be generalized as the combination of two stators with n slots forming a final stator with $2n$ slots. The concept begins first with the identification of working harmonic. In a stator containing n slots, with p number of pole-pairs, the working harmonic is usually p. The stator shift angle is noted as the electrical angle by which the second stator would be shifted relative to the first stator. The units of the stator shift angle are in the electrical degreees of the p harmonic. In other words, if the electrical shift of the second stator is θ degrees the mechanical shift of the second stator is θ/p degrees. An example is of the steps done to achieve the final results is reported in Fig.5.2:
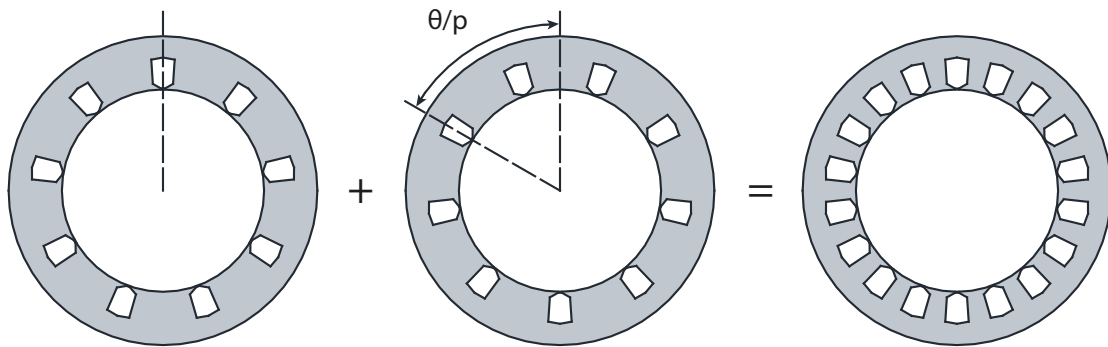
Figure 5.2: Example of stator shifting done on a stator lamination with 9 slots

If the electrical shift angle θ lies around 180 deg, it is obvious that the two working harmonics from either of the stators are equal and opposite and would cancel each other. The only two operable ranges for the final stator are the shift angles around 360 deg and 720 deg. In the first case in general the superharmonic is reduced while in the second range it is the fundamental one to be reduced. It must be remembered that the FCSW PMARel motors with double-layer windings (as all the reference ones previously designed) have a lower fundamental harmonic component than the single-layer windings. If in theory this technique could be realized for all the possible electrical shift angles, in practice this isn't always true. In fact the mechanical shift angle related to a particular electrical shift angle couldn't be possible for two reasons:

- the cross-section area of one slot intersects the one of the consecutive slot;

- the teeth thickness between two conecutive slots is too much thin and consequently this deals with iron saturation and mechanical problems.
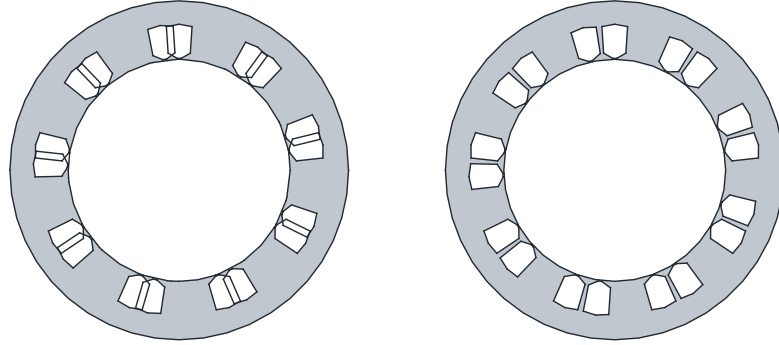
This two problems are shown in Fig.5.3:

Figure 5.3: Example of stator shifting problems on a stator lamination with 9 slots. On the left the stator slots intersect one with each other. On the right the teeth thickness between two consecutive slots is too much thin.

To extend the method also to a range around 180 *deg* and 540 *deg* it must be done a consideration about the attenuation factor sinusoidal variation. If the second winding is connected to the first one out of phase of 180 *deg* electrical degrees the winding factor behaviour becomes sinusoidal and not cosinusoidal anymore. In particular the final winding factor could be computed as:

$$k_{final} = k_{initial} \cdot sin\left(\frac{n \cdot \alpha}{2 \cdot p}\right) \qquad (5.2)$$

and the sinusoidal and cosinusoidal behaviours are shown in Fig.5.4:
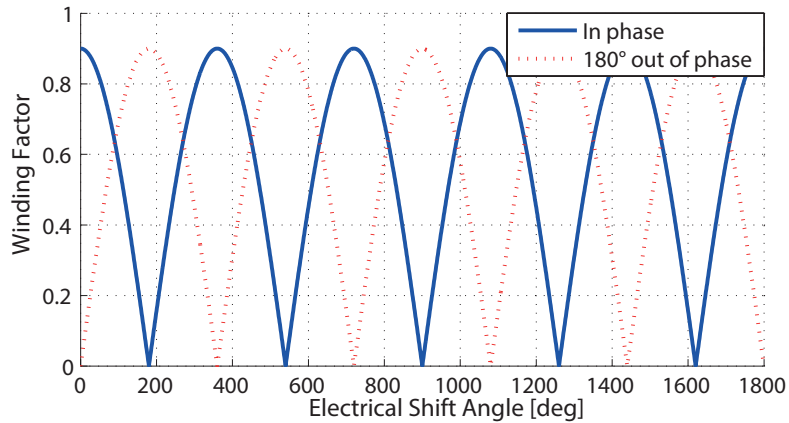
Figure 5.4: Example of comparison between sinusoidal and cosinudoidal behaviour about winding factor variation.

In this way the possibility of choice have been doubled and the two main problems, shown in Fig.5.3, could be avoided choosing an operable shift angle range around 180 *deg* or 360 *deg*. In fact, if these problems can be found around 360 *deg* it is possible to operate around 180 *deg* to avoid them.

5.2 Configuration with 9 stator slots and 8 poles

This is the first motor configuration which has been considered. At the beginning, in keeping with 5.1, it has been analyzed the harmonic order about the winding factor of the motor. In particular the main and the secondary harmonics and the main sub-harmonic have been considered as shown in Fig.5.5:
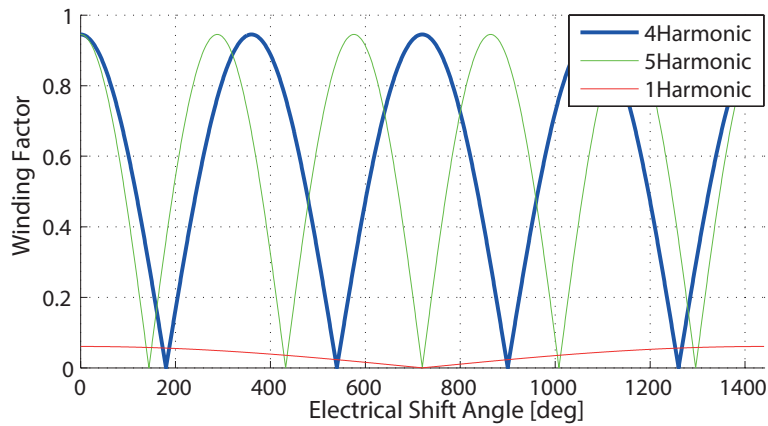

Figure 5.5: Winding factor variation for different harmonics. The main harmonic (ν=p=4) has been highlighted in bold

Being this a FCSW PMARel motor, to keep constant the 4th harmonic which is the main one (ν=p=4), has been decided to chose an electrical shift angle equal to 380 deg. In this way, the 4th harmonic amplitude remains almost the same while the amplitudes related to the harmonics of 5th and 1st order are considerably decreased. The range around 180 deg is not possible to realize in practice because the cross-section area of two consecutive slots intersect one with each other as it is shown in Fig.5.6:
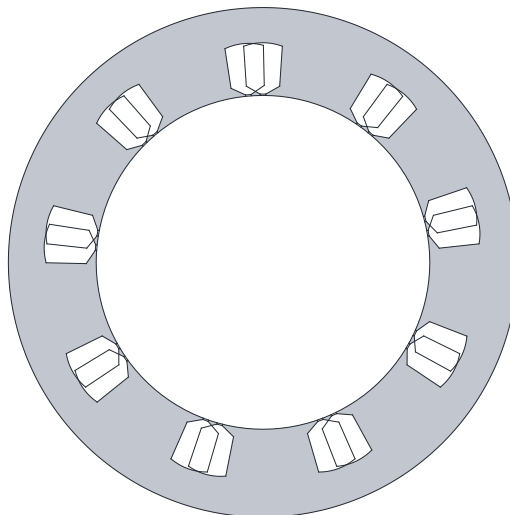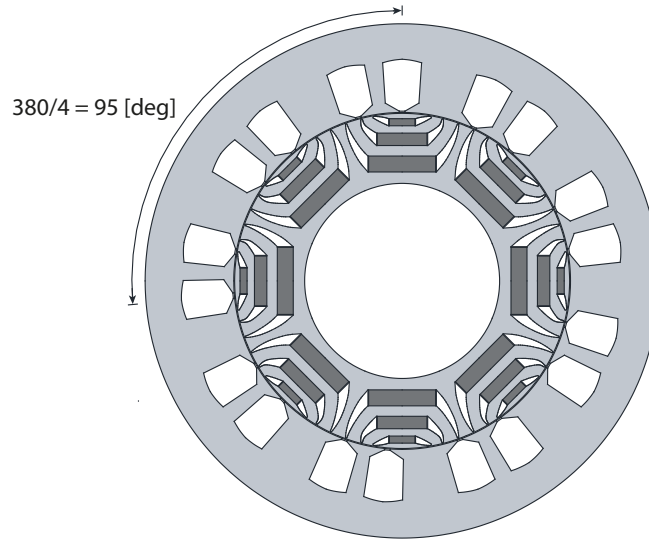

Figure 5.6: Cross-section area of a 9/8 PMARel motor with a stator shifting of 180 deg electrical degrees equal to 45 deg mechanical ones. It is clear the problem due to the intersection of two consecutive slot areas.

To realize this effect on the motor, the stator slots number must be doubled. Each slot will have half cross-section area than the single slot related to the reference FCSW PMARel motor with the same configuration. So it will moves from $1085\ mm^2$ to $542.5\ mm^2$. In the same way, keeping fixed the current density into the slot equal to $6\ A/mm^2$, the peak current at nominal conditions must be halved moving from $3627\ A$ to $1814\ A$. As a consequence, also the slot matrix has been changed as follow:

$$ka = [\ +1\ 0\ -1\ -0.5\ +0.5\ +1\ 0\ -1\ 0\ +0.5\ 0\ 0\ 0\ 0\ 0\ -0.5\ 0];$$
$$kb = [\ 0\ 0\ 0\ 0\ -0.5\ 0\ +1\ 0\ -1\ -0.5\ +0.5\ +1\ 0\ -1\ 0\ +0.5\ 0\ 0];$$
$$kc = [\ 0\ -1\ 0\ +0.5\ 0\ 0\ 0\ 0\ 0\ 0\ -0.5\ 0\ +1\ 0\ -1\ -0.5\ +0.5\ +1];$$

and the new motor geometry is shown in Fig.5.7:

Figure 5.7: Cross-section area of a 18/8 PMARel motor with a stator shifting of 380 deg electrical degrees equal to 95 deg mechanical ones

The new winding belongs again to FCSW family also if now it is more similar to a distributed one. The slot number per pole per phase becomes equal to:

$$q_s = \frac{Q_s}{m \cdot 2p} = \frac{18}{3 \cdot 8} = 0.75 \tag{5.3}$$

The only difference is due to the different teeth thickness along the stator. Besides the slot pitch is expressed as:

$$Y_q = \frac{Q_s}{2p} = \frac{18}{8} = 2.25 \tag{5.4}$$

From the matrix slot could be noticed how in practice it has been shortened from 2.25 to 2.

After all these considerations the motor has been simulated. In particular the mechanical interval selected has been equal to 15 deg, while the MTPA operating point has been found to amount to $\alpha ie = 47\ deg$. The results computed in terms of torque performance are shown in Fig.5.8:
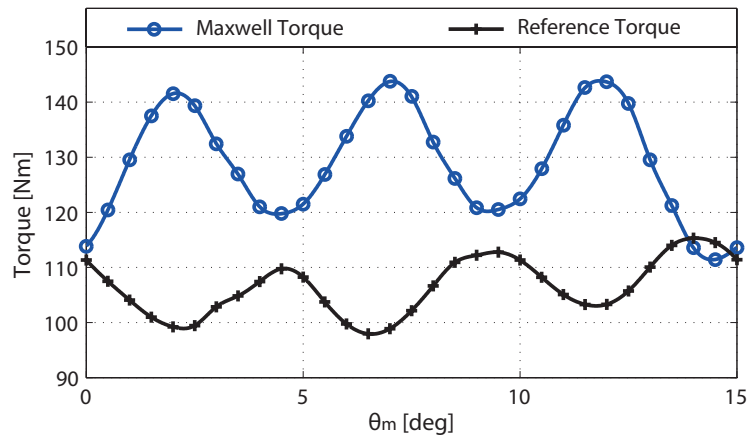
Figure 5.8: Torque value for different mechanical angles calculated through Maxwell stress tensor at nominal conditions compared with reference torque behaviour. PMARel motor 18/8 configuration with stator shifting of 380 *deg* electrical degrees

Elaborating this torque behaviour it is possible to find out that:

Average Maxwell Torque = 128.8 Nm
Average d-q torque = 128.8 Nm
Torque ripple = 25.09 %

Comparing these results with the reference PMARel motor, it is clear how with this technique the average torque has been increased about 21 %. However also the torque ripple has been increased about 9 %, so the first positive result has been balanced out by a negative one. Focusing the attention on the harmonic order reported in Fig.5.9 could be done some considerations:
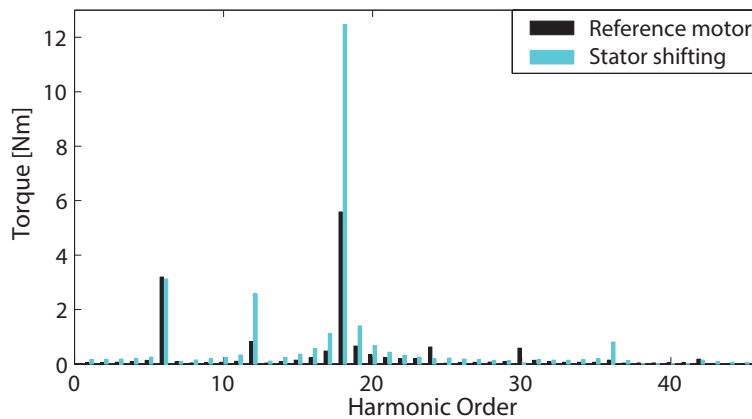
Figure 5.9: Harmonic order comparison between the reference PMARel motor and the PMARel motor 18/8 configuration with stator shifting of 380 *deg* electrical degrees.

The torque ripple increase is clearly due to the harmonic of 12th, 18th and 36th order. The first two have been doubled their amplitudes in absolute value if compared to the reference machine. Instead the 6th one remains almost the same. The average torque is increased

because of a more distributed stator M.M.F.

Also through the results could be seen how the new motor could be considered a compromise between the motor with pure distributed winding and the motor with the pure fractional-slot one.

5.3   Configuration with 12 stator slots and 8 poles

The stator shifting adopted in the FCSW PMARel motor with 12 stator slots and 8 poles has been done chosing an electrical shift angle equal to 180 deg, which in mechanical degrees it could be expressed as:

$$\frac{180}{p} = \frac{180}{4} = 45 \ [deg] \tag{5.5}$$

In particular in Fig.5.10 have been shown the main and the secondary harmonics on which has been focused the attention. It must be noticed the absence of sub-armonic belonging to the winding factor.
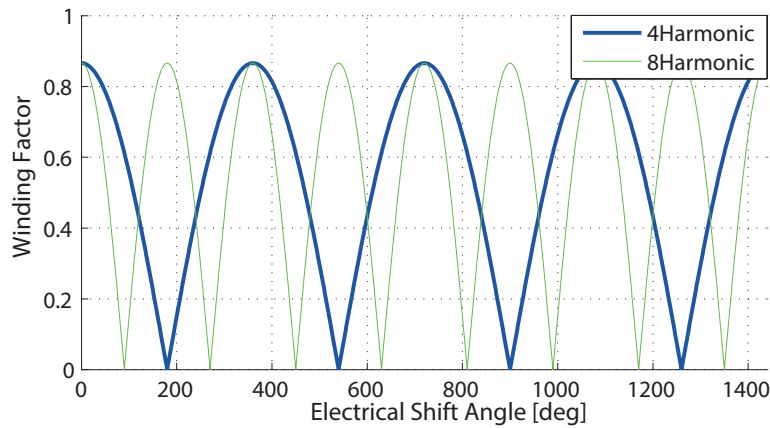
Figure 5.10: Winding factor variation for different harmonics. The main harmonic (ν=p=4) has been highlighted in bold

The shifting which has been selected deletes completely the 8th harmonic while the main one (ν=p=4) remains constant in amplitude. To obtain this effect on the motor performance it must be doubled the number of stator slots from 12 to 24. The cross-section area of each slots halves from 810 m^2 to 405 mm^2. This keeping fixed again the density current into the slot to 6 A/mm^2. As a consequence the peak current at nominal conditions used in the following simulations has been considered equal to 1370 A and the new slot matrix related to this kind of motor configurations has been changed as follow:

ka = [+0.5 0 -0.5 -0.5 0 +0.5 +0.5 0 -0.5 -0.5 0 +0.5
+0.5 0 -0.5 -0.5 0 +0.5 +0.5 0 -0.5 -0.5 0 +0.5];

kb = [0 +0.5 +0.5 0 -0.5 -0.5 0 +0.5 +0.5 0 -0.5 -0.5
0 +0.5 +0.5 0 -0.5 -0.5 0 +0.5 +0.5 0 -0.5 -0.5];

kc = [-0.5 -0.5 0 +0.5 +0.5 0 -0.5 -0.5 0 +0.5 +0.5 0
-0.5 -0.5 0 +0.5 +0.5 0 -0.5 -0.5 0 +0.5 +0.5 0];

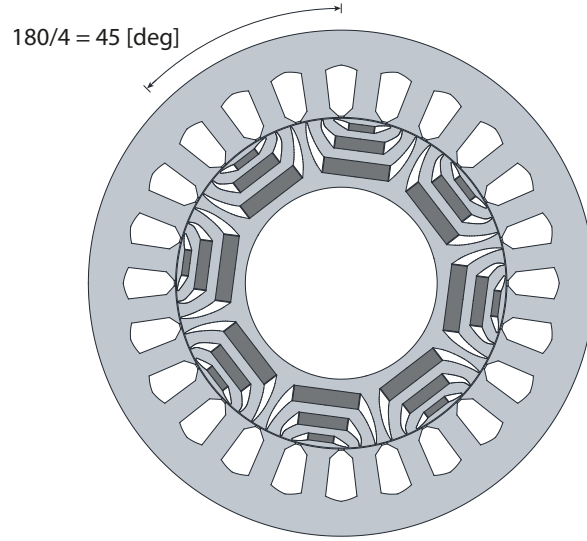and the new motor geometry is shown in Fig.5.11:

Figure 5.11: Cross-section area of a 12/8 PMARel motor with a stator shifting of 180 *deg* electrical degrees equal to 45 *deg* mechanical ones

The new winding is now very similar to a distributed one because the slot number per pole per phase becomes equal to:

$$q_s = \frac{Q_s}{m \cdot 2p} = \frac{24}{3 \cdot 8} = 1 \qquad (5.6)$$

The only difference is due to the different teeth thickness along the stator. Besides the slot pitch is expressed as:

$$Y_q = \frac{Q_s}{2p} = \frac{24}{8} = 3 \qquad (5.7)$$

From the matrix slot could be noticed how in practice it has been shortened from 3 to 2. In this FCSW PMARel motor configuration it is not possible to select an elctrical shift angle around 360 *deg* because of the intersection between two consecutive slot cross-section areas.In Fig.5.12 is shown this physical problem for a 380 *deg* electrical degrees stator shifting.
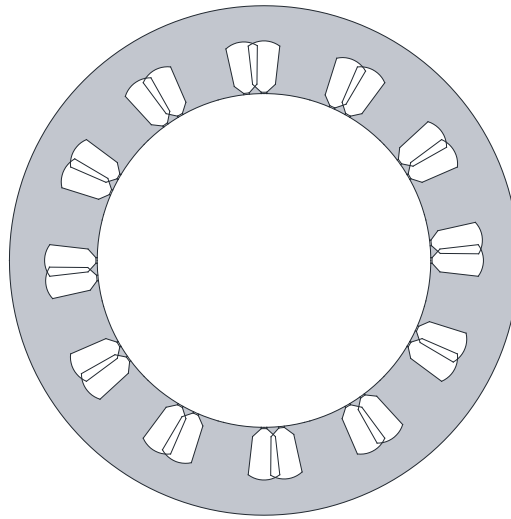
Figure 5.12: Cross-section area of a 24/8 PMARel motor with a stator shifting of 380 *deg* electrical degrees equal to 95 *deg* mechanical ones. It is clear the problem due to the intersection of two consecutive slot areas.

The new PMARel motor with the stator shifting has been simulated considering again a mechnical interval equal to 15 *deg* and a current angle $\alpha_{ie} = 54$ *deg* to work in MTPA conditions. Fig:5.13 shows the resulting torque behaviour.
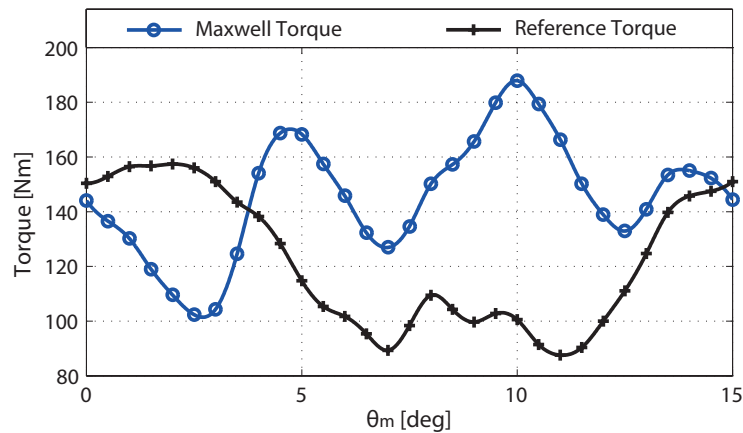

Figure 5.13: Torque value for different mechanical angles calculated through Maxwell stress tensor at nominal conditions compared with reference torque behaviour. PMARel motor 24/8 configuration with stator shifting of 180 *deg* electrical degrees

It results:

Average Maxwell Torque = 145.6 Nm
Average d-q torque = 144.2 Nm
Torque ripple = 58.75 %

It must be noticed how the average torque has been increased about 16 % if compared with the reference PMARel motor with the same configuration. In particular, in the first 4 *deg* mechanical degrees this parameter has been worsen while later it has been

considerably improved. The torque ripple could be considered almost the same. The shifting angle adopted deals with the better torque performance obtained. There are not negative aspects than before as in Sect.5.2 where torque ripple has been got worse. The attention has been focused on the harmonic order related to the torque ripple which is reported in Fig.5.14:
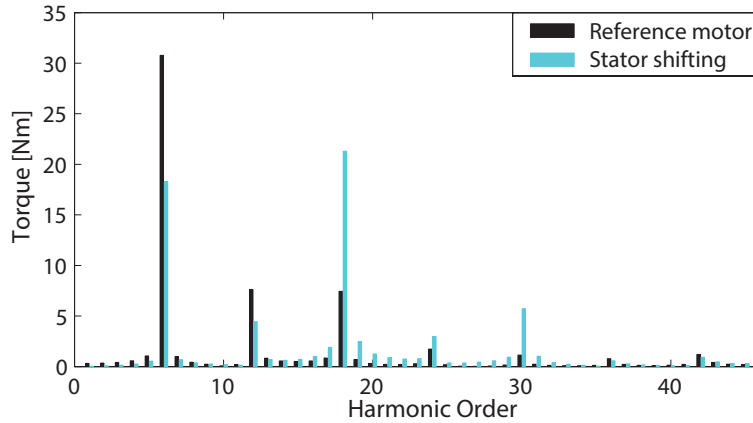

Figure 5.14: Harmonic order comparison between the reference PMARel motor and the PMARel motor 24/8 configuration with stator shifting of 180 *deg* electrical degrees

Some considerations could be done about how the harmonic spectrum changes through this technique. The contribution to the torque ripple is different with the stator shifting because the harmonic with the higher amplitude is the 18th and not the 6th anymore. The best effects have been found in the harmonic of 6th and 12th order because their amplitudes have been reduced very well. The reason that why torque ripple doesn't change is due to the strong improvement of the harmonic of 18th, 24th and 30th order.
The new motor could be considered a compromise between the motor with pure distributed winding and the motor with the pure fractional-slot one.

5.4 Configuration with 12 stator slots and 10 poles

The third FCSW PMARel motor to be analyzed has a dfferent number of poles and this deals with a lower interval of the electical shift angle related to the winding factor. In Fig.5.15 have been shown the trends about the main (5th) and the secondary (7th) harmonics. Besides also the sub-harmonic (1st) has been reported.
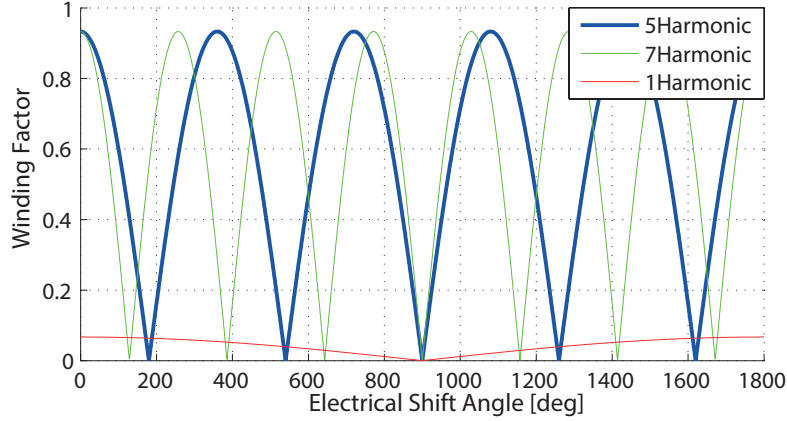
Figure 5.15: Winding factor variation for different harmonics. The main harmonic (ν=p=5) has been highlighted in bold

In this case the electrical shift angle has been chosen equal to 380 deg. In this way the amplitude of the main harmonic (ν=p=5) remains almost the same while the secondary one and the sub-harmonic have been increased. To obtain this effect on the motor, the number of the stator slots must be doubled. As a consequence, keeping fixed to 6 A/mm^2 the current density into the slots, the cross-section area of each one moves from 810 mm^2 to 405 mm^2. Besides the peak current at nominal conditions must be halved from 2739 A to 1370 A. This considerations led up to have a new slot matrix which becomes:

ka = [+1 0 -0.5 -0.5 0 +1 0 -0.5 0 0 +0.5 0 -1 0 +0.5 +0.5 0 -1 0 +0.5 0 0 -0.5 0];

kb = [0 0 +0.5 0 -1 0 +0.5 +0.5 0 -1 0 +0.5 0 0 -0.5 0 +1 0 -0.5 -0.5 0 +1 0 -0.5];

kc = [0 -1 0 +0.5 0 0 -0.5 0 +1 0 -0.5 -0.5 0 +1 0 -0.5 0 0 +0.5 0 -1 0 +0.5 +0.5];

and the new motor geometry related to this stator shifting is shown in Fig.5.16:
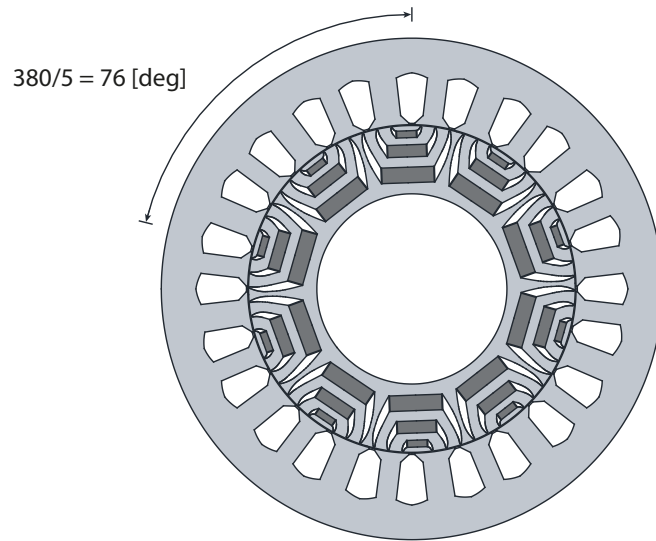
Figure 5.16: Cross-section area of a 12/10 PMARel motor with a stator shifting of 380 *deg* electrical degrees equal to 76 *deg* mechanical ones

The new winding belongs again to FCSW family also if now it is more similar to a DW. The slot number per pole per phase becomes:

$$q_s = \frac{Q_s}{m \cdot 2p} = \frac{24}{3 \cdot 10} = 0.8 \tag{5.8}$$

The only difference is due to the different teeth thickness along the stator. Besides the slot pitch is expressed as:

$$Y_q = \frac{Q_s}{2p} = \frac{24}{10} = 2.4 \tag{5.9}$$

From the matrix slot could be noticed how in practice it has been shortened from 2.4 to 2.

In this PMARel motor configuration it is not possible to select an elctrical shift angle around 180 *deg* because of the intersection between two consecutive slot cross-section areas.In Fig.5.17 is shown this physical problem for a 180 *deg* electrical degrees stator shifting.
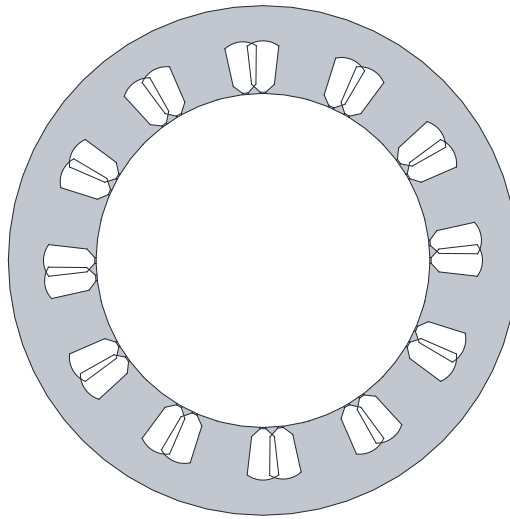
Figure 5.17: Cross-section area of a 24/10 PMARel motor with a stator shifting of 180 *deg* electrical degrees equal to 36 *deg* mechanical ones. It is clear the problem due to the intersection of two consecutive slot areas.

Since the geometry of the machine has been changed, the current angle related to MTPA conditions change from $\alpha_{ie} = 53$ *deg* to $\alpha_{ie} = 52$ *deg*. The mechanical range has been considered equal to 12 *deg*. Fig.5.18 shows the resulting torque behaviour.
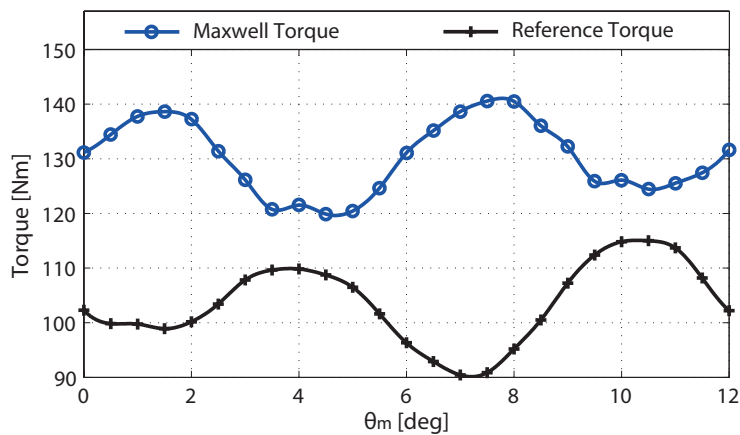

Figure 5.18: Torque value for different mechanical angles calculated through Maxwell stress tensor at nominal conditions compared with reference torque behaviour. PMARel motor 24/10 configuration with stator shifting of 380 *deg* electrical degrees

It results:

Average Maxwell Torque = 130.4 Nm
Average d-q torque = 129 Nm
Torque ripple = 15.86 %

From the comparison with the reference PMARel motor it is clear that the average torque has been strongly increased about 26 % and that also the torque ripple behaviour has been

improved. In fact it is lower than before about 8 %. The best torque ripple result respect to the Sect.5.3 is due to the amplitudes of the secondary harmonic. In fact in this case the 7th is decreased while in Sect.5.3 the 8th is completely deleted. Besides the main (ν=p=5) decreases a few its amplitude while in the previous case it (ν=p=4) remains fixed. There is also the presence of a sub-harmonic which contributes to the torque ripple. Instead the average torque increases in both cases because there is a more distributed stator M.M.F. at the air-gap. At the end the attention has been focused on the harmonic order analysis related to the torque ripple as it is shown in Fig.5.19:
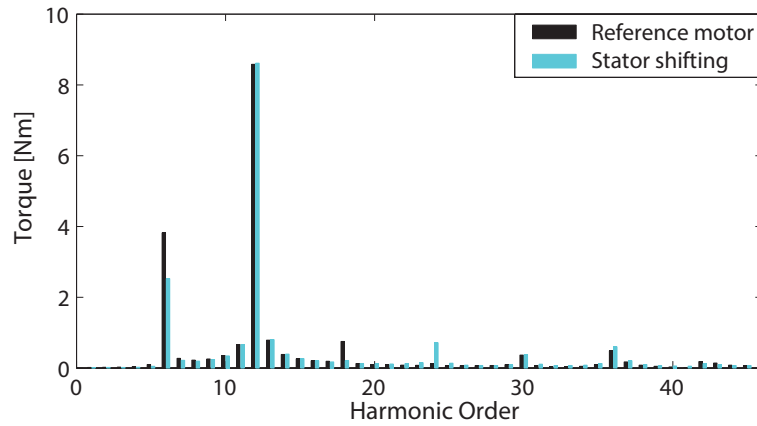

Figure 5.19: Harmonic order comparison between the reference PMARel motor and the PMARel motor 24/10 configuration with stator shifting of 380 deg electrical degrees.

The reason of torque ripple improvement is due to the 6th harmonic which has been decreased togheter with the 18th one. All the others have been remained almost the same except the 24th harmonic which has been introduced.

5.5   Configuration with 15 stator slots and 10 poles

This is the last configuration which has been considered. The winding factor harmonic spectrum doesn't present sub-harmonics but only a main one (5th) and a secondary one (10th). It is all reported in Fig.5.20 where are compared their behaviours. The stator shifting has been done considering an electrical shift angle equal to 180 *deg*.
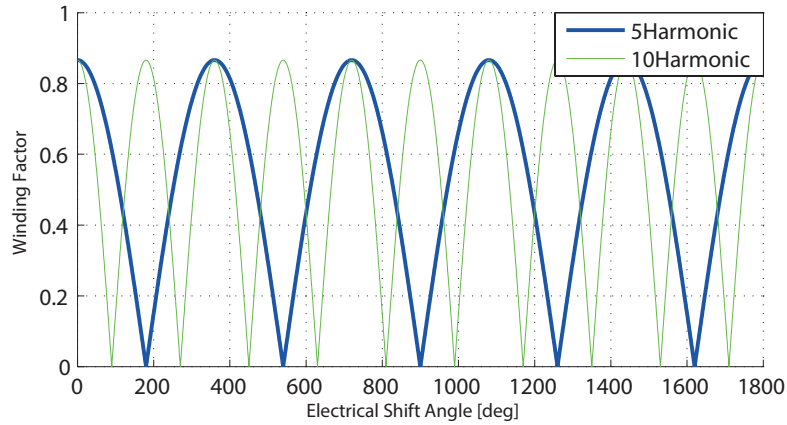

Figure 5.20: Winding factor variation for different harmonics. The main harmonic (ν=p=5) has been highlighted in bold

The choice which has been done deals with the elimination of the 10th harmonic, while the amplitude of the 5th one remains constant. To reach the same result in the motor the stator slots must be doubled and keeping fixed the current density to 6 A/mm^2, the peak current must be halved. So, the cross-section area of each slot moves from 652 mm^2 to 326 mm^2 and the peak current at nominal conditions moves from 2207 A to 1104 A. This considerations led up to have a new slot matrix which becomes:

ka = [+0.5 0 -0.5 -0.5 0 +0.5 +0.5 0 -0.5 -0.5 0 +0.5 +0.5 0 -0.5
       -0.5 0 +0.5 +0.5 0 -0.5 -0.5 0 +0.5 +0.5 0 -0.5 -0.5 0 +0.5];

kb = [0 +0.5 +0.5 0 -0.5 -0.5 0 +0.5 +0.5 0 -0.5 -0.5 0 +0.5 +0.5
       0 -0.5 -0.5 0 +0.5 +0.5 0 -0.5 -0.5 0 +0.5 +0.5 0 -0.5 -0.5];

kc = [-0.5 -0.5 0 +0.5 +0.5 0 -0.5 -0.5 0 +0.5 +0.5 0 -0.5 -0.5 0
       +0.5 +0.5 0 -0.5 -0.5 0 +0.5 +0.5 0 -0.5 -0.5 0 +0.5 +0.5 0];

and the new motor geometry related to this stator shifting is shown in Fig.5.21:
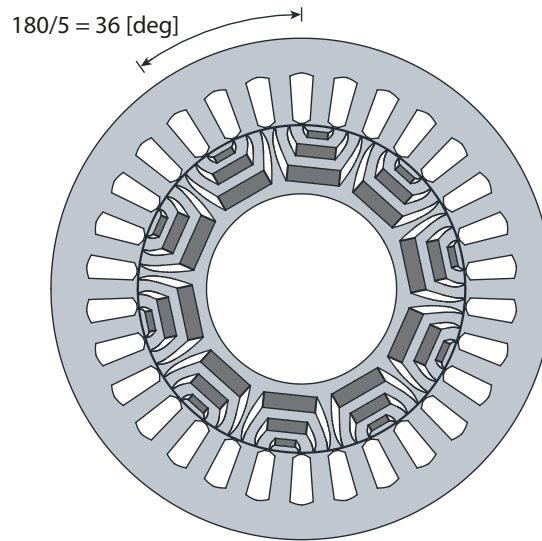
Figure 5.21: Cross-section area of a 15/10 PMARel motor with a stator shifting of 180 *deg* electrical degrees equal to 36 *deg* mechanical ones

The new winding is now very similar to a DW because the slot number per pole per phase becomes:

$$q_s = \frac{Q_s}{m \cdot 2p} = \frac{30}{3 \cdot 10} = 1 \tag{5.10}$$

The only difference is due to the different teeth thickness along the stator. Besides the slot pitch is expressed as:

$$Y_q = \frac{Q_s}{2p} = \frac{30}{10} = 3 \tag{5.11}$$

From the matrix slot could be noticed how in practice it has been shortened from 3 to 2. In this PMARel motor configuration it is not possible to select an elctrical shift angle around 380 *deg* because of the intersection between two consecutive slot cross-section areas.In Fig.5.22 is shown this physical problem for a 380 *deg* electrical degrees stator shifting.
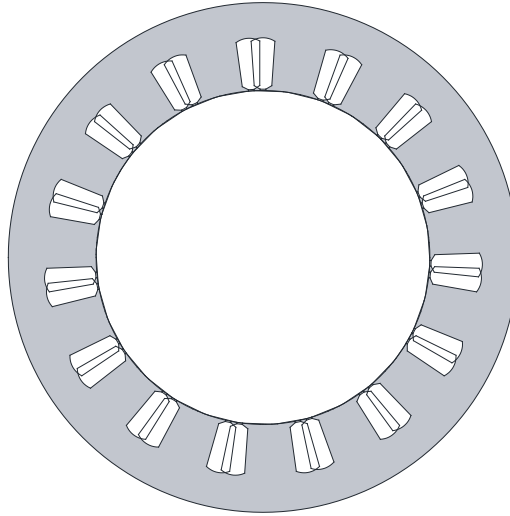
Figure 5.22: Cross-section area of a 30/10 PMARel motor with a stator shifting of 380 deg electrical degrees equal to 76 deg mechanical ones. It is clear the problem due to the intersection of two consecutive slot areas

The current angle related to the MTPA operating point has been fixed equal to $\alpha_{ie} = 51\ deg$. In the reference PMARel motor it was equal to $\alpha_{ie} = 47\ deg$ electrical degrees. The mechanical interval simulated has been fixed equal to 12 deg and Fig.5.23 shows the resulting torque behaviour.
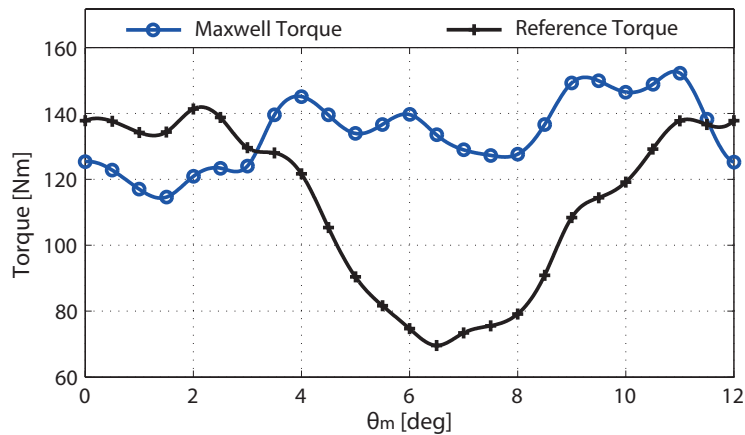

Figure 5.23: Torque value for different mechanical angles calculated through Maxwell stress tensor at nominal conditions compared with reference torque behaviour. PMARel motor 30/10 configuration with stator shifting of 180 deg electrical degrees

It results:

Average Maxwell Torque = 133.9 Nm
Average d-q torque = 133.3 Nm
Torque ripple = 28.14 %

The technique adopted deals with an improvement in terms of torque performace if com-

pared to the reference PMARel motor. In particular the average torque has been increased about 18 % and the torque ripple has been strongly reduced from 63.48 % to 28.14 %. This is the best result among all the different motor configurations which have been analyzed. The average torque in per cent has reached the same growth than all the others motors, but it is on torque ripple where has been obtained the best effect. This probably because of the elimination of the 10th harmonic and all its multiples and also because of the higher stator slots number and poles number than all the others. In this way rotor and stator M.M.Fs have been more distributed and so their harmonic spectrums don't contain all the harmonics as the pure fractional-slot winding. As a consequence, probably some harmonics that in the reference PMARel motor interact one with each other, now don't interact anymore without to give contribute to torque ripple. To better understand the results it has been done the torque ripple harmonic analysis. The harmonic spectrum is shown in Fig.5.24:
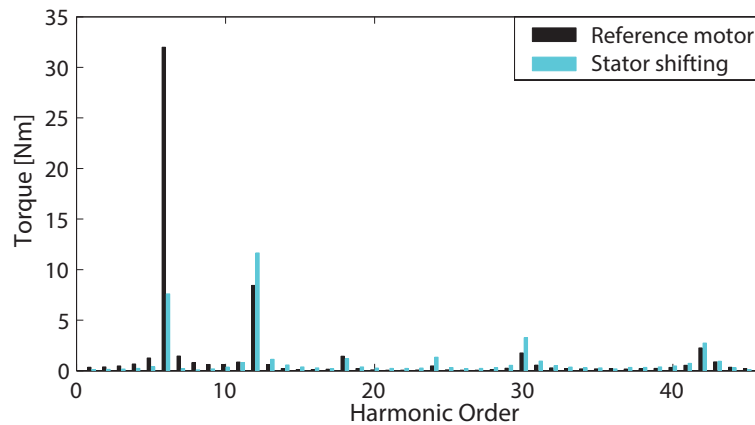

Figure 5.24: Harmonic order comparison between the reference PMARel motor and the PMARel motor 30/10 configuration with stator shifting of 180 *deg* electrical degrees

It is evident that the 6th harmonic has been reduced of about 6 times. This balances out the increase, in absolute value, of the amplitude related to the harmonic of 12th, 24th and 30th order and gives the possibility to reach a torque ripple more than 2 times lower. The reduction of the 6th harmonic could be noticed also in Fig.5.23 where between 2 *deg* and 11 *deg* mechanical degrees Maxwell torque behaviour has been made smoother.

5.6   Final considerations

At the end of the analysis for all FCSW PMARel configurations it could be done a comparison with the reference ones previously considered. In particular this is reported in Table.5.1:

Table 5.1: Comparison between reference FCSW PMARel motor configurations and the same ones after the stator shifting technique. This for different kinds of configurations and at nominal conditions.

	Maxwell Average Torque [N·m]	Torque Ripple [%]
Reference 9/8	106.5	16.29
9/8 Stator shifting	128.8	25.09
Reference 12/8	125.96	59.02
12/8 Stator shifting	145.6	58.75
Reference 12/10	103.5	23.73
12/10 Stator shifting	130.4	15.88
Reference 15/10	113.1	63.48
15/10 Stator shifting	133.86	28.14

Some main considerations must be highlighted about the stator shifting introduced in this chapter:

- this technique couldn't be applied to the motor for all the electrical shift angles. If theoretically this is possible, when it must be physically done on the motor there's the problem of stator slots overlapping which limits the choice to a more restricted range;

- stator shifting on motors with 3 slots/ 2 poles configuration modifies the winding into a distributed type one. In both cases the stator slot number per pole per phase becomes equal to $q_s = 1$;

- for all PMARel motor configurations it is possible to achieve an average torque improvement between 16 % and 26 % in comparison with the reference ones. This deals with a reduction of the difference from the average torque related to DW PMARel motor;

- stator shifting on torque ripple has different effects which changes depending on the case;

- copper savings due to pure fractional-slots windings are reduced to reach a better motor behaviour in terms of torque performance. However the copper use is still lower than the one necessary for distributed winding;

- there is a better saturation of stator tooth and back-iron due to the improvement of the stator M.M.F distribution at the air-gap.

Chapter 6

Rotor skewing of shifted stator

In this last chapter has been tried to improve the torque ripple introducing a technique on the rotor structure. The alghoritm which has been developed by *Fusar* in [5] has been used. This because in the previous chapters two solutions have been studied both related to the stator, while now the main aim is to manage the rotor to improve again the results presented above. In particular, the *stator shifting* as seen before deals with an increase of average torque. So in the following step it will be matched with the *rotor skewing* to try to keep fixed the positive results in terms of average torque and at the same time to reduce the torque ripple.

6.1 The concept of rotor skewing

6.1.1 Physical description

The rotor skewing adopted is not equal to the one made on the asynchronous rotor. In fact, while in this last case it is done in a continuos way, in the PMARel motors it must be done in a discrete way. This is because of the PMs presence which can't be twisted as the rotor laminations. In particular through the rotor skewing the rotor is divided into m parts, each one in a different angular position than all the others. The kind of rotor skewing studied has not the m parts all with the same stack length and so they must be weighted by a specific coefficient k_i called *weighing coefficient*. Each one of them is included between 0 and 100. It has been decided that they have to be equal only to 0, 10, 20, 30, 40, 50, 60, 70, 80, 90 and 100. Their total sum must be always equal to 100. In fact it must be verified the equivalence:

$$L_{stk} = \sum_{i=1}^{m} k_i \cdot L_i \tag{6.1}$$

where L_{stk} is the total stack length of the motor, L_i is the lenght of each single rotor parts after the skewing and k_i is the specific weighing coefficient for each part. The reason why the rotor is splitted in this way could be found in the alignment (which in this case is done at nominal conditions), essential to reach the MTPA operating point of the motor related to a specific α_{ie} current angle. In fact, if the rotor is not aligned, the torque behaviour is different and surely the average torque will be lower. In particular, the idea of this kind of rotor skewing is based considering aligned the central part, while all the others have been rotated of $\Delta\theta = 1 \ deg$ mechanical degrees one from each other. Choosing always m as odd

number, the angular distribution of all the rotor parts must be done in a symmetrical way respect to the central one. This means that, for example, if $m = 9$, the disalignment of the first part must be equal to $+4$ *deg* mechanical degrees, the second one must be equal to $+3$ *deg*, the third one to $+2$ *deg*, the fourth one to $+1$ *deg* and the central part must be equal to 0 *deg*. Carring on in this way, the angular rotation of the following parts must be done increasing step by step the skewing angle of 1 *deg* until to arrive to the ninth part which will have an angular rotation of -4 *deg* mechanical degrees respect to the aligned rotor part. This method will generate m different torque behaviours similar among them but shifted horizontally one from each other. This effect gives the possibility to balance out the maximum value of a specific behaviour with the minimum related to another one reducing the torque ripple. The better the final result in terms of torque performance, the better will be the combination of the weighing coefficients adopted.

6.1.2 Considerations about the current angle

At this point could be thought that the new PMARel motor will have a current angle, related to the MTPA operating point, difficult to identify. Actually there isn't this problem because α_{ie} could be considered equal to the one found for the rotor part aligned which could be considered a good estimation. The reason of this is that a certain angular rotor position amounts to a fixed α_{ie}, which amplitude is done by the rotor position value multiplied for the pair-poles, while the sign is opposed to the one of the angular rotor position. This because to wheel ahead the rotor means to wheel back the currents. To better explain this latter concept an example is done.

Example:

It is considered a rotor splitted into $m = 7$ parts as follow:

1. rotor position $\theta_{r1} = +3$ *deg* and stack length percentage 10 %;

2. rotor position $\theta_{r2} = +2$ *deg* and stack length percentage 30 %;

3. rotor position $\theta_{r3} = +1$ *deg* and stack length percentage 10 %;

4. rotor position $\theta_{r4} = 0$ *deg* and stack length percentage 20 %;

5. rotor position $\theta_{r5} = -1$ *deg* and stack length percentage 10 %;

6. rotor position $\theta_{r6} = -2$ *deg* and stack length percentage 0 %;

7. rotor position $\theta_{r7} = -3$ *deg* and stack length percentage 20 %.

Above all it must be highlighted that although at the beginning it has been considered that the rotor has been splitted into m parts, the best skewing configuration not necessarily must be made up by m parts but could be done by a lower number of sections as shown in this example. That being said, the attention must be focused on the current angles related to the mechanical ones about the different rotor parts. Considering that $\alpha_{ieALG} = 47$ *deg*, when $\theta_r = 0$ *deg* and that $p = 4$, it will be computed that:

$$\alpha_{iem} = \alpha_{ieALG} - \theta_{rm} \cdot p \tag{6.2}$$

1. $\alpha_{ie1} = \alpha_{ieALG} - \theta_{r1} \cdot p = 47 - 3 \cdot 4 = 35$ *deg*

2. $\alpha_{ie2} = \alpha_{ieALG} - \theta_{r2} \cdot p = 47 - 2 \cdot 4 = 39 \ deg$

3. $\alpha_{ie3} = \alpha_{ieALG} - \theta_{r3} \cdot p = 47 - 1 \cdot 4 = 43 \ deg$

4. $\alpha_{ie4} = \alpha_{ieALG} - \theta_{r4} \cdot p = 47 - 0 \cdot 4 = 47 \ deg$

5. $\alpha_{ie5} = \alpha_{ieALG} - \theta_{r5} \cdot p = 47 + 1 \cdot 4 = 51 \ deg$

6. $\alpha_{ie6} = \alpha_{ieALG} - \theta_{r6} \cdot p = 47 + 2 \cdot 4 = 55 \ deg$

7. $\alpha_{ie7} = \alpha_{ieALG} - \theta_{r7} \cdot p = 47 + 3 \cdot 4 = 59 \ deg$

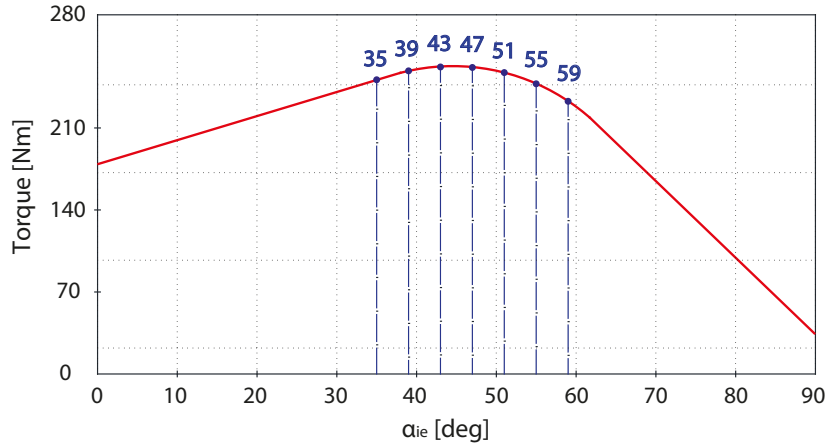and they are all represented in Fig.6.1:

Figure 6.1: Distribution of current angle in a sample curve torque-alphaie

At this point, to find the final current angle of the new motor, a weighted average angle has to be found among all the current angles obtained. It could be expressed as:

$$\alpha_{ieNEW} = \frac{1}{\sum\limits_{i=1}^{m} k_i} \cdot \sum_{i=1}^{m} k_i \cdot \alpha_{iei} \tag{6.3}$$

and substituting the corrispondig values it could be calculated that:

$$\alpha_{ieNEW} = \frac{10 \cdot 35 + 30 \cdot 39 + 10 \cdot 43 + 20 \cdot 47 + 10 \cdot 51 + 0 \cdot 55 + 20 \cdot 59}{100} = 45.8 \ [deg] \tag{6.4}$$

It is clear that the real current angle related to MTPA conditions is not so far from the one before the rotor skewing ($47 \ deg \simeq 45.8 \ deg$). This open the possibility to simulate the motor always with the same current angle equal to $\alpha_{ie} = 47 \ deg$ and it is very important because gives the advantage to semplify the simulation difficulty without to be too much in error as far as the result is concerned. On the contrary, the error which is introduced through going to operate in different conditions from the MTPA ones, deals with precautionary torque performance. In fact, the average torque obtained will be lower than the real one. The torque ripple will be very similar to the real one in percentage value as it has been seen in Fig.2.17. It could be considered fixed in absolute value whether the α_{ie} or not. In other words, the torque performance obtained are a few lower than the real

ones of the PMARel motor with rotor skewing. In Fig.6.2 is reported an example of a
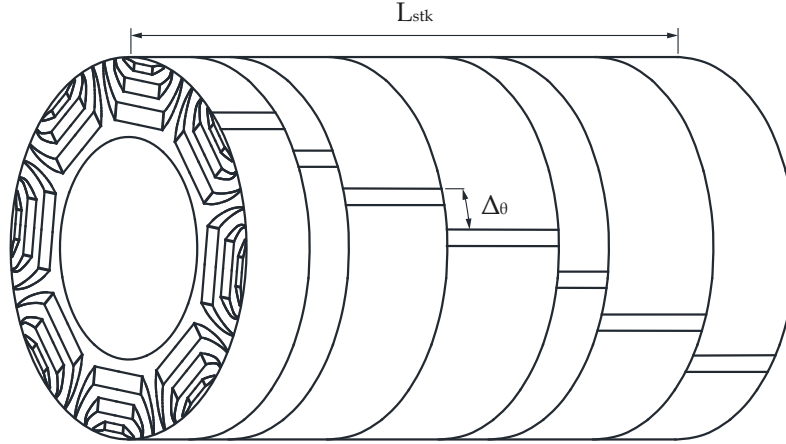skewed rotor according to the technique described:

Figure 6.2: Rotor skewing of a rotor which has been splitted into $m = 7$ parts with an
angular rotor skewing $\Delta\theta$ between two consecutive sections

6.1.3   Analytical model

In practical terms to apply this method on the simulations, the different m parts in which
the rotor has been splitted are simulated, always considering fixed the α_{ie} to the value
obtained before the rotor skewing. In this way a matrix $T_{skewing}(m, n)$ with m lines
and n columns has been computed, where n depends from the step adopted during the
torque computation with the change in mechanical position. Later has been analytically
generated another matrix $COMBO(k, m)$ with k lines and m columns. The k represents
the total possible linear combinations (made by weighing coefficients) on which a rotor
could be splitted having fixed m. As a consequence, k is function of m and in particular
the higher m, the higher will be k. The two matrices must be multiply between them
obtaining in this way a final matrix $T_{results}(k, n)$ where each element represents a single
torque value in a fixed rotor position which has been computed as:

$$T_{(k,n)}(\theta) = \frac{1}{\sum\limits_{i=1}^{m} k_i \cdot L_{stk}} \cdot \sum_{i=1}^{m} k_i \cdot L_{stk} \cdot T_i(\theta) \tag{6.5}$$

A matrix has been obtained where k different torque behaviours are described (one for
each linear combination of rotor skewing generated). All of them are composed by n torque
values whose number depends on the mechanical angle step chosen. So it has been possible
to compute the average torque and torque ripple for all the k combinations representing
them in a graphic where comes into view the best combinations.

6.2   Configuration with 9 stator slots and 8 poles

The rotor skewing has been done dividing into $m = 7$ parts with different lengthes the rotor. It has all been done matched to the stator shifting introduced in Cap.5. This PMARel motor configuration has been simulated considering always a density current into the slots equal to 6 A/mm^2 at nominal conditions. 8000 different possible combinations have been computed and the final results in terms of torque performance are shown in Fig.6.3 where a zoom has been done on the more interesting area to highlight in red the combination chosen.
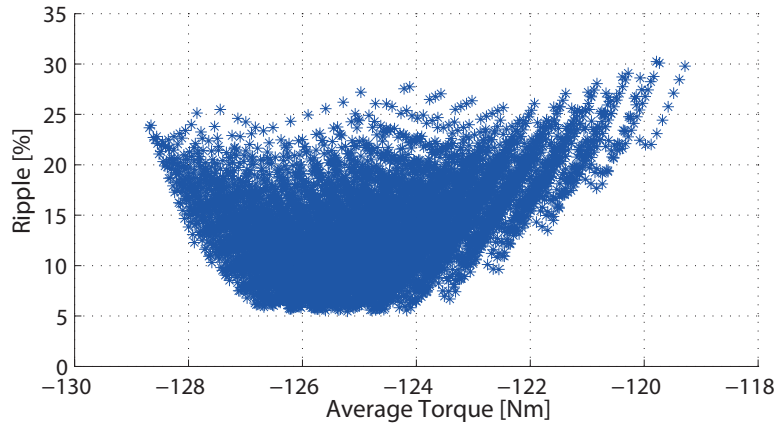
(a) Rotor skewing combinations computed
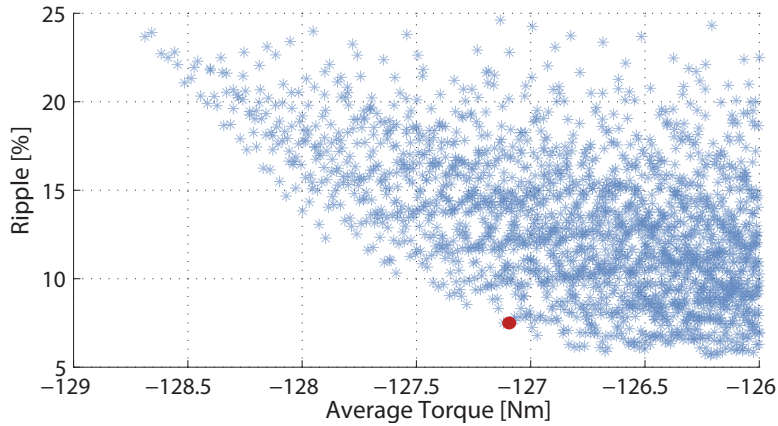
(b) Zoom of the area where the skewing combination adopted is highlighted in red

Figure 6.3: Representation of all the possible rotor skewing combinations of a 18/8 PMARel motor with stator shifting. The rotor has been splitted into 7 parts

The partition of the rotor is reported in Tab.6.1:

Table 6.1: Rotor skewing partition in a 18/8 PMARel motor

Angular rotor position [deg]	+3	+2	+1	0	-1	-2	-3
Weighing coefficient	0	10	40	10	20	20	0

It is clear how the chosen machine exhibits a rotor built up by 5 parts and this is positve because the executive difficulties has been made easier. Torque values:

Average Maxwell Torque = 127.1 Nm
Average d-q torque = 126.8 Nm
Torque ripple = 7.49 %

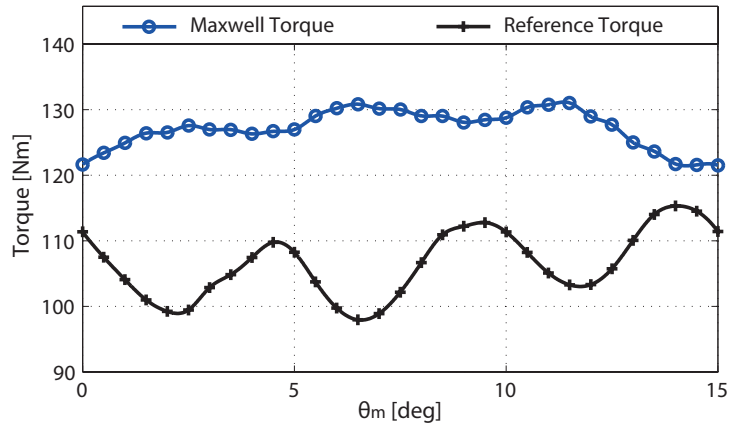and the torque behaviour have been shown in Fig.6.4:

Figure 6.4: Torque value for different mechanical angles calculated through Maxwell stress tensor at nominal conditions. PMARel motor 18/8 configuration with stator shifting of 380 *deg* electrical degrees matched with rotor skewing

From the comparison with the PMARel motor with only the stator shifting, the average torque remains almost the same. The torque ripple has been considerably reduced reaching interesting performance from an industrial point of view. In particular, it must be noticed that respect the reference PMARel motor the average torque is about 19 % higher while the torque ripple is about 9 % lower. The reason of this improvement is due to the improvement of the harmonic spectrum of the torque behaviour, shown in Fig.6.5.
The 18th harmonic, the main one which influences the torque ripple, is considerably reduced, while harmonic of 24th and 30th order could be considered completely deleted. The 6th harmonic remains the same while the 12th one is increased. This worsening has been balanced out by all the others positive results given by the stator shifting and rotor skewing union. In the end have been remained only three harmonics: 6th, 12th and 18th.
To close, it must be remembered that the best result in terms of torque performance has been a motor with $T_{Avg} = 125.2\ Nm$ and $Ripple = 5.47$ %. It hasn't been considered because it has been prefered to keep an higher average torque since torque ripple is however lower than 10 %.
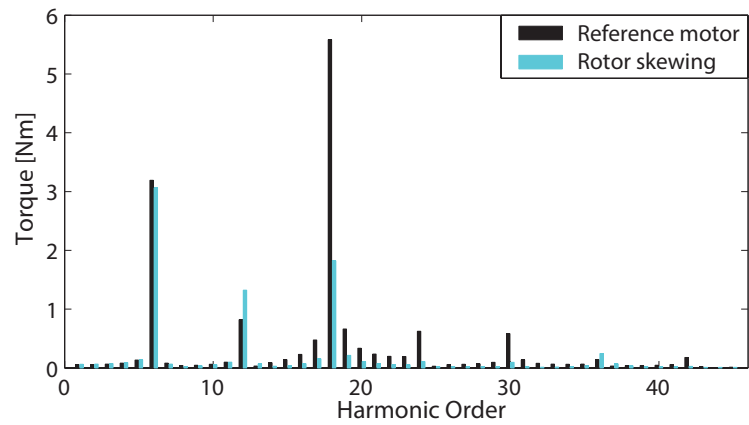
Figure 6.5: Harmonic order comparison between the reference PMARel motor and the PMARel motor 18/8 configuration with stator shifting of 380 *deg* electrical degrees matche with rotor skewing

6.3   Configuration with 12 stator slots and 8 poles

Through the method introduced at the beginning of this chapter, and with the same conditions described in Sect.6.2, 8000 different configurations has been analyzed and the final results, in terms of torque performance, are shown in Fig.6.6a.

Fig.6.6b shows a zoom of the most interesting area about torque performance.The PMARel motor configuration chosen has been highlighted in red.
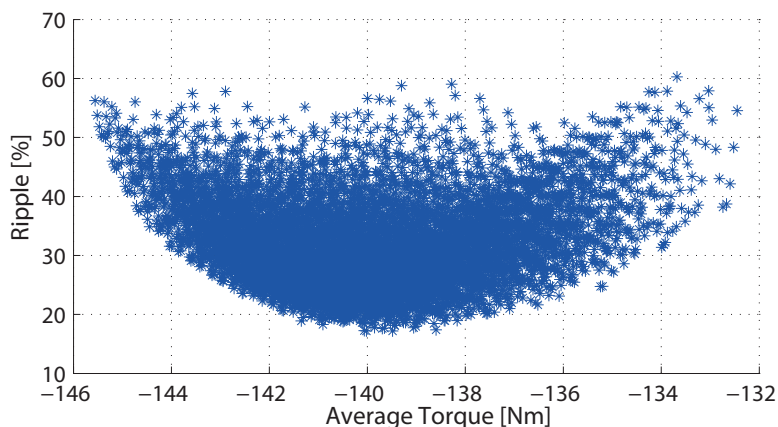
(a) Rotor skewing combinations computed
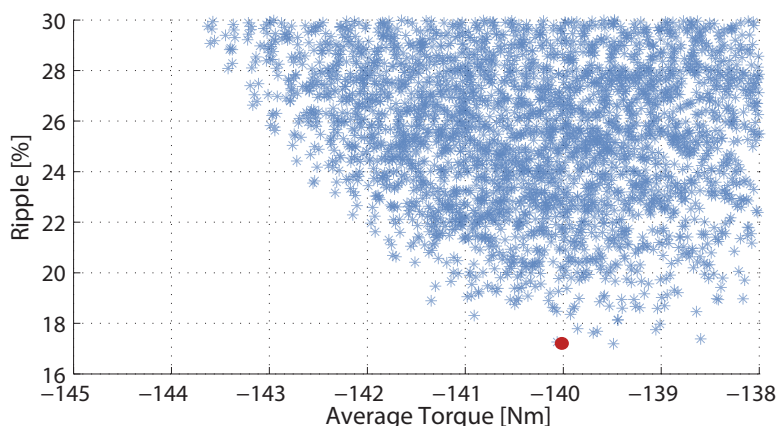
(b) Zoom of the area where the skewing combination adopted is highlighted in red

Figure 6.6: Representation of all the possible rotor skewing combinations of a 24/8 PMARel motor with stator shifting. The rotor has been splitted into 7 parts

The rotor skewing gives the opportunity to reach lower torque ripple if compared with the reference PMARel motor, but it remains high if the results obtained in Sect.6.2 are considered. This is because the departure situations in these cases are different since the 12 slots/ 8 poles configuration continues to show the worst behaviour in torque ripple. Instead the average torque has lost only a few torque units due to the not correct rotor alignment has previosuly described. The configurations which has been chosen is the one highlighted in red in Fig.6.6b. The equivalent rotor structure is reported in Tab.6.2:

Table 6.2: Rotor skewing partition in a 24/8 PMARel motor

Angular rotor position [deg]	+3	+2	+1	0	-1	-2	-3
Weighing coefficient	10	10	20	10	20	10	20

In this case, differently from Sect.6.2, the rotor is made up by 7 parts increasing the complexity of the machine. However, this choice guarantees better results which has been obtained above all those computed in terms of torque ripple. The final torque performance are:

Average Maxwell Torque = 140.0 Nm
Average d-q torque = 139.0 Nm
Torque ripple = 17.2 %

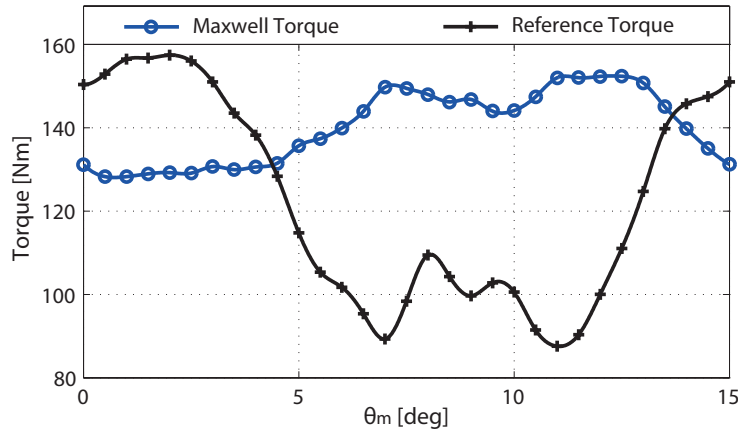and the torque behaviour is shown in Fig.6.7:

Figure 6.7: Torque value for different mechanical angles calculated through Maxwell stress tensor at nominal conditions. PMARel motor 24/8 configuration with stator shifting of 180 *deg* electrical degrees matched with rotor skewing

If it has been compared with the reference PMARel motor it must be highlighted that the torque ripple has been reduced about 42 % and the average torque has been improved about 11 %. In particular, it is evident the improvement from 4 *deg* to 14 *deg* mechanical degrees. Focusing the attention on the harmonic spectrum of the torque behaviour reported in Fig.6.8 the reason of the lower torque ripple is due to the elimination of all the harmonics except the 6th, 12th and 18th. In particular the latter two have been halved their values and the 6th harmonic, which is the main one, has been strongly reduced. To reach similar results as those in Sect.6.2 in terms of torque ripple will be splitted the rotor into an higher number of m parts.
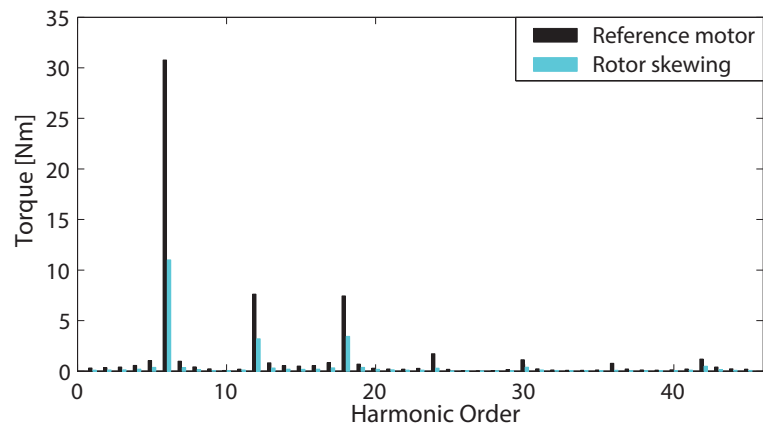
Figure 6.8: Harmonic order comparison between the reference PMARel motor and the PMARel motor 24/8 configuration with stator shifting of 180 *deg* electrical degrees matched with rotor skewing

6.4   Configuration with 12 stator slots and 10 poles

As in Sect.6.2 and Sect.6.3 also for this kind of PMARel motor configuration 8000 different rotor structures have been analyzed and the results are shown in Fig.6.9 a, while in Fig.6.9 b is reported a zoom of the most interesting area about torque performance. The PMARel motor configuration chosen has been highlighted in red.
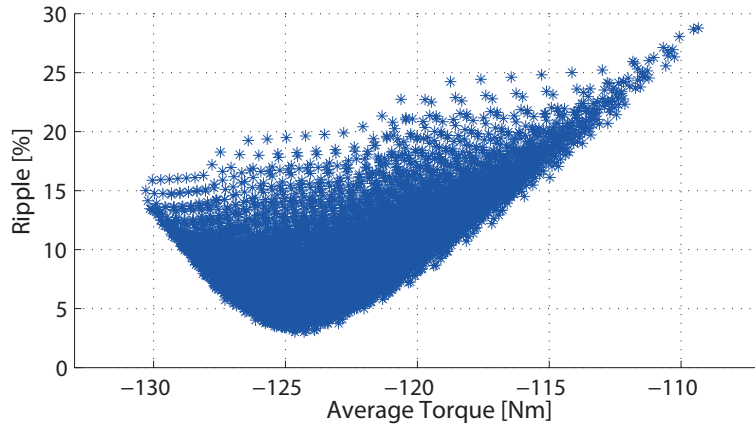
(a) Rotor skewing combinations computed
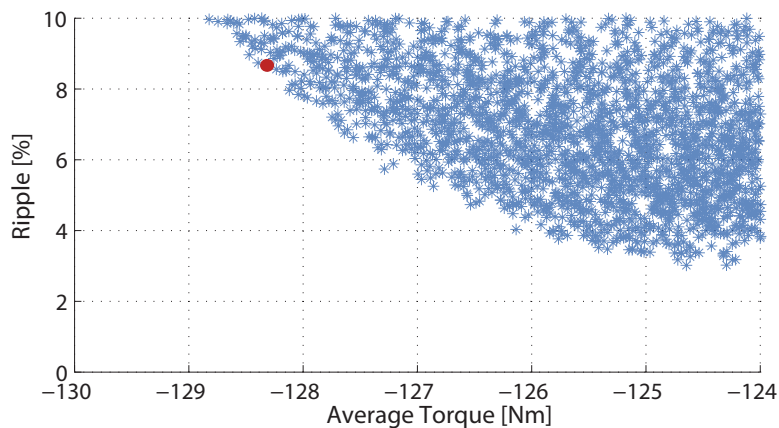
(b) Zoom of the area where the skewing combination adopted is highlighted in red

Figure 6.9: Representation of all the possible rotor skewing combinations of a 24/10 PMARel motor with stator shifting. The rotor has been splitted into 7 parts

The rotor related to the PMARel motor pointed out in Fig.6.9 b has a structure made up as reported in Tab.6.3:

Table 6.3: Rotor skewing partition in a 24/10 PMARel motor

Angular rotor position [deg]	+3	+2	+1	0	-1	-2	-3
Weighing coefficient	0	20	50	10	20	0	0

It is composed only by 4 parts and this deals with a more feasible industrial construction than the case where the rotor is made up by 7 sections. The final torque performance

related to this kind of rotor, linked with the PMARel motor which adopted also the stator shifting techique, are:

Average Maxwell Torque = 128.3 Nm
Average d-q torque = 126.8 Nm
Torque ripple = 8.65 %
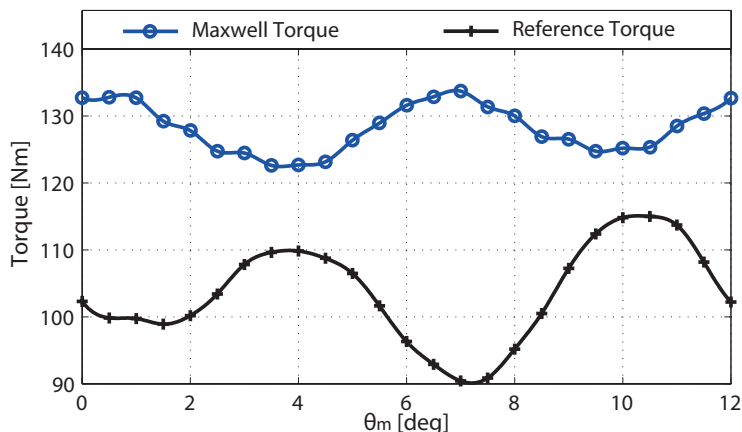
and the torque behaviour is shown in Fig.6.10:

Figure 6.10: Torque value for different mechanical angles calculated through Maxwell stress tensor at nominal conditions. PMARel motor 24/10 configuration with stator shifting of 380 deg electrical degrees matched with rotor skewing

It is evident the improvement obtained with the final structure if compared with the reference one. In particular the average torque has been increased of about 24 % and the torque ripple has been reduced of about 15 %. This is clear observing the Maxwell torque behaviour in Fig.6.10 which is smoother than the reference one. From the harmonics point of view, some considerations could be done about the final PMARel motor spectrum that is shown in Fig.6.11.
The union between stator shifting and rotor skewing has reduced all the harmonics values except the 24$^{\text{th}}$ one, which it is increased. The final motor structure deals with a torque ripple mainly influenced by only two harmonics: the 6$^{\text{th}}$ and the 12$^{\text{th}}$. Both of them have been reduced. In particular the 12$^{\text{th}}$ harmonic has been halved and the 6$^{\text{th}}$ reaches about 30 % if compared with the reference configuration. To close, it must be remembered that have been computed motors with better torque ripple (the best one is charachterized by $T_{Avg} = 124.6\ Nm$ and $Ripple = 3$ %). It hasn't been considered because it has been prefered to keep an higher average torque since the torque ripple is however lower than 10 %.
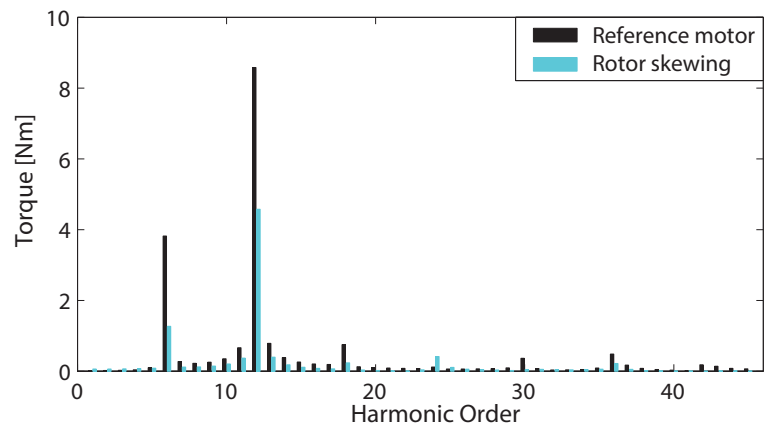
Figure 6.11: Harmonic order comparison between the reference PMARel motor and the PMARel motor 24/10 configuration with stator shifting of 380 *deg* electrical degrees matched with rotor skewing

6.5   Configuration with 15 stator slots and 10 poles

Basing the study on the same method, 8000 different rotor structures have been studied considering the possibility to split the rotor into 7 parts with different lengthes. The results obtained, in terms of torque performance, are shown Fig.6.12 a, while in Fig.6.12 b a zoom of the most interesting area about torque performance is reported. The PMARel motor configuration chosen has been highlighted in red.
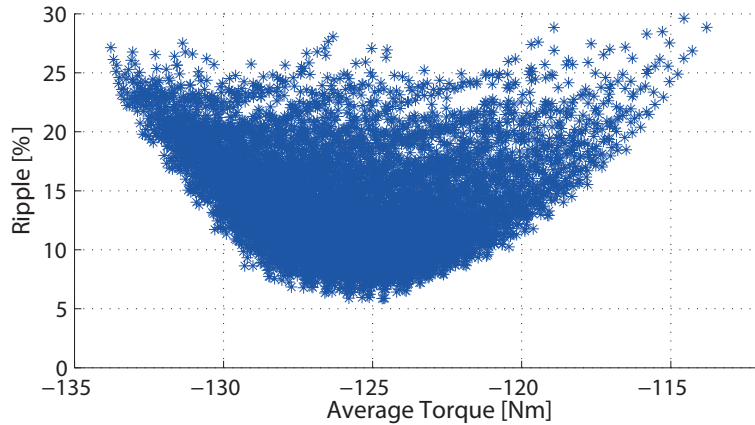
(a) Rotor skewing combinations computed
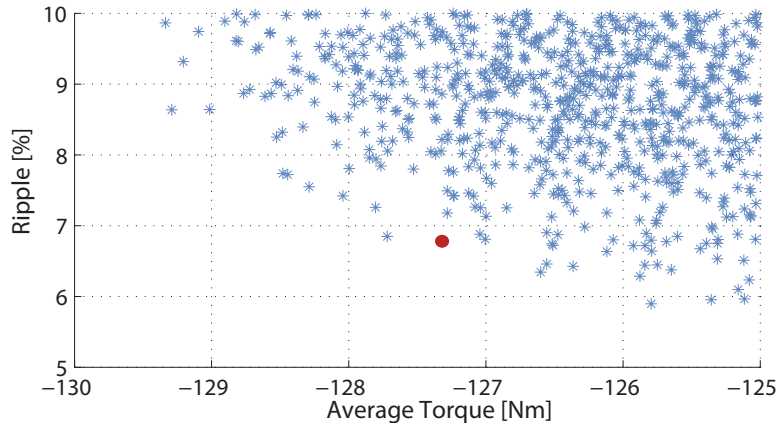
(b) Zoom of the area where is highlighted in red the skewing combination adopted

Figure 6.12: Representation of all the possible rotor skewing combinations of a 30/10 PMARel motor with stator shifting. The rotor has been splitted into 7 parts

The rotor related to the PMARel motor pointed out in Fig.6.12 b has a structure made up as reported in Tab.6.4:

Table 6.4: Rotor skewing partition in a 30/10 PMARel motor

Angular rotor position [deg]	+3	+2	+1	0	-1	-2	-3
Weighing coefficient	10	30	10	0	30	20	0

It is composed only by 5 parts and this deals with a more feasible industrial construction

than the case where the rotor is made up by 7 sections. The final torque performance related to this kind of rotor, linked with the PMARel motor which adopted also the stator shifting technique, are:

Average Maxwell Torque = 127.3 Nm
Average d-q torque = 126.5 Nm
Torque ripple = 6.77 %

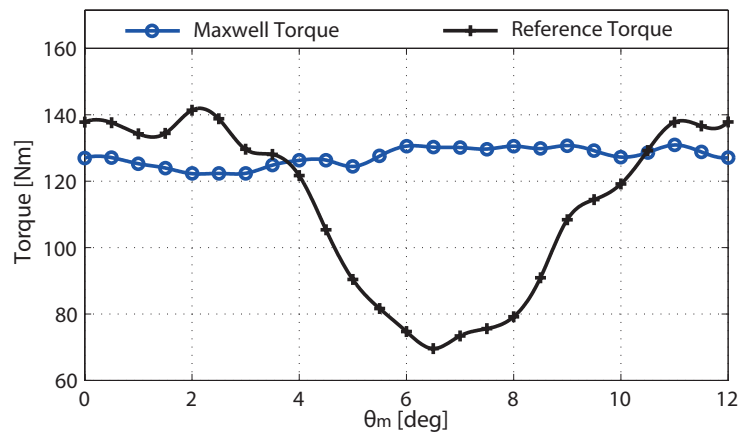and the torque behaviour is shown in Fig.6.13:

Figure 6.13: Torque value for different mechanical angles calculated through Maxwell stress tensor at nominal conditions. PMARel motor 30/10 configuration with stator shifting of 180 *deg* electrical degrees matched with rotor skewing

The comparison with the reference PMARel motor highlights the importance of the final result especially between 4 *deg* and 11 *deg* mechanical degrees. The average torque obtained is almost the highest possible, while the torque ripple reaches a very interesting value. The latter parameter is became almost 57 % lower than the reference motor and the average torque has been increased almost about 13 %. The harmonic spectrum related to this last one torque behaviour is shown in Fig.6.14.

The technical solution composed by the stator shifting and rotor skewing union, operates on the harmonic spectrum deleting all the harmonics except the main one, which is the 6th. This latter is considerably reduced reaching approximately 12 % of the initial amplitude. The presence of this only harmonic could be seen also in Fig.6.13 where the Maxwell torque has only one period in 60 *deg* electrical degrees. This means that in 360 *deg* electrical degrees there are 6 periods.

To close, it must be remembered that the best result in terms of torque performance has been a motor with $T_{Avg} = 125.8 \ Nm$ and $Ripple = 5.9$ %. It hasn't been considered because it has been prefered to keep an higher average torque since the torque ripple is however lower than 10 %.
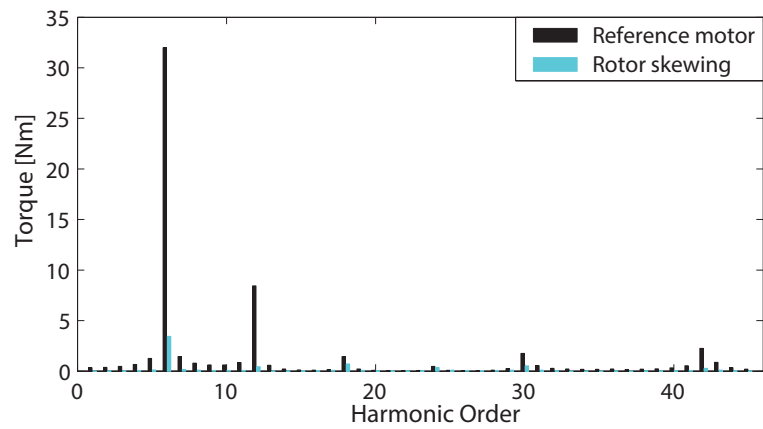
Figure 6.14: Harmonic order comparison between the reference PMARel motor and the PMARel motor 30/10 configuration with stator shifting of 180 *deg* electrical degrees matched with rotor skewing

6.6 Final considerations

The final torque performance which have been reached at the end of the study are very interesting if compared with the FCSW PMARel motors sized at the beginning. A brief summary is reported in Tab.6.5:

Table 6.5: Comparison between reference FCSW PMARel motor configurations and the same ones after the union of stator shifting and rotor skewing techniques at nominal conditions

	Maxwell Average Torque [N·m]	Torque Ripple [%]
Reference 9/8	106.5	16.29
9/8 Rotor skewing	127.1	7.49
Reference 12/8	125.96	59.02
12/8 Rotor skewing	140.0	17.2
Reference 12/10	103.5	23.73
12/10 Rotor skewing	128.3	8.65
Reference 15/10	113.1	63.48
15/10 Rotor skewing	127.3	6.77

There are some main considerations to do about the rotor skewing:

- the method used to apply this technique to the rotor has been based on a discrete rotor split which is possible because of the windings absence. As a consequence the PMs will have different lenghtes according to the weighing coefficient related to each rotor part;

- the average torque always decreases after the rotor skewing and this deals with the phenomenon shown in Sect.6.1.2. In fact, the light error in the current angle valuation deals with a lower torque because the motor doesn't work in MTPA conditions;

- the torque ripple is always considerably improved going under 10 % in all cases except in the 12 slots/ 10 poles PMARel motor configuration;

- if compared with the reference PMARel motors the average torque has been increased between 11 % and 24 % while the torque ripple has been decreased between 9 % and 57 %;

- if compared with the PMARel motors with only the stator shifting the average torque has been decreased between 1 % and 5 % while the torque ripple has been decreased between 7 % and 42 %;

- the final harmonic spectrum is always composed by the harmonic of 6th, 12th and 18th order. In the 12 slots/ 10 poles PMARel motor configuration there are only the first two harmonics and in the 15 slots/ 10 poles PMARel motor configuration there is the presence only of the 6th.

Conclusions

From the analyses that have been carried out it could be said that SPM motor remains a simple configuration with great torque performance due to the high average torque and low torque ripple. This only if PMs are made up by NdFeB. If they are composed by Ferrite it has been seen how the torque behavior gets worse with the additional problem of PMs degmagnetization. The DW PMARel motor using Ferrite PMs has the same torque performance about SPM configuration. Torque ripple is worse especially at overload conditions. Focusing the attention on its behaviour on varying of the current vector angle it could be highlighted how it remains almost the same in absolute value. Instead in per cent it changes, decreasing when the average torque increases and vice versa. In PMARel configuration the main torque contribution is done by the reluctance torque and PMs secondly takes part on its generation. This is because of the rotor anisotropy absence in SPM rotor.

The comparison among different FCSW PMARel motors and DW PMARel motor has generally shown an average torque drop in the range between 28.6 % and 38 % when it is adopted a FCSW instead of a DW. This reduction is due to the reluctance torque, while the PMs torque remains always the same except in 12/8 PMARel motor where it has an anomalous behaviour. In fact it isn't smooth but very variable achieving also negative values.

Linked to this torque behaviour the torque ripple becomes worse than the DW PMARel motor. These two main effects depend on the periodicity and are emphasized for its higher values. In particular, the highest average torque and torque ripple have been always obtained in motors being part of 3 slots/2 poles configuration.

Different techniques have been tried to improve the FCSW motors torque performance. The first one has been the *tooth cut*, and among different kinds, the symmetrical cut has given the best results. In particular it influences the $L_d - L_q$ parameter going to decrease the reluctance torque and as a consequence the average torque in all the FCSW PMARel configurations. It must be highlighted that it always acts on slot harmonics of the stator M.M.F. For lower periodicity there is a torque ripple improvement about the 8 %, while for higher ones it remains almost the same.

The *stator shifting* technique always improved the average torque. It increases between 16 % and 26 % in comparison with the reference FCSW PMARel motors. This means that the torque difference from the DW PMARel motor is reduced and it is about from 15 % and 25 %. Torque ripple changes in different ways due to the FCSW configurations. In both 3 slots/2 poles configurations it continues to keep the highest level also if in 30/10 PMARel motor the torque ripple is decreased about 35 %.

FCSW related to 3 slots/2 poles type after *stator shifting* become DW.

Combining *stator shifting* with *rotor skewing* it is possible to reduce considerably the torque ripple going under 10 % in all cases except for 12/8 PMARel motor. It is the worst FCSW configuration from this point of view also if it is the one with the highest average torque. However it is the less interesting because its torque performance doesn't satisfy the industrial needs despite of a final DW has been adopted. In all FCSW motors the *rotor skewing* doesn't decrease the average torque.

For each FCSW PMARel motor which has been analyzed is shown in Fig.6.15 a summary of average torque behaviour and in Fig.6.16 a summary of torque ripple behaviour. Both depending on the technique adopted. For both the torque performance, it is worth noticing the positive effect of the design choices.
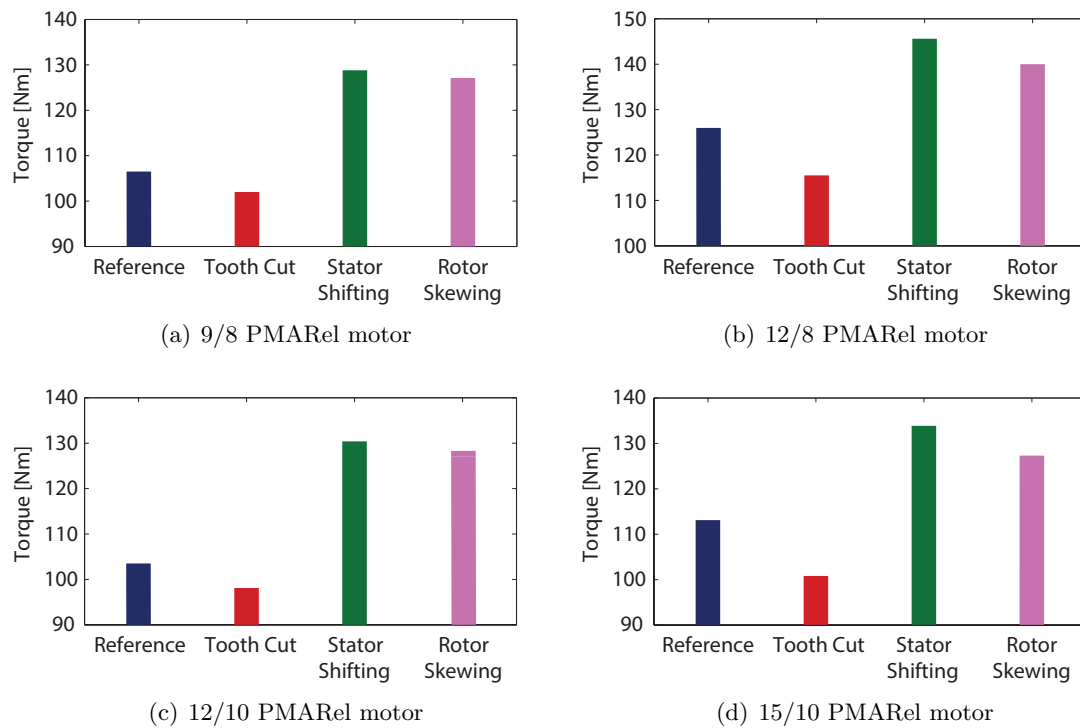

(a) 9/8 PMARel motor

(b) 12/8 PMARel motor

(c) 12/10 PMARel motor

(d) 15/10 PMARel motor

Figure 6.15: Average torque behaviour summary for each FCSW PMARel motor configuration. The DW PMARel motor has an average torque of 171.8 Nm
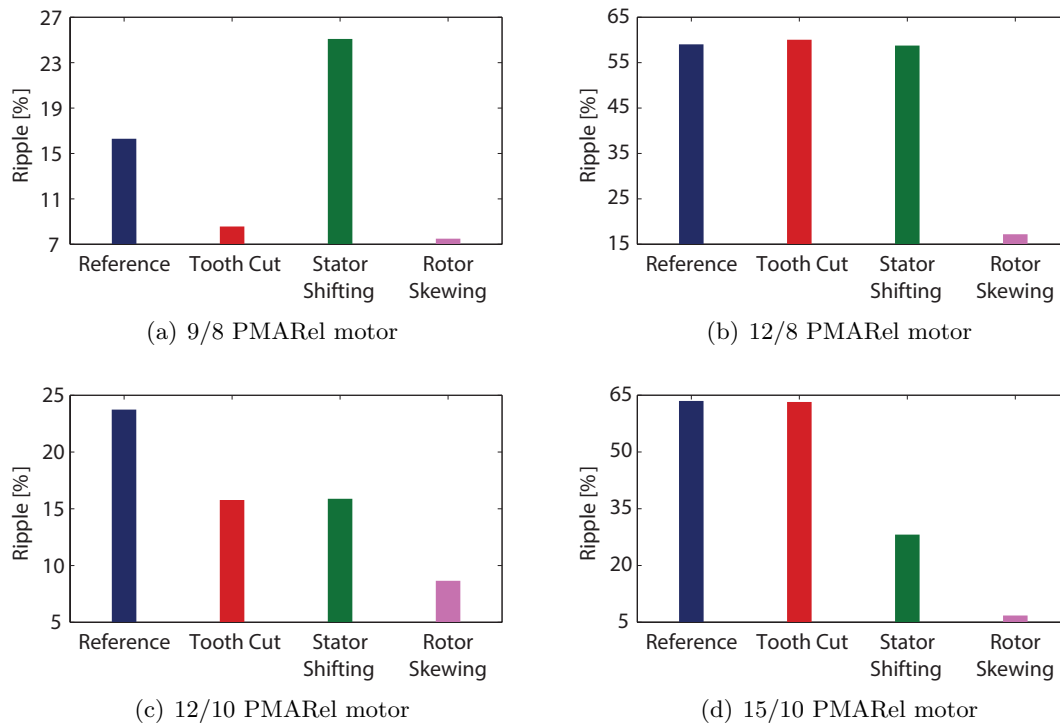
Figure 6.16: Torque ripple behaviour summary for each FCSW PMARel motor configuration. The DW PMARel motor has a torque ripple of 13.05 Nm

To conclude the study, from the various comparisons the 12/10 PMARel motor results to be the best configuration among the FCSW motors that have been analyzed. It could guarantee the best torque ripple (until the 3 %) and an average torque equivalent to all the others FCSW types. This without becoming a DW after *stator shifting*.
Using FCSW PMARel motors it is not possible to reach the same results of SPM motor. If torque ripple is better, the average torque remains quite low ($\simeq$ 75 %). The DW PMARel motor is the unique solution which reaches a similar average torque nder nominal and overload conditions of the SPM motor one, while its torque ripple is comparable with the SPM motor one.

Bibliography

[1] N. Bianchi. *Metodologie di progettazione delle macchine elettriche*. Cleup, Nov 2004.

[2] N. Bianchi. *Calcolo delle macchine elettriche col metodo degli elementi finiti*, chapter 9, pages 176–181. Cleup, Nov 2004.

[3] A. Vagati, M. Pastorelli, G. Francheschini, and S.C. Petrache. Design of low-torque-ripple synchronous reluctance motors. *Industry Applications, IEEE Transactions on*, 34(4):758–765, Jul 1998.

[4] B. Boazzo, A. Vagati, G. Pellegrino, E. Armando, and P. Guglielmi. Multipolar ferrite-assisted synchronous reluctance machines: A general design approach. *Industrial Electronics, IEEE Transactions on*, 62(2):832–845, Feb 2015.

[5] R. Fusar. Analysis and damping techniques for torque ripple reduction in a 24-slot 16-pole fractional slot windings pmasynrel motor. Master's thesis, University of Padua, Department of Industrial Engineering, Jul 2015.

[6] L. Alberti, M. Barcaro, and N. Bianchi. Design of a low-torque-ripple fractional-slot interior permanent-magnet motor. *Industry Applications, IEEE Transactions on*, 50(3):1801–1808, May 2014.

[7] P.B. Reddy, Kum-Kang Huh, and A.M. EL-Refaie. Generalized approach of stator shifting in interior permanent-magnet machines equipped with fractional-slot concentrated windings. *Industrial Electronics, IEEE Transactions on*, 61(9):5035–5046, Sept 2014.